

**STRUCTURAL AND FUNCTIONAL ANALYSIS OF
CROSSVEINLESS 2 / BMP-2 / CHORDIN INTERACTION**

**Dissertation zur Erlangung des
naturwissenschaftlichen Doktorgrades
der Bayerischen Julius-Maximilians-Universität Würzburg**

vorgelegt von

Liyan Qiu

(Shandong, China)

Würzburg, 2008

Eingereicht am:

Mitglieder der Promotionskommission:

Vorsitzender:

1. Gutachter:

Prof. W. Sebald

2. Gutachter:

Prof. R. Benz

Tag des Promotionskolloquiums:

Doktorurkunde ausgehändigt am:

Contents

Contents

1 Introduction	1
1.1 TGF- β superfamily and BMP subfamily.....	1
1.2 TGF- β signaling pathway and receptors.....	2
1.3 Structure of TGF- β -like proteins and BMPs.....	4
1.4 Crystal Structure of BMPs with receptor ectodomains.....	6
1.5 Binding affinity and specificity of BMP/receptor interactions.....	9
1.6 Modulator proteins of BMP signaling.....	10
1.6.1 Noggin and Follistatin.....	11
1.6.2 Von Willebrand Factor type C domain (VWC) containing proteins.....	14
1.6.2.1 Chordin	15
1.6.2.2 Crossveinless 2.....	19
2 Material and methods	25
2.1 Bacterial strains.....	25
2.2 Vectors.....	25
2.3 Oligoes for molecular cloning.....	25
2.4 Solutions.....	27
2.5 Proteins.....	28
2.6 Molecular biology methods.....	28
2.6.1 Agarose gel electrophoresis of DNA.....	28
2.6.2 Isolation of plasmids from <i>E. coli</i>	28
2.6.3 Transformation of <i>E. coli</i> strains.. ..	29
2.6.4 Determination of DNA concentration and purity	30
2.6.5 Molecular cloning of VWC domains and mutants.....	30
2.6.5.1 Cloning of CV2-VWC domains.....	30
2.6.5.2 Cloning of CV2-VWC1 mutants.....	31
2.6.5.3 Cloning of multi-VWC fragments.....	32

Contents

2.7 Expression of proteins.....	32
2.7.1 Expression of thioredoxin fusion proteins in TB-Medium.....	32
2.7.2 Expression of ¹⁵ N labelled and ¹⁵ N ¹³ C labelled thioredoxin fusion CV2-VWC1.....	33
2.7.3 Selenomethionine labelled thioredoxin fusion CV2-VWC1 and mutants.....	34
2.7.4 Expression of proteins in SF9 cells.....	35
2.8 Purification of proteins	37
2.8.1 Bacteria sonication.....	37
2.8.2 Nickel-chelating chromatography	37
2.8.3 Ni-NTA chromatography.....	38
2.8.4 Anion and cation exchange chromatography.....	38
2.8.5 High Performance Liquid Chromatography (HPLC).....	39
2.8.6 Gel filtration chromatography.....	40
2.8.7 Calibration of the superdex 200 column.....	41
2.8.8 BMP-2 affinity chromatography.....	42
2.9 Thrombin cleavage.....	43
2.10 Protein chemistry methods	44
2.10.1 Proteins marker.....	44
2.10.2 SDS-Polyacrylamid-Gelelektrophorese (SDS-PAGE)	44
2.10.3 Coomassie Brilliant Blue staining	45
2.10.4 Silver staining	45
2.10.5 Concentrating the protein solution.....	46
2.10.6 Determination of the protein concentration.....	46
2.10.7 Biosensor interaction analysis	47
2.10.8 Mass spectrometry.....	48
2.10.9 Western blotting.....	48
2.11 Crystallization solutions and methods.....	49
2.11.1 Crystallization solutions.....	49

Contents

2.11.2 X-ray Crystallization of BMP-2 and CV2-VWC1 complex.....	49
2.11.3 Cryoprotection of crystals.....	50
2.12 Biological Activity in Cell Lines.....	50
3. Results	52
3.1 Preparation of VWC domains of CV2.....	52
3.1.1 Expression and purification of CV2-VWC1 domain	52
3.1.2 Expression and purification of other 4 remaining CV2-VWC domains...	59
3.1.3 Preparation of ¹⁵ N-labelled CV2-VWC1 and ¹⁵ N ¹³ C-double Labelled CV2-VWC1	64
3.1.4 Binding affinity and specificity of BMPs for CV2 and CV2-VWC domains.....	66
3.2 Identification of CV2 binding site for Chordin.....	67
3.3 Crystallization of the BMP-2 /CV2-VWC1 binary complex.....	70
3.3.1 Preparation of BMP-2 and CV2-VWC1 complex.....	70
3.3.2 Crystallization of the binary complex of wt BMP-2/CV2-VWC1 and preliminary analysis of the native data.....	71
3.3.3 Crystallization of the Selenomethionine-labelled complex of BMP-2 and CV2-VWC1.....	80
3.3.4 NMR analysis of CV2-VWC1.....	86
3.4 Structure of the binary complex of BMP-2 and CV2-VWC1.....	87
3.4.1 Binding epitopes of BMP-2 for CV2-VWC1.....	87
3.4.2 Key interactions between CV2-VWC1 and BMP-2.....	91
3.5 Biological activity of CV2 and CV2-VWC1 in cell assay and in vivo.....	97
3.5.1 Inhibition of BMP-2 signaling by CV2 and CV2-VWC1.....	97
3.5.2 BMP-2 variants that inhibit CV2 and CV2-VWC1.....	97
3.5.3 Biological activity of CV2-VWC1/CV2 in vivo.....	100
4. Discussion	102
4.1 Expression and purification of VWC domains.....	102
4.2 Binding affinity and specificity of VWC domains.....	103

Contents

4.3 VWC domains are multifunctional binding modules that exert multiple binding characteristics.....	107
4.4 Mechanism of CV2 and CV2-VWC1 modulate BMP signaling	108
5. References.....	112
Abbreviations.....	124
Abstracts.....	126
Acknowledgement.....	130
Crriculum Vitae.....	131
ERKLÄRUNG	132

1. Introduction

1.1 TGF- β superfamily and BMP subfamily

The transforming growth factor- β (TGF- β) superfamily forms a group of structurally related cytokines. According to similarities of amino acid sequences, the TGF- β superfamily can be classified into bone morphogenetic proteins (BMPs), growth and differentiation factors (GDFs), TGF- β s, activins and others (Fig. 1.1) (1, 2). The TGF- β superfamily of growth factors comprises seven genes in *Drosophila melanogaster* and at least 30 genes in mammals, including 3 TGF- β isoforms, 4 activin β -chains, the protein nodel, 10 bone morphogenetic proteins (BMPs) and 11 growth and differentiation factors (GDFs) (3). These proteins are found in almost all cell types and are involved in numerous cellular processes, including bone and joint development, cell proliferation and differentiation, and dorsal/ventral patterning of the animal embryo, trauma and wound repair (4, 5).

BMP proteins were first isolated on the basis of their bone-inducing activity in mammalian tissues and were therefore named as BMPs (4). BMPs account for most of the TGF- β superfamily of peptides, and the proteins display extensive conservation among species (6). BMPs were found to play crucial roles in embryogenesis and organogenesis during vertebrate and invertebrate development (7). During embryonic life, BMPs regulate neurogenesis and hematopoiesis, and induce somite formation. BMPs regulate multiple cellular processes such as cell proliferation and differentiation, apoptosis and pattern formation and tissue specification during embryonic development (7, 8). After birth, BMPs play a role in the maintenance of bone mass. They induce the differentiation of marrow stromal cells toward the osteoblastic lineage, therefore increasing the pool of mature bone forming cells, and enhance the differentiated function of osteoblasts (9). Dysregulated function of BMPs and other TGF- β like proteins results in a variety of diseases ranging from skeletal abnormalities to metabolic disorders (10).

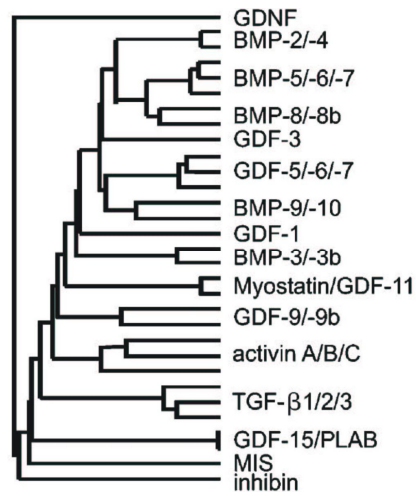


Figure 1.1 Phylogenetic comparisons of mature ligands in the TGF-β superfamily (reviewed by Sebald et al.). Only human proteins are included with the exception of BMP-8b and GDF-3 which are from mouse (2).

1.2 TGF-β signaling pathway and receptors

Activity of TGF-β superfamily members is initiated by binding to both type I and type II serine/threonine kinases receptors, leading to phosphorylation of the cytoplasmic serine/threonine kinase domains (11, 12). In mammals, seven type I receptors and five type II receptors have been identified (Fig. 1.2A) (1, 12). The type I receptors have similar sizes (50-55 KDa) and 60-90% amino acid sequence identity in their kinase domains. Type I receptors are more similar to each other than they are to the known type II receptors (approximately 70 KDa) (13, 14). Both type I and type II receptors are composed of an N-terminal extracellular ligand binding domain, a transmembrane region, and a C-terminal serine/threonine kinase domain.

Type I receptors contain a conserved sequence (SGSGSG) known as the GS domain (also called type I box) in their cytoplasmic juxtamembrane region (15, 16). The activation of the type I receptor involves the phosphorylation of its GS domain by the type II receptor; hence an active receptor signaling complex comprises both types of receptors bound to ligands (17, 18). The type I receptors then transduce downstream signals by phosphorylating receptor-activated Smad proteins. Based on functional and

Introduction

structural differences, Smads can be classified into three subfamilies: receptor-activated Smads (R-Smad), common-partner Smads (Co-Smad), and inhibitory Smads (I-Smad) (13). Whereas Smad1, Smad5, and Smad8 are phosphorylated by BMP type I receptors (ALK-2, ALK-3, and ALK-6), Smad2 and Smad3 are activated by TGF- β and Activin type I receptors (ALK-5 and ALK-4). The R-Smad and Co-Smad (Smad4) form a hetero-oligomer which translocates into the nucleus and regulates expression of ligand-responsive genes. Inhibitory Smads include Smad6 and Smad7, which negatively regulate TGF- β signaling by competing with R-Smads for receptors or Co-Smads interaction, and by targeting the receptor for degradation (13).

There are two distinct modes of the ligand-receptor interaction in the TGF- β superfamily signaling (11). One is represented by members of BMP subfamily and the other exemplified by TGF- β s and Activins. BMP ligands, such as BMP-2 and BMP-4, exhibit a high affinity for the extracellular ligand binding domains of type I BMP receptors and a low affinity for type II receptors. The preassembled type I receptor-ligand complex has a higher binding affinity for the type II receptor (11). In contrast to BMPs, TGF- β s and Activins display high affinity for the type II receptors. The ligand binds tightly to the type II receptor first, which allows the subsequent incorporation of the type I receptor, forming a large ligand-receptor complex involving a ligand dimer and four receptor molecules (11).

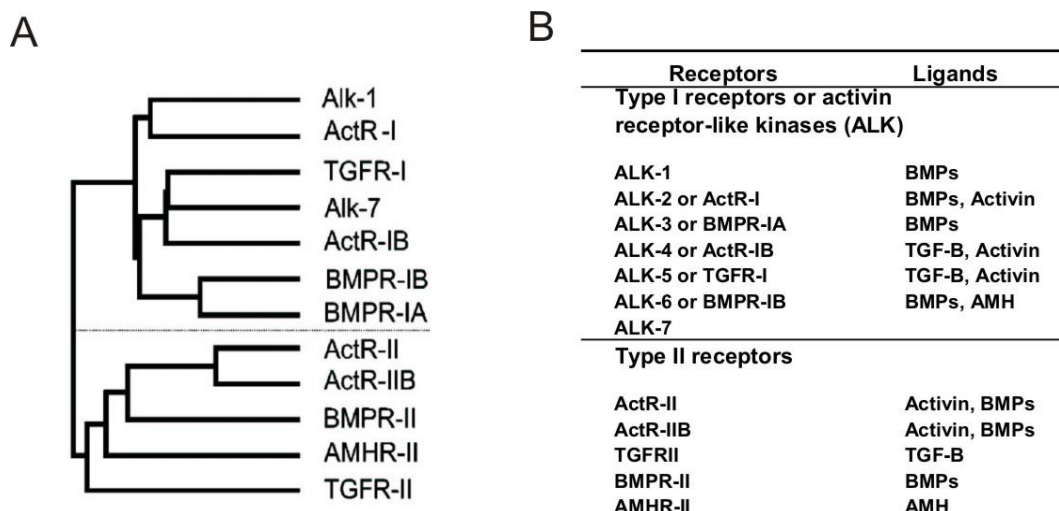


Figure 1.2 A. Sequence similarities of receptor ectodomains in the TGF- β superfamily (reviewed by Sebald et al (2)). B. Type I and type II receptors involved in the signaling pathway of TGF- β superfamily members and their ligands (reviewed by Balemans W et al (19)).

The interactions of two kinds of receptors with ligands are promiscuous, and this means the receptor can bind with different TGF- β superfamily proteins and one ligand can bind to different receptor chains (Fig.1.2B). However, accumulated evidence shows that there is specificity in these interactions. BMPR-IA preferentially binds to BMP-2 over BMP-7 and GDF-5, BMPR-IB binds preferentially to GDF-5 and BMP-7 over BMP-2 (20, 21). ActR-IB binds the activins and myostatin (22). TGFR-I is specific for the TGF- β s and possibly for myostatin. Moreover, Type II receptor chains are less discriminatory in binding with ligands. ActR-II, ActR-IIB and BMPR-II have been shown to interact with BMP-2, BMP-7 and GDF-5.

1.3 Structure of TGF- β -like proteins and BMPs

Like all members of TGF- β superfamily, BMPs are synthesized as precursor proteins, consisting of a signal peptide, pro-domain and mature peptide. BMPs are matured by cleavage of a large proprotein by proteases. The mature monomer of TGF- β superfamily represents the C-terminal segment of about 100 residues and 6-41 additional residues at the N-terminus (2). The proprotein has about three times the

Introduction

length of the mature protein. BMP-2 is synthesized as a 453 residues proprotein, which becomes glycosylated, proteolytically cleaved and dimerized to yield the mature homodimeric protein consisting of 114 C-terminal proprotein residues. Similar to other members of TGF- β superfamily, BMP-2 contains a conserved cystine-knot which comprises two consensus sequences, C43-X-G-X-C47 and C111-X-C113. The cystine bridges between C43/C111 and C47/C113 form a ring-like structure with the main chain. A third disulfide bond C14/C79 passes through the ring thus forming the knot (2, 23, 24).

According to the structures of TGF- β superfamily members that have been characterized, typical features include two separated antiparallel β -sheets, the second of which adopts a twisted crossover conformation, and a four-turn α -helix approximately perpendicular to the strands (23). The β -sheets can be further divided into nine β -strands. The monomer is commonly described as an open left hand with the N-terminal end as the thumb, the two β sheets (each two-stranded) as the two fingers and the central α -helix as the wrist (Fig. 1.3A). To date, the crystal structure of TGF- β 2, TGF- β 3, GDNF, BMP-7, BMP-2, GDF-5, BMP-6, BMP-9 and solution structure of TGF- β 1 have been determined (25, 26). There are little differences in some structural elements between BMPs and TGF- β s at the basis of their common structure (Fig. 1. 3A) (23).

The native BMP-2 is a homodimer and the subunits are covalently linked by a single disulfide bond (Cys78 from both subunits). The BMP-2 dimer is antiparallel associated (23). In the BMP-2 dimer, the wrist of one monomer fits into the concave side of the fingers of the other monomer (Fig. 1.3B). Intersubunits contacts are formed by interaction of helix α 3 from one monomer with the β -sheets of the other monomer. The topology of BMP-2 dimer is highly conserved within the TGF- β superfamily, but it is different to other cystine-knot proteins, like PDGF, VEGF and NGF. (27, 28).

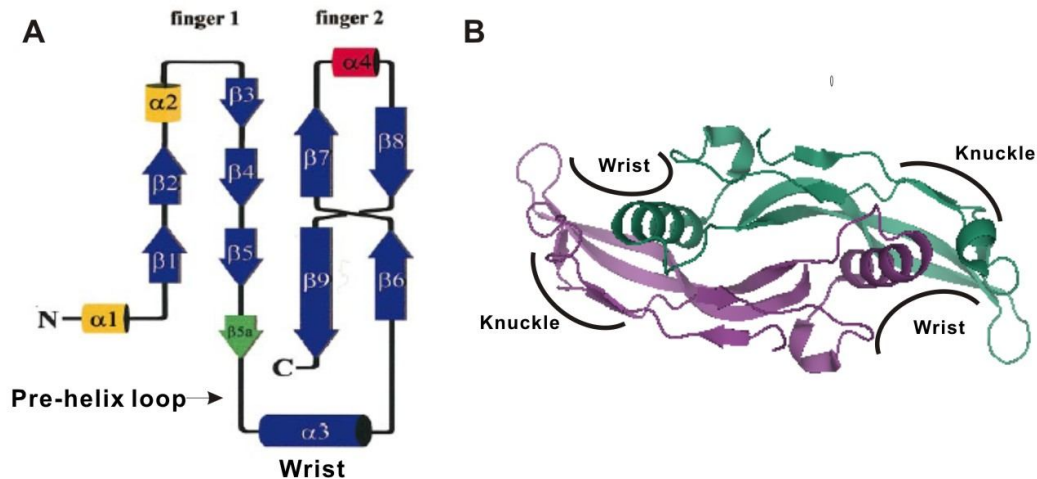


Figure 1.3 Secondary structure elements (A) and crystal structure of BMP-2 (B). A, Helices are indicated as cylinders, β -strands as arrows. Secondary structure elements that are part of the TGF- β /BMP basic-scaffold are colored blue. Orange helices ($\alpha 1$ and $\alpha 2$) are uniquely found in TGF- β s, while the red helix is unique to BMP-7 ($\alpha 4$), and the green helix is unique to BMP-2 ($\beta 5\alpha$) (23). B, Ribbon model presents a view of BMP-2 along the 2-fold axis and shows the location of the wrist and knuckle epitopes.

BMP-2 has low solubility properties under physiological conditions, similar to other BMP members and TGF- β s and GDFs. One explanation is that the surface of BMP-2 exposes 4 large hydrophobic areas (23).

1.4 Crystal Structure of BMPs with receptor ectodomains

Crystal structure of BMP-2 and BRIA is composed of one BMP dimer and two BRIA extracellular domains, which interact with the wrist epitope of the ligand. The contact is from both BMP-2 monomers, which is formed by the wrist of one monomer and the inner finger region of the concave side of the other monomer (29) (Fig. 1.4A). In the BMP-7/ActRII-ec complex, the type II receptor binds to the knuckle epitope formed only by the back side of the finger regions of one BMP-7 monomer (21) (Fig. 1.4B). The ternary complex of BMP-2/BRIA/ActIIB (ActII) comprises one BMP-2 dimer, two BRIA and two ActIIB (ActII) ectodomains. In the crystal structure, the receptor ectodomains bind independently and have no direct contacts. The BMPs function as rigid scaffolds, which hold the receptor ECDs together for transactivation (30, 31) (Fig.

1.4C and 4D).

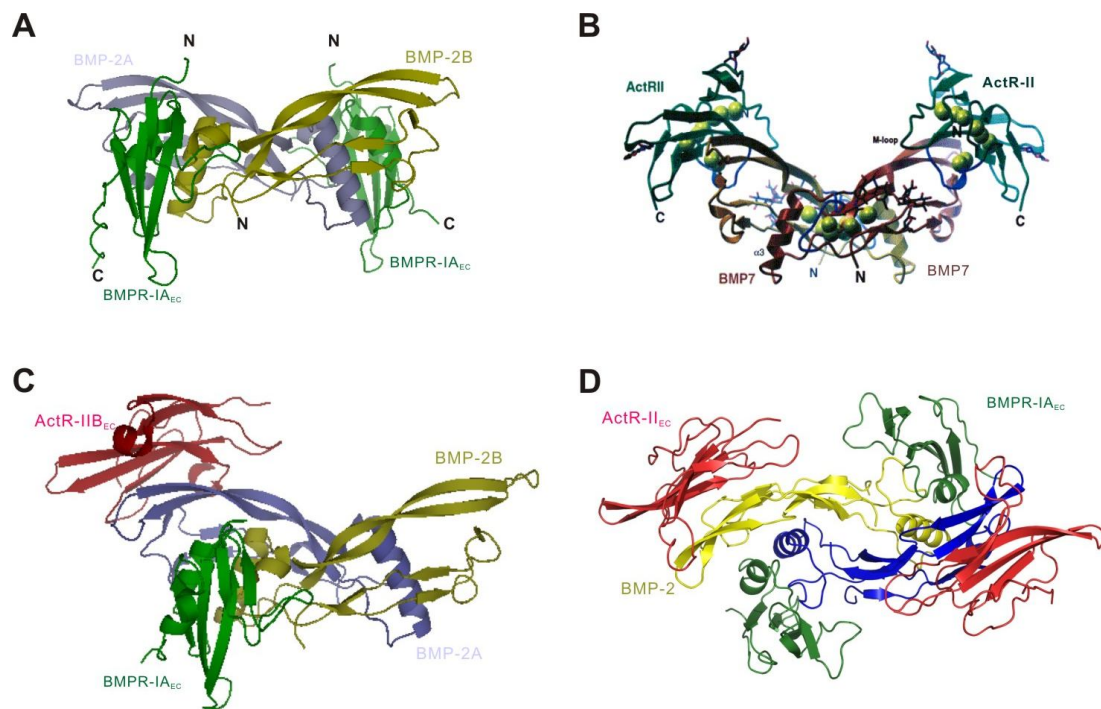


Figure 1.4 Crystal structures of BMPs with receptor ectodomains. A, BMP-2 and the receptor BMPR-IA ectodomain. (30). B, BMP-7 and the receptor ActR-II ectodomain (22). C, Crystal structure of BMP-2 bound to one receptor ectodomain of BMPR-IA and ActR-IIB (31). D, Ternary complex of BMP-2/BMPR-IA/ActR-II (32).

In the complex of BMP-2 and BRIA, the total buried solvent accessible surface area upon binding of one receptor molecule is 2.260\AA^2 . Of the 1130\AA^2 in the BMP-2 dimer that are buried, 68% is from BMP-2_A and 32% is from BMP-2_B. Altogether, 27 residues from BRIA and 26 residues from BMP-2 are involved in ligand-receptor interactions, of which 15 are from BMP-2_A and 11 are from BMP-2_B (29). The interaction of BMP-7 and ActRII is hydrophobic with a buried surface area of 676\AA^2 per subunit. It is mainly composed of side chain interactions providing a structural scaffold on which the binding specificity can be encoded by amino acid identities (21).

BMPs and other TGF- β like proteins have two kinds of functional epitopes for receptor binding. The crystal structure of BMP-2 and BRIA_{ec} complex shows that

Introduction

elements of both BMP-2 monomers build the “wrist” epitope and binds type I receptor ectodomains (ECD) (Fig. 1.5A). The pre- α -helix loop and the α -helix from one monomer (the wrist of the hand-like monomer) together with the concave side of the fingers of the second monomer create this epitope (32, 33). Central to the hydrophobic interface of BMP-2/BMPR-IA is Phe85 of BRIAec, which sticks out of the receptor helix α 1 and fits into a hydrophobic pocket on the ligand where it is surrounded by 8 hydrophobic residues from both BMP-2 monomers. The residue Phe85 is conserved in all type I receptors, raising the possibility that this “knob-into-hole” motif possibly determines the specificities of type I receptor/ligand interactions. The “knuckle” epitope is also hydrophobic. It is constituted by one monomer only and binds type II receptor ectodomains (Fig. 1.5B) (21). Both epitopes are promiscuous and each of them can interact with several different receptor chains.

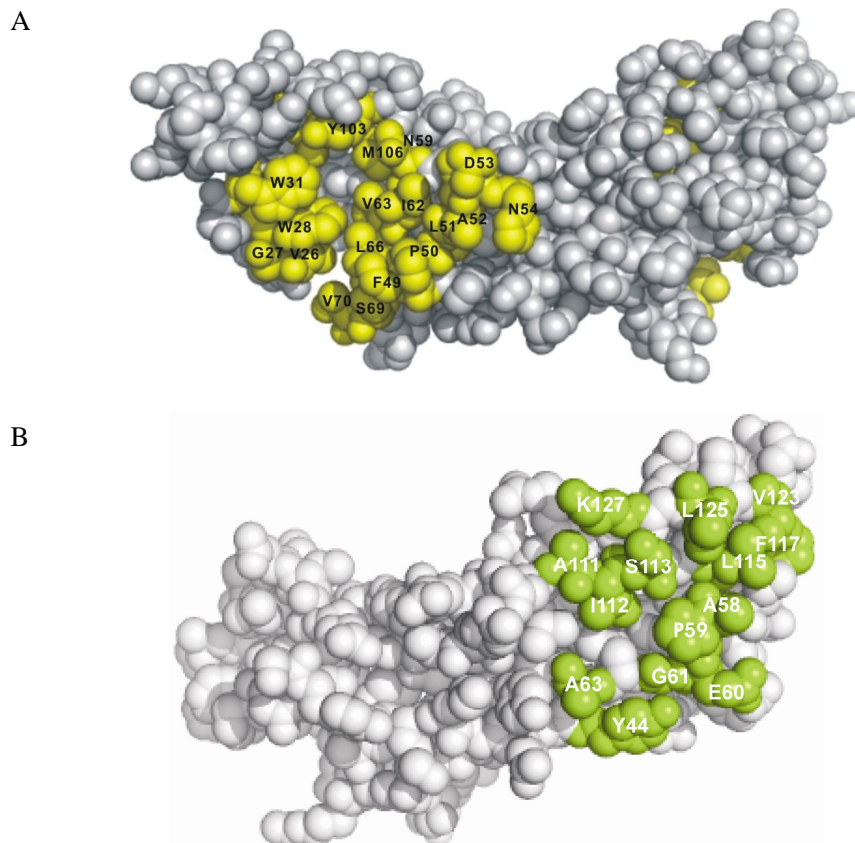


Figure 1.5 A Structural epitopes of BMP-2/BMP-7 for binding of type I and type II receptors. A, Residues buried in the surface in the wrist epitope of BMP-2 in complex with BMP-IA ectodomain (2, 33). B, Residues buried in the surface in the knuckle epitope of BMP-7 in complex with ActR-II ectodomain (21).

1.5 Binding affinity and specificity of BMP/receptor interactions

The residues of BMP-2 that determine binding affinity and specificity for both type I and type II receptor binding have been identified by submitting a large array of BMP-2 mutants by Biacore interaction analysis with the receptor ectodomains (33, 34).

In the early study, mutational analysis identified only side chains of minor importance (33, 35, 36 and 37). The elusive binding determinants for BMP-2/BMPR-IA interaction were finally identified by scrutinising the ten hydrogen bonds predicted to occur at the interface (34). A BMP-2 L51P mutant which has lost one of the central hydrogen bonds due to the introduced proline showed about 5000-fold lower affinity to BRIA and BRIB than the wild type, but still has the similar affinity to type II receptors. Thus L51P is known as “receptor-dead” mutant. The amide and carbonyl of Leu51 of BMP-2 form two hydrogen bonds with Q86 of BRIA. Interestingly, the mutant Q86A has a 100-fold reduced affinity for BMP-2 compared to that of the wild type receptor (34). Residue Leu51 is invariant in members of the BMP-2-BMP-4, BMP-5-BMP-6-BMP-7, and GDF-5-GDF-6-GDF-7 protein subfamilies, all of which interact functionally with the receptors BRIA and BRIB. Gln 86 of BRIA is invariant in the BRIB receptor but not in other type I chains. This suggests that the hydrogen bonds between these residues are important for the binding of all the BMPs and GDFs to the BRIA and BRIB receptors (34).

The binding of the “receptor-dead” BMP-2 mutant L51P to modulator proteins such as Noggin, chordin and gremlin is unchanged (34) indicating that binding determinants of BMPs for type I receptor and Noggin are different. This allows the L51P mutant to neutralize Noggin inhibition on BMP induction of alkaline phosphatase (ALP) in C2C12 cells. Thus, L51P mutant could be used as a receptor-inactive inhibitor of Noggin.

Mutational analysis of BMP-2 has identified A34, H39, S88, L90, and L100 in the knuckle epitope as minor binding determinants for BMPR-II and ActR-II (33). However, no binding hot-spot was found in the knuckle epitope. The central hydrogen bond with type II receptors ActR-II and ActR-IIB can be disrupted in the BMP-2 S88A mutant with minor effects on binding affinity (31). This central H-bond is highly conserved and exists also in the ActA-ActR-IIB contact, which in contrast determines high-affinity binding (31). Remarkably, some BMP-2 mutants at the border of the knuckle epitope exhibit strongly increased affinity specifically for ActR-IIB, e.g. L100K and L100K/N102D (31) or for BMPR-II (E109R) (38). In contrast, other mutations, e.g., BMP-2 A34D, disrupt binding of type II receptors resulting in antagonistic variants (30).

1.6 Modulator proteins of BMP signaling

The BMP signaling is subject to stringent regulation at multiple levels. These include the intracellular modulation, membrane receptor modulation and extracellular modulation (19). Intracellularly, Inhibitory Smads (I-Smads), i.e., Smad6 and Smad7, as intracellular regulators, can antagonize the TGF- β signaling pathway either by interacting with phosphorylated type I receptors and thereby preventing the activation of R-Smads, or through competition with Co-Smads for the formation of the R-Smad/Co-Smad complexes (39). The inhibitory regulation of I-Smads is likely regulated by negative feedback signal from TGF- β superfamily members (40). At the cell surface, pseudoreceptors like Bambi (Bmp and activin membrane-bound inhibitor) can attenuate BMP signaling. The Bambi gene encodes a transmembrane protein highly similar in amino acid sequence to type I serine/threonine kinase receptors in the extracellular domain. However, the Bambi intracellular domain is short and lacks a serine/threonine-kinase domain that is essential for transducing TGF- β signaling (41, 42). Biochemical assays showed that Bambi interacts directly with serine/threonine kinase receptors and antagonizes BMP signaling (41). Finally, a large number of

Introduction

modulator proteins exist in the extracellular space, which inhibit and/or enhance the receptor-mediated activity of BMPs by directly binding to BMPs. These proteins include Noggin, Follistatin, members of the DAN family, Chordin and others (Fig. 1.6).

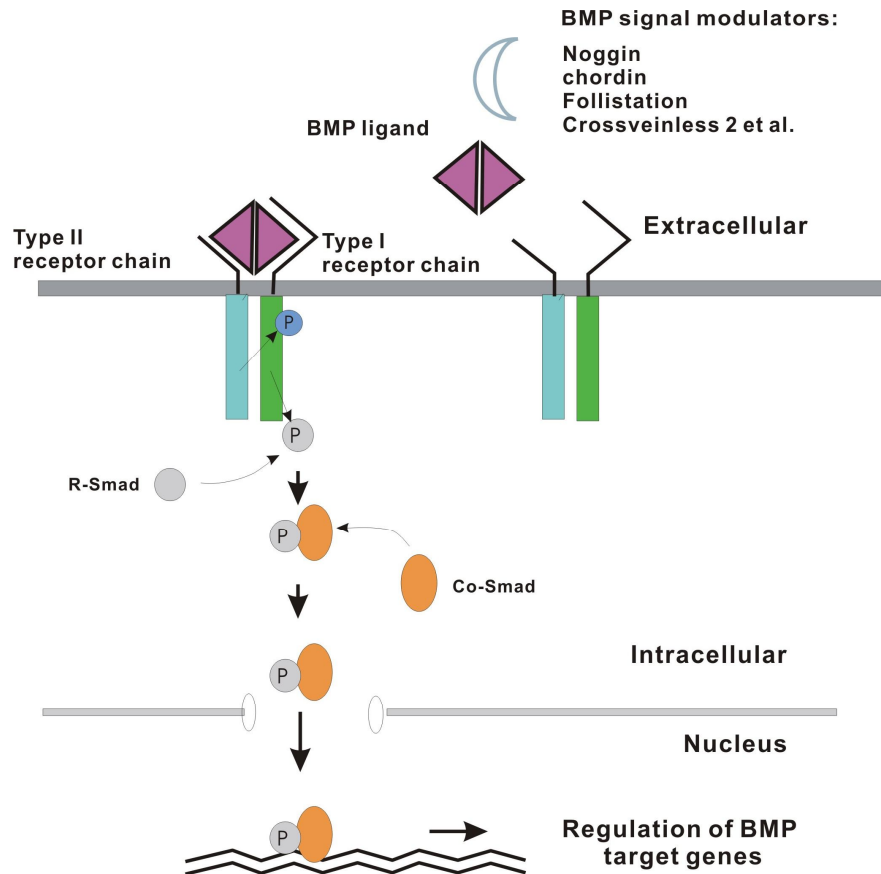


Figure 1.6 BMP signal pathway (modified from Balemans et al.).

1.6.1 Noggin and Follistatin

One of the most investigated BMP extracellular regulators is Noggin. Noggin is expressed during early stages of gastrulation in the Spemann organizer, where it promotes the development of dorsal tissues, such as muscle and nervous tissue (43). Only one single Noggin homolog was identified in the vertebrates, in the zebrafish embryo, where three Noggin isoforms have been isolated, namely Noggin1, Noggin2, and Noggin3. Although the zebrafish Noggin isoforms show different expression

Introduction

patterns, all have dorsalizing activities by antagonizing BMP signaling (44).

Noggin is a secreted and homodimeric protein whose primary structure consists of an acidic aminoterminal region and a cytokine-rich carboxyterminal region containing a cystine knot (45). A central, highly basic heparin-binding segment retains Noggin at the cell surface. Noggin is known to bind BMPs/GDF5 with very high affinity (46, 47), and the binding is almost irreversible due to a slow dissociation rate constant. The crystal structure of Noggin and BMP-7 complex has revealed for the first time how one of the regulators binds to the ligand and prevents it from contacting membrane receptors. It shows that Noggin occupies both two knuckle and two wrist epitopes of the receptor binding sites, and inhibits BMP signaling in this strong manner (Fig. 1.7) (45). Each monomer of Noggin contains an extended N-terminal clip segment of about 20 residues, which wraps around a BMP-7 monomer, directly occupying part of the wrist epitope. A proline residue in this segment, Pro35, fills the BMP-7 hydrophobic pocket that normally accommodates Phe85 in the type I receptor. Interestingly, Noggin contains a cysteine knot topology that is similar to that of BMPs, which suggests that they evolved from a common ancestral gene (45).

The BMP-7 binding affinity of the site-specific variants of Noggin is correlated with alterations in bone formation and apoptosis in chick limb development, showing that Noggin functions by sequestering its ligand in an inactive complex (45). Furthermore, familiar Symphalangism (48) results from the heterozygous mutation P35S in the clip region, confirming the importance of the N terminus of Noggin in vivo.

Introduction

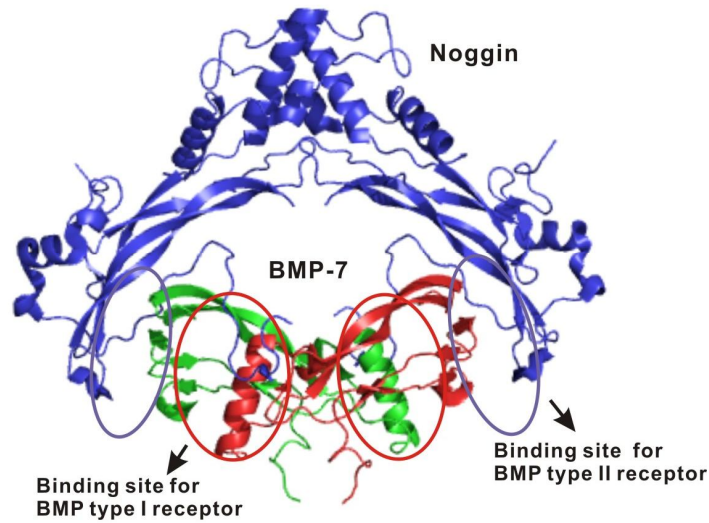


Figure 1.7 Crystal structure of Noggin-BMP-7 complex provides a paradigm for the mechanism of BMP inhibition by a secreted antagonist.

The three-dimensional structure of Noggin-BMP-7 complex provides a paradigm for the mechanism of BMP inhibition by a secreted antagonist. However, for the interaction of BMPs and Noggin the functional epitope(s), i.e. the residues determining binding affinity and specificity, are still poorly understood.

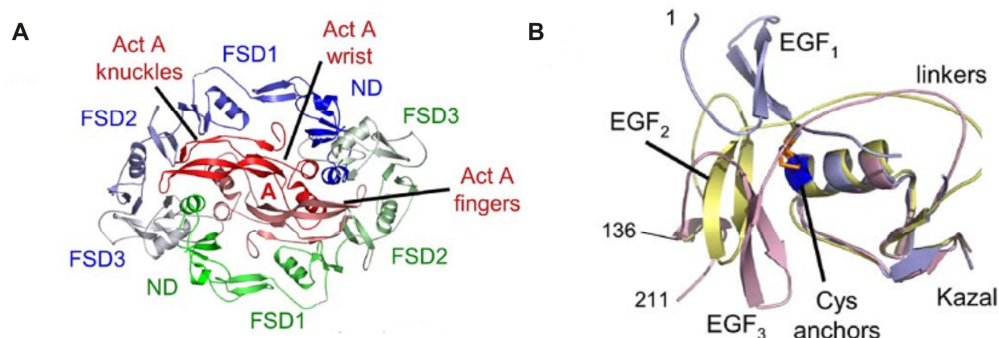


Figure 1.8 Overview of the Follistatin:ActivinA Complex. A, Ribbon diagram of the follistatin:activin complex (topview). B, Overlay of the individual follistatin domains 1-3 using their Kazal-like domains (49).

The crystal structure of Follistatin, another BMPs signal regulator, was also determined (49, 50). In Follistatin-activin complex, two follistatin monomers surround the dimeric ligand and bury the binding sites for type I and type II receptors (Fig. 1.8) (49, 50). Mutational analysis revealed that only residues at the type II

receptor-binding surface of activin are critical for high-affinity follistatin binding, and the interaction surface of activin for type II receptors and follistatin are overlapping but not identical (51). Furthermore, a dissection of the follistatin domain structure revealed that the unique N-terminal Fs0 domain, which as a pseudo type I receptor contacts the wrist epitope of activin, appears to be dispensable for activin interaction (50).

1.6.2 Von Willebrand Factor type C domain (VWC) containing proteins

Among the BMP signaling regulatory members, there is a large number of extracellular regulator proteins that contain von Willebrand factor type C domain (VWC domain, also called cysteine-rich domain, CR domain). The VWC domains have ten cysteins with a conserved spacing pattern: typically with a conserved CXXCXC motif in the middle and a CCXXC motif in the C-terminus. In this nomenclature 'X' can be any amino acid. In addition, a glycine and a tryptophan residue located between the first two cysteins are highly conserved (52, 53). The VWC domains exist in about 500 extracellular proteins from *Drosophila* to human (83 proteins in *Homo sapiens* and 85 proteins in *Mus musculus*) (54). Many VWC-containing proteins act as extracellular modulators in the BMP/TGF- β signaling pathway. They act as an antagonist or agonist of TGF- β signal by binding to a range of TGF- β superfamily members through their VWC domains (55, 56, 57, 58). For instances, one VWC domain-containing protein CTGF (connective tissue growth factor) inhibits BMP signaling, but promotes TGF- β activity (55), while the multi-VWC domain-containing protein Kielin could enhance BMP signaling while suppress TGF- β activation (56, 57, 58).

Numerous extracellular proteins that contain large numbers of VWC domains such as CRIM-1, Kielin/kielin chordin-like protein (KCP), Crossveinless-2 (CV2) and Neuralin/ CHL have been identified (Fig. 1.9). (59, 60, 61, 62, 63). To date, there are

~ 500 proteins containing more than one VWC domains, and some of which have physical interactions with BMPs.

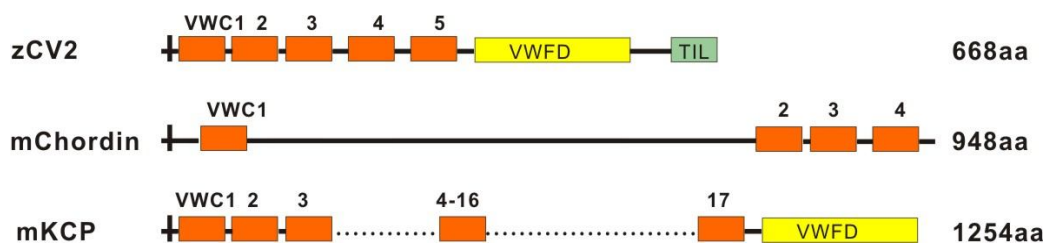


Figure 1.9 Domain compositions of VWC-containing proteins of zebrafish Corssveinless 2 (zCV2), mouse Chordin (mChordin) and mouse Kielin/Kielin Chordin like protein (KCP). The black boxes indicate signal peptide; red boxes indicate Von Willebrand factor type C domain (VWC); green box indicates trypsin inhibitor-like cysteine-rich domain (TIL); yellow boxes indicate Von Willebrand factor type D domain (VWFD).

1.6.2.1 Chordin

Among the increasing number of VWC-containing proteins, one representative is the widely studied Chordin/Sog (the *Drosophila* homology of Chordin). Chordin is a protein of 120 kDa with 4 VWC domains secreted by Spemann's organizer (64). It binds to BMPs in the extracellular space, preventing the interaction of BMPs with their receptors (65). Chordin plays important roles in the dorsalventral patterning determination of the animal embryo (66). The BMP antagonist activity of chordin has been pinpointed to the VWC domains (52, 54).

Chordin mainly acts as an antagonist of BMP signaling by binding to BMPs via its VWC domains, but this could be regulated by Tollid or Tsg. The regulation of Sog/Chordin activity in *Drosophila*, zebrafish, *Xenopus* and mice has been extensively studied, in particularly its inactivation after cleavage by the metalloprotease Xolloid or Tolloid (65, 67, 68, 69). It has been shown that the cleavage of Chordin by Xolloid/Tolloid releases BMP from an inhibitory Sog/Dpp or Chordin/BMP complex. This cleavage occurs at two sites, resulting in proteolytic fragments containing the individual VWC1, VWC4, and a longer product containing both VWC2 and VWC3 (53). The antagonistic activity of Chordin is stringent in the

Introduction

presence of Tsg, through the formation of a Chordin:BMP:Tsg ternary complex. After cleavage of Chordin by Xolloid, BMP is released from chordin, but remains bound to Tsg (BMP:Tsg binary complex). Following this, Tsg dislodges BMP from the Chordin VWC domains, allowing the efficient transfer of BMP to the receptor and signaling (Fig. 1. 10) (70, 71, 72, 73).

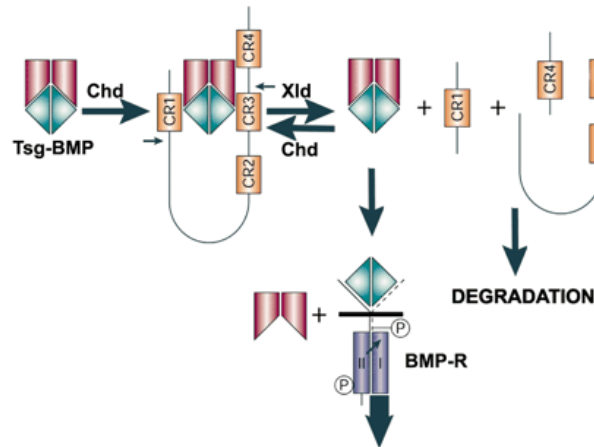


Figure 1.10 Model for a biochemical pathway that regulates BMP signaling in the extracellular space. Tsg-BMP complexes can be bound by full-length Chordin to form a ternary complex that is a potent BMP antagonist. Xolloid cleaves Chordin releasing Tsg-BMP binary complexes and Chordin fragments. In the presence of full-length Chordin, the binary complex will re-bind to Chordin, re-forming the ternary complex. Full-length Chordin is then cleaved by Xolloid. Tsg is able to dislodge BMP from Chordin and to destabilize the Chordin proteolytic products, displacing the equilibrium. This model explains why Tsg has the dual ability to increase BMP antagonism by full-length Chordin and to promote BMP signaling after Xolloid cleavage (from Larrain J et al., 2001).

Shimmi et al (2005) proposed a model for Patterning Dorsal Tissues in the *Drosophila* embryo, where Sog and Tsg play important roles (Fig. 1.11). Homodimers and heterodimers of Dpp and Scw are produced throughout the dorsal domain. Sog is expressed and secreted in the ventral lateral region and diffuses toward the dorsal side. Dpp and Scw homodimers do not bind to Sog and Tsg with high affinity. As a result, they are free to bind with receptors, but they produce only low-level signals that can activate targets such as *pnr*. In contrast, Dpp/Scw heterodimers bind with high affinity to Sog and Tsg. Net flux of the complex toward the dorsal midline leads to an increase in the heterodimer concentration at the midline. Tld processes Sog at the midline to release the ligand, which then binds to a receptor complex containing both Sax and

Introduction

Tkv. This complex produces a synergistic high signal that activates high-level response genes such as *race* and leads to specification of the amnioserosa (74).

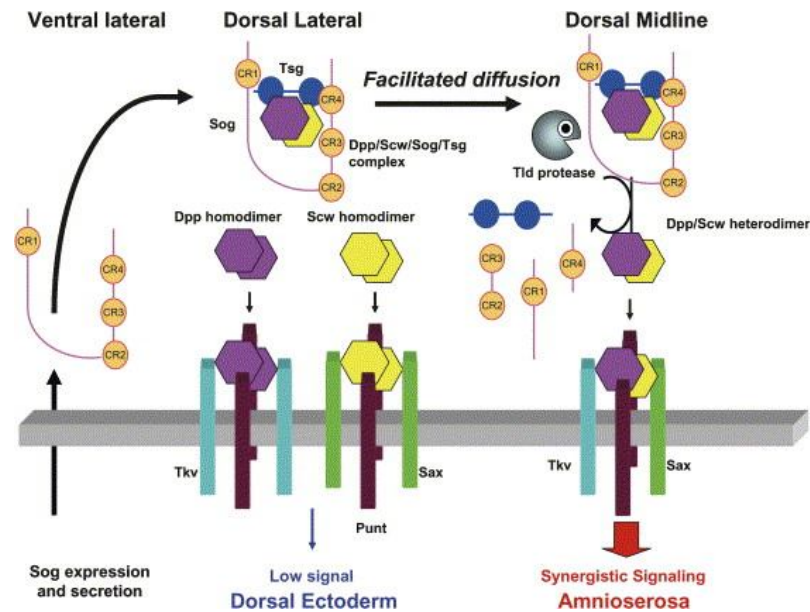


Figure 1.11 Schematic model for Patterning Dorsal Tissues in the *Drosophila* Embryo (from Shimmi et al., 2005).

The binding affinity of chordin VWC domains to BMP-2/-7 and GDF-5 was analyzed (54). VWC1 and VWC3 of chordin were found to bind to BMP-2. However, BMP-7 bound to immobilized VWC1 with an affinity about 5 times higher than that of BMP-2 to VWC1. It bound to VWC3 very weakly but bound to VWC4 with 100-fold higher affinity (23 nM) than that of BMP-2 to VWC4. GDF-5 bound to chordin with a very low affinity (binding affinities for chordin VWC1 and VWC3 are only 180 nM and 1 μ M). No binding was found between chordin VWC2 and BMP-2/-7 or GDF-5. These results suggest that BMP-2 preferentially binds to VWC1 and VWC3 of chordin; BMP-7 binds to VWC1 and VWC4, and GDF-5 binds weakly to chordin and its VWC domains (54).

BMP regulator proteins have different specificities and affinities for BMPs (54). Therefore, different binding epitopes for the modulators may exist in the BMPs. To better understand the regulatory mechanisms of these proteins, it is necessary to know how these binding epitopes are constructed, how they overlap with the

Introduction

receptor-binding wrist and knuckle epitopes, and whether inhibitors could be generated that are specific for each type. Chordin is one of the investigated proteins whose binding epitopes for BMPS are well examined among the BMP regulator proteins.

Binding affinity analysis by biacore showed that many of the knuckle epitope BMP mutants such as A34D, S88P, L90A, V98P, L100P, L100K and L100K/N102D, bound to Chordin with reduced affinity, suggesting that the binding epitopes of BMP-2 for chordin overlap with the knuckle epitope (54). M106A, a BMP wrist epitope mutant, also exhibited 11-fold lower affinity for chordin. M106A has a 100-fold lower affinity for chordin VWC1 than that for the wild type, suggesting that M106 is a hot spot for binding with VWC1. M106A bound to chordin-VWC1 with ten-fold lower affinity than to chordin-VWC3, although the other determinants of the BMP-2 knuckle epitope for chordin-VWC1 and -VWC3 are very similar (54). In general, mutational analysis of BMP-2 predicted an overlapping of the binding epitope for Chordin mainly with the knuckle epitope for type II receptors. However, the reduced binding affinities of chordin to the M106A variant suggest that its binding epitope is also partially overlapping with the wrist epitope.

Co-precipitation experiments showed that chordin competes with type I receptors (BMPR-IA or BMPR-IB) for BMP-4 binding (28, 45). In a Biacore interaction analysis, 100 nM full length Chordin was found to completely inhibit the binding of 50 nM BMP-2 to both immobilized BMPR-IA and ActR-IIB (54). Chordin-VWC1 was able to block the binding of BMP-2 to BMPR-IA and ActR-IIB at high concentration. However, chordin-VWC3 that mainly binds to the knuckle epitope of BMP-2, displays no inhibition on BMP-2/BMPR-IA interaction even with 4 μ M, and it could inhibit BMP-2/ActR-IIB binding by only 50% at this concentration. These results indicate that the single VWC domains are able to inhibit the binding of BMP-2 to type I and/or type II receptor(s) *in vitro* and their inhibitory efficiency correlates with the binding affinities for BMP-2.

Cell culture experiments showed that Chordin inhibited alkaline phosphatase (ALP) activity induced by 10 nM BMP-4 with an IC₅₀ value of about 15 nM (75). However, neither VWC1 nor VWC3 of chordin showed inhibitory activity up to a concentration of 1 μM. Interestingly, the chordin-VWC1 domain, at a concentration of 1 μM, inhibited BMP-2/BMPR-IA and BMP-2/ActR-IIB interactions in an *in vitro* competition experiment, but could not inhibit BMP-2-induced ALP activity at the same concentration (54). Thus, for the single VWC domain the *in vitro* and *in vivo* activities are not strictly correlated. One explanation is the binding affinity of Chordin VWC domains to BMPs is not high enough, therefore no inhibitory activity could be induced in the cell assay.

1.6.2.2 Crossveinless 2

Crossveinless 2, another member of Chordin-like protein family, is an evolutionary conserved extracellular regulator of the Dpp/BMP signaling pathway. CV2 was first detected in *Drosophila* where it is required for signaling of BMP homologs Dpp and Gpp during the formation of cross-veins in the developing wing (76, 77). Accumulating evidence has show that CV2, as a VWC domain-containing protein, plays important roles in embryogenesis, dorsalventral patterning and organogenesis through regulation of BMP signaling (78, 79, 80, 81, 82).

The expression of zebrafish CV2 is correlated with that of BMP, and it is under the positive control of BMP signaling (78). Mouse CV2 is expressed dynamically during development, particularly in areas of high BMP activity such as the posterior primitive streak, ventral tail bud and prevertebral cartilages (79, 83). CV2 +/- knocked-in mice analysis showed that CV2 is expressed in a number of developing skeletal structures and internal organs such as vertebral body and arch, ribs, skull and long bones, lung and kidney during the organogenetic stages (79). CV2 has been identified as BMP-binding endothelial cell precursor-derived regulator (BMPER) which is expressed in flk-1 positive endothelial precursor cells (81). In adult animals CV2 is strongly expressed in the lung, but less in brain and heart. In addition, primary

chondrocytes but not osteoblasts express high levels of CV2 (82).

Like Chordin, CV2 is also a secreted protein and can physically interact with BMPs. CV2 binds BMP-2, BMP-4 and BMP-6/-7 with high affinity but interacts only weakly with GDF-5 (78, 81). The affinity of CV2 binding to BMP members are similar to BMP-2 binding to type I receptor BRIA (34). Both CV2 regulated enhancement and inhibition of BMP signaling have been reported. Loss-of-function analysis of CV2 by morpholino knockdowns show that CV2 acts as a BMP signal-promoting factor during early dorsoventral patterning of zebrafish embryos (78). While gastrulation is normal in CV2 knockout mice, a number of later defects are observed in the development of skeleton, eye and kidney, consistent with the phenotypes that can also be genetically enhanced by the loss of BMP signaling (79). In invertebrates, CV2 was reportedly only required for enhancing BMP signaling during wing vein development (80). Gain of function results are not as clear as that of loss of function, and both pro- and anti- BMP signaling have been described. Microinjection of CV2 mRNA into the *Xenopus* embryo results in the formation of a secondary axis similar to that induced by Noggin and Chordin (80, 81). In cell culture experiments, hCV2 was found to inhibit BMP-dependent Osteoblast and Chondrocyte differentiation (82). Mouse CV2 can reduce activation of the BMP-dependent luciferase reporter (81). These phenotypes could not be only explained by CV2 overexpression, because CV2 could also enhance BMP-4 mediated phosphorylation of Smad1 in cell culture (84); Coinjection of CV2 and BMP-4 mRNA into *Xenopus* animal pole blastomeres synergistically induce the ectopic expression of *xbra.*, which is significantly higher than injection of the same amount of BMP-4 mRNA alone (85).

A processing site (G₃₅₂DPH) is located between the fifth VWC domain and the VWFD domain of full-length zebrafish CV2 (Fig. 1.10) (78, 81), which is also confirmed in *Drosophila* CV2. After the cleavage the N- and C-terminal parts are detected to associate by a disulfide bond, which is likely formed by C383 and C520 in *Drosophila* CV2 (78). The cleavage converts CV2 from a dorsalizing to a ventralizing

Introduction

factor in zebrafish embryos, since injection of CV2-N construct containing VWC domains 1-5 into the zebrafish embryos led to a ventralized phenotype, and the cleavage-resistant mutant (CV2-CM) construct in which the cleavage site was destroyed caused a strong dorsalization. Wild type CV2 can both dorsalize and ventralize, and the effect was similar with the coinjection of CV2-N and CV2-CM (78). Both cleaved and uncleaved CV2 strongly bind BMPs, and the binding was via its N-terminal VWC domain (78). In *Drosophila* the GDPH cleavage of CV2 is not caused by the proposed low pH that can trigger the cleavage occurrence via an autocatalytic process in other secreted proteins (86). Until now, the existence types of CV2 *in vivo* are unclear, but it is possible that the cleavage exists during the embryogenesis, and the proteolytic cleavage is an important regulatory factor for CV2 modulating BMPs signaling. However, it was found that *drosophila* CV2 promoting BMP signaling does not require the cleavage of CV2 (Serpe et al., unpublished).

It is likely that binding to the extracellular matrix for uncleaved CV2 is another factor for its regulation of BMPs signaling. Studies have shown that the uncleaved CV2-CM bound to extracellular matrix (ECM), but the cleaved one did not. CV2 contains 67 basic amino acids as potential binding site for HSPGs. Deletion of 4 amino acids that conforms to a consensus heparin binding sites from mutant CV2-CM reduced the affinity of heparin binding. Injection of this mutant led to a strongly reduced dorsalizing activity compared with CV2-CM (78). The association of BMP modulator proteins Noggin and Chordin with ECM via the HSPG binding have shown an important role in the regulation of BMP signaling (86, 87, 88, 89). Thus, more information is required to understand the effect of heparin binding of CV2.

Introduction

MLCLSPPVTYNLLFWFLILQTPQSTAPLITGTEASCENEGEVLHIPNITDNPCISCCVCLNQ
KAECKOEKCAPLAEDCALVVKOTGACCEKCKGLLKGTSYNSSHHWISPVKPCVTYS
QEGVITEAEMRCVIHCKNPKIHPKKCCPTCPGCIFEGNLYKEDEEFHPEGNPCIKCVCT
GGQSMCHKLVCPVLSCPSHLTHTPPGQCCPRCRGQRRVFDLSPGSCLFHSEVYENGSSIS
YDNCTTCTCVDSTVLCRKRCSPPGSCHGTACCEACQSHLKMEDVKYCRVKSSKIYRDGD
RWSSVNCSLCTCVKGNIQCPKICVPITSCPSNKILNRTGCCPVCTDKPGVCTVFGDPHY
NTFDGRTEFNFGTCKYVLTKDCSPAASFTVLVKNDARRTRSF~~SWTKSVELHTSGLSISLH~~
QH~~LT~~VRQNGTRIALPFHSTGVHIDLDGYLLKLT~~TIAGLEITWDGDSLVEVVAAPHLK~~GQ
L~~CGLCGNYNGQRRD~~SLGGDGQFKFDV~~DELAESWRVEDNELCEVQNR~~RPTSFLCAGT
VKV~~KLRAHRT~~CQKLKSWEFQKCHSAVDFTSFYKSCV~~TDMCECPVHK~~NCFCE~~SFIAYS~~R
AREREGIHVHWRPELTCMSTHCKHGAVYDTCGPGCTKSCHN~~WNEIGPCQR~~PC~~AG~~CHC
PASLVMFQGHCIKPTSCPGR

Figure 1.12 Amino acid sequence of zebrafish CV2. VWC1 domain is shown in red, VWC2 domain is shown in green, VWC3 is shown in blue, VWC4 is shown in purple and VWC5 is shown in gold. All VWC domains are underlined. The c-terminal including VWFD domain and TIL domain are marked in brown colour. The GDPH processing site is underlined.

Other BMP extracellular regulators also contribute to the CV2 regulating mechanism. Another chordin like protein KCP, which containing 17 VWC domains in the mouse protein, can enhance BMPs signaling but reduce TGF- β /Activin signaling. It has overlapping function with CV2 in regards to BMP signaling. KCP knockout mice show no gross structural defects, but are more susceptible to renal interstitial fibrosis, a condition which can be suppressed by enhanced BMP signaling (85). The kidney defects observed in CV2^{-/-} mutants are enhanced by loss of KCP (79).

It is possible that both pro- and anti- BMPs signaling functions of CV2 exist together *in vivo*, and there is a balance between the two functions. The interaction of CV2 with other unknown factors, the heparin binding, the spatial and temporal expression of CV2 should always be considered comprehensively in explaining the mechanism of CV2 regulating BMP signaling.

Crossveinless 2 contains 5 closely spaced VWC domains in the N-terminal segment, a von Willebrand Factor D (VWFD) domain and a trypsin inhibitor-like cysteine-rich (TIL) domain in the C-terminal region (Fig. 1.9). The linkers between 5 VWC

Introduction

domains are very short, varying from 2 to 13 amino acids. Every domain contains 8 or 10 cysteines and the conserved CXXCXC/CCXXC consensus. Each VWC domain of CV2 contains about 50-60 amino acids from the first cysteine to the last cysteine (Fig. 1.12). It has been demonstrated that the BMP binding of CV2 is strictly confined to its VWC1-5 domains (78), therefore, the VWC domain has been taken as the main target of this thesis.

To date, only one structure of the VWC domain has been determined. The solution structure of Collagen IIA (ColIIA) VWC domain exhibits a two subdomain architecture tethered by a flexible linkage (PDB code: 1u5m). The N-terminal subdomain contains a double-stranded anti-parallel β -sheets and a triple stranded anti-parallel β -sheet. The C-terminal subdomain adopts a more irregular structure (Fig. 1.13). In this structure, disulfide bonds were assigned as C1-C4, C2-C8, C3-C5, C6-C9 and C7-C10. This study established for the first time the two-domain architecture of the VWC domain and the similarity of the subdomain 1 of VWC with fibronectin type I (FNI) module (90).

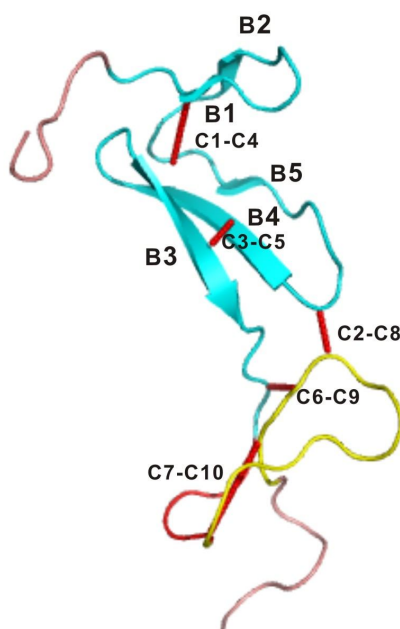


Figure 1.13 Solution Structure of Collagen IIA VWC domain. The N-terminal subdomain is colored blue and C-terminal domain is colored yellow. 5 β -strands and 5 disulfide bonds are marked (modified from O'Leary et al., 2004).

Introduction

However, the VWC protein used for the NMR structure determination does not exhibit the BMP-binding affinity originally claimed for the procollagen VWC domain (90, 52). Thus, it remains uncertain if the NMR structure of Collagen IIA VWC domain represents the functional protein, and it is still unknown if other VWC domains share the similar structure. The binding of CV2 to BMP-2/-7 and GDF-5 occurs via its N-terminal segment containing VWC1-5 (78), although which specific domain(s) are involved is not known.

Hitherto, no three dimensional structure of the complex of BMPs with VWC domains is available. The aim of this thesis was to solve the crystal structure of the complex of BMP-2 and VWC domains, define their binding affinity and specificity, and test the biological relevance of the VWC/BMP interaction, in order to provide a structural basis for the interaction of BMP and VWC domains.

In this thesis, we first present the crystal structure of the BMP-2 and CV2-VWC1 binary complex, and then describe how the binding epitopes of BMP-2 and CV2-VWC1 are constructed, and how they overlap with the receptor-binding wrist and knuckle epitopes.

The structure determined for BMP-2 bound to the VWC1 domain of CV2 provides new and interesting data, which in the future will augment an understanding of the cooperation of BMP-2 and CV2 during animal development. The structural data together with mutational analysis demonstrates a new binding mode for a BMP modulator protein differing from the interaction of BMP-7 and Noggin (44) or Activin and Follistatin (49, 50). These results provide the first paradigm of VWC structure and BMP binding and are likely relevant for the 201 VWC domains present in about 70 other human proteins.

2. Material and methods

2.1 Bacterial strains

Table 2.1: Bacteria stains and their features.

Strain	Genotype	Features
MM 294	F-supE44 hsdR17 endA1 thi-1 lambda	Host for cloning and plasmid propagation (ATCC 39607)
XL1-Blue	recA1 endA1 gyrA96 thi-1 hsdR17 supE44 relA1 lac	Host for cloning and plasmid propagation (Stratagene)
BL21 (DE3)	F- ompT hsdSB (rB- mB-) gal dcm	Host for protein expression with selenomethionine labeling (Novagen)
OrigamiB (DE3)	F- ompT hsdSB(rB- mB-) gal dcm lacY1 aphC (DE3)	Host for protein expression (Novagen)

2.2 Vectors

PET 32a: T7 Promoter; lacI Sequence; Thioredoxin A (N-terminal);
6 x Histidine-tag
Modification: Delete base pairs from 223 to 297 from the original vector (92).

pACGP67B : Polyhedrin promoter; gp67 secretion signal
Modification (By Dr. Joachim Nickel): Add 6 x Histidine-tag and thrombin cleavage sites.

2.3 Oligoes for molecular cloning

Primers of the CV2-VWC domains

Pet-S: CCCGCGAAATTAATACGACTC
VWC1Ws: CTGGTGCCACGCGGTTCTTGGTTAATCACCGGTACAGAG
VWC1Wa: CTCTGTACCGGTGATTAACCAAGAACCGCGTGGCACCAG
VWC1A: CGCGCTCAGCCTATTAACCTTTGCATTTTTCACA

Material and Methods

VWC2S: ATACCATGGCCAAAGGTTGTCTTCTGAAA
VWC2A: CGCGCTCAGCCTATTACCCTGGACATGTAGGGCA
VWC3S: ATACCATGGCCCCAGGGTGCATTTTTGAG
VWC3A: CGCGCTCAGCCTATTAGCTGCCTGGCGATAAGTC
VWC4S: ATACCATGGCCCGGGGTCAGACCAGGGTG
VWC4A: CGCGCTCAGCCTATTATTTACGTCTTCCATCT
VWC5S: ATACCATGGCCCAGTCTCACCTCAAGATG
VWC5A: CGCGCTCAGCCTATTACACGCCTGGCTTGTCAG

Primers of the CV2-VWC1 mutants

VWC1- Δ Clip1Ns: CTGTGCCACGCGGTTCTTGTGAAAACGAGGGAGAA
VWC1- Δ Clip1Na: TTCTCCCTCGTTTTACACAAGAACCGCGTGGCACCAG
L1A1: TGTACCGGTGATTGCCCAAGAACCGCG
L1A2: GTTTTACAGCTAGCCTCTGTACCGGTGATTGCCCA
L1R1: TGTACCGGTGATTCGCCAAGAACCGCG
L1R2: GTTTTACAGCTAGCCTCTGTACCGGTGATTCGCCA
I2A1: CTCTGTACCGGTGGCTAACCAAGAACC
I2A2: CTCGTTTTACAGCTAGCCTCTGTACCGGTGGCTAA
I2R1: CTCTGTACCGGTGCGTAACCAAGAACC
I2R2: CTCGTTTTACAGCTAGCCTCTGTACCGGTGCGTAA
I18As: AAGTGTTACACGCGCCCAACATCACA
I18Aa: TGTGATGTTGGGCGCGTGTAACACTT
I18Rs: AAGTGTTACACCGCCCCAACATCACA
I18Ra: TGTGATGTTGGGGCGGTGTAACACTT
I18Ks: AAGTGTTACACAAGCCCAACATCACA
I18Ka: TGTGATGTTGGGCTTGTGTAACACTT
I18Es: AAGTGTTACACGAGCCCAACATCACA
I18Ea: TGTGATGTTGGGCTCGTGTAACACTT
I21As: ACATCCCCAACGCGACAGACAACCCC

Material and Methods

I21Aa:	GGGGTTGTCTGTGGCGTTGGGGATGT
I21Rs:	ACATCCCCAACCGCACAGACAACCCC
I21Ra:	GGGGTTGTCTGTGCGGTTGGGGATGT
I27As:	ACAACCCCTGCGCGTCCTGCGTCTGT
I27Aa:	ACAGACGCAGGACGCGCAGGGGTTGT
I27Rs:	ACAACCCCTGCCGCTCCTGCGTCTGT
I27Ra:	ACAGACGCAGGAGCGGCAGGGGTTGT
A36Rs:	TGAATCAGAAACGCGAGTGTAAGCAG
A36Ra:	CTGCTTACACTCGCGTTTCTGATTCA

Primers of the CV2-VWC1 mutants for selenomethionine labeling

S28Ms:	ACCCCTGCATCATGTGCGTCTGTCTG
S28Ma:	CAGACAGACGCACATGATGCAGGGGT
N33Ms:	GCGTCTGTCTGATGCAGAAAGCGGAG
N33Ma:	CTCCGCTTTCTGCATCAGACAGACGC
K39Ms:	AAGCGGAGTGTATGCAGGAGAAGTGT
K39Ma:	ACACTTCTCCTGCATACTCCGCTT
E41Ms:	AGTGTAAGCAGATGAAGTGTGCACCG
E41Ma:	CGGTGCACACTTCATCTGCTTACACT

2.4 Solutions

1. **Luria-Bertani Medium (LB medium):** 10 g Tryptone, 5 g Yeast extract, 10 g NaCl in 1 L dH₂O, pH 7.2.

2. **Luria-Bertani-Agar:** LB-medium containing 15 g Agar/L.

Other solutions are listed according to relevant experiments protocols.

2.5 Proteins

BMP-2: Produced by Christian Soeder and Prof. Walter Sebald in the Department of Physiological Chemistry II.

Selenomethionine labelled wide type BMP-2 and BMP-2 (Y41M,Y91M): Prepared by Dionys Weber, Christian Soeder and Prof. Walter Sebald.

CV2 and CV2-N: Prepared by Dr. Jinli Zhang, Nicole Hopf and Prof. Walter Sebald.

GDF-5: Prepared by Dr. Joachim Nickel and Prof. Walter Sebald.

2.6 Molecular biology methods

Standard methods for DNA isolation and manipulation were performed as described in Qiagen manual. Phenol/chloroform extraction and ethanol precipitation were used for purification and concentration of DNA. Quantification of DNA was carried out by using a Bio UV-Visible spectrophotometer at 260 nm as well as by comparing the fluorescent intensity with DNA markers on agarose gels.

2.6.1 Agarose gel electrophoresis of DNA

1.0% - 2.0% (w/v) agarose gels were used to separate DNA fragments. The buffer system was 1 × TAE buffer. The gels were supplemented with the ethidium bromide, detected under the UV light and photographed. Lambda DNA /PstI 24 were used as standard markers. DNA fragments were excised and isolated from agarose gels using gel extraction kit (Promega) according to manual.

2.6.2 Isolation of plasmids from *E. coli*

Buffer 1: 25 mM Tris-Cl pH 8.0, 50 mM Glucose, 10 mM EDTA

Buffer 2: 0.2 M NaOH, 1% (w/v) SDS

Material and Methods

Buffer 3: 3.0 M Kac pH 4.8

TE buffer: 10 mM Tris-Cl, pH 7.5. 1 mM EDTA

5 ml LB-medium was inoculated with a single colony and grown overnight at 37°C, 170 rpm. 4.5 ml of this culture was harvested by centrifugation (15000 rpm, 4°C, and 1 min) and resuspended in 200 µl buffer 1 by vortexing. The suspension was mixed with 300 µl buffer 2 by inversion and incubated on ice for 5 min. Then 300 µl buffer 3 was added and incubated on ice for 5 min. After centrifugation for 10 min (15000 rpm, 4°C), the supernatant was transferred into a fresh eppendorf tube. 300 µl phenol and 300 µl chloroform were added to the supernatant, and centrifuged (15000 rpm, 4°C and 5 min) after mixture. The supernatant was transferred to a new EP tube and mixed with 600 µl chloroform and centrifuged again (15000 rpm, 5 min). After taking away the supernatant, DNA was precipitated by addition of equal volume of isopropanol and centrifugation (15000 rpm, 4°C and 10 min). DNA pellet was washed once with 500 µl 70% ethanol, dried under vacuum and resuspended in 20 µl TE buffer.

All plasmid maximal preparations were carried out with Qiagen Plasmid Midi Kit according to the manual.

2.6.3 Transformation of *E. coli* strains

E. coli competent cells were prepared in the laboratory. XL1-Blue, MM294, Origami (DE3) and BL21 (DE3) cells were transformed by the heat-shock method: 50-100 ng plasmids DNA was mixed with 60-80 µl competent cells previously thawed on ice for approximately 10 min, and incubated on ice for 30 min. Subsequently, the mixture was subjected to heat shock at 42 °C for 90 seconds and put back on ice for 2 min. 800 µl LB medium without antibiotics was added and the mixture was incubated at 37°C for 60 min. After centrifugation at 4000 rpm for 5 min, 600-700 µl of supernatant was discarded, and bacteria resuspended in the remaining LB were plated

onto a selective LB plate and incubated overnight at 37 °C.

2.6.4 Determination of DNA concentration and purity

The concentration and the purity of double stranded plasmid DNA were determined based on the Beer-Lambert Law by measuring absorbance at 260 nm and 280 nm:

$$A_{260} = \epsilon_{260} c l \text{ and } A_{260} \times 50 = \mu\text{g/ml (when } l = 1 \text{ cm)}$$

A_{260} is the absorbance at 260 nm, ϵ_{260} is the molar absorption coefficient, c is the molar concentration and l is the optical path. For a protein-free and RNA-free solution of DNA the ratio of A_{260}/A_{280} should be close to 2. Protein contaminants would reduce the ratio, whereas RNA contamination would increase it. To further estimate the concentration and purity of DNA preparations, agarose gel electrophoresis was carried out.

2.6.5 Molecular cloning of VWC domains and mutants

2.6.5.1 Cloning of CV2-VWC domains

cDNA of VWC1 amplified by recombinant PCR was inserted into the modified pET32a vector at XbaI and Bpu1102I sites (Fig. 2.1A). Other VWC domains were cloned into plasmid pET32a at NcoI and Bpu1102I sites (Fig. 2.1B). Plasmids containing VWC domains were transformed into MM294 for plasmid propagation. DNA minimal preparation followed by enzyme digestion was performed to select the positive clones. DNA maximal preparation was used to isolate plasmid DNA for sequencing (performed by the Department of Humangenetic, Biocenter of the University of Wuerzburg). Positive plasmids were transformed into host cell Origami (DE3) for protein expression.

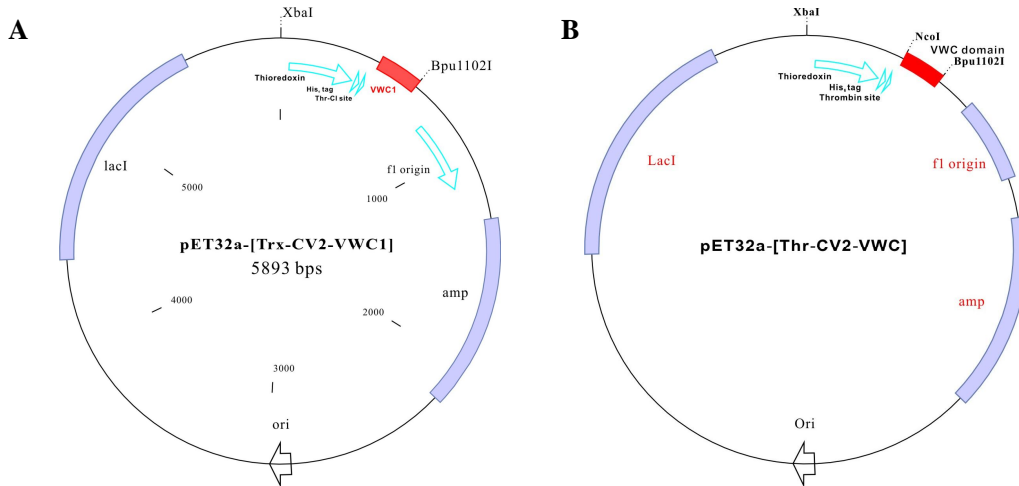


Figure 2.1. **A:** Expression vector of pET32a-[Thr-CV2-VWC1] **B:** Expression vector of pET32a-[Thr-CV2-VWC] domains.

2.6.5.2 Cloning of CV2-VWC1 mutants

PCR products of CV2-VWC1 mutants were amplified by recombinant method and cloned into pET32a at NcoI and Bpu1102I sites (Fig. 2.2). Clones were transformed into MM294 for DNA propagation. Positive clones were transformed into Origami (DE3) for protein expression.

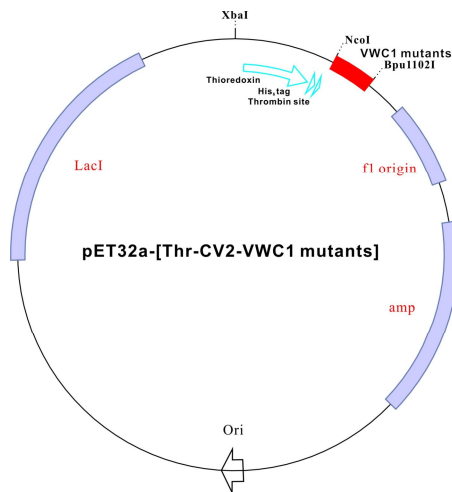


Figure 2.2. Expression vector of pET32a-[Thr-CV2-VWC1] mutants.

2.6.5.3 Cloning of multi-VWC fragments

Multi-VWC fragments were amplified by recombinant PCR and cloned to pACGP67b/TH transfer vector at EcoRV and BamHI sites. Clones were co-transfected with BaculoGold DNA into SF9 cells for protein expression.

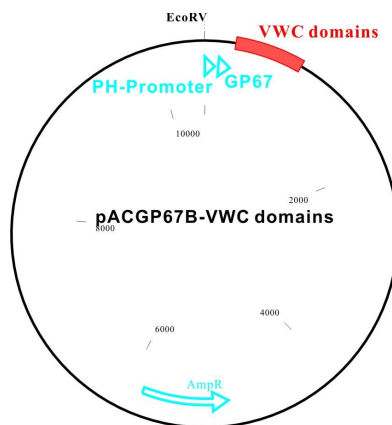


Figure 2.3 Map of the transfer vector of pACGP67B containing CV2-VWC domains.

2.7 Expression of proteins

2.7.1 Expression of thioredoxin fusion proteins in TB-Medium

TB-Medium: 13.3 g/l Tryptone; 26.6 g/l Yeast Extract; 4.4 ml/l Glycerin

80 ml 10 × Pi added to 720 ml TB-Medium before use

10x Pi: 0.17 M KH_2PO_4 , 0.72 M K_2HPO_4

Wash buffer: 20 mM Tris/HCl; pH 7.5; 150 mM NaCl

A single clone was inoculated into 2 ml TB medium containing appropriate antibiotics and grown at 37°C for 8 h. This pre-culture was used to inoculate a new 120 ml TB culture which was left to grow at 37°C for 15-17 h. Bacteria from 40 ml cultures was added to 800 ml TB medium, which were shaken at 30°C, 150 rpm, until they reached an OD_{600} of 0.6. 0.8 ml of 1 M IPTG was added for protein induction, and the cultures were left to grow for 15 h-17 h at 20°C, 120 rpm. The bacteria were then harvested by

Material and Methods

centrifugation at 4°C for 10 min, 6000 rpm, and washed by resuspension in the wash buffer followed by centrifugation. The bacteria pellets were stored at –20°C until next step.

2.7.2 Expression of ¹⁵N labelled and ¹⁵N¹³C labelled thioredoxin fusion CV2-VWC1

M9 minimal medium:

10× M9: 60 g Na₂HPO₄; 30 g KH₂PO₄; 5 g NaCl; add 1000 ml dH₂O; pH 7.2 – 7.4; autoclaved

1000x MgSO₄: 1 M MgSO₄ x 7 H₂O; autoclaved

1000x CaCl₂: 1 M CaCl₂ x 2 H₂O; autoclaved

100x

Trace elements: 5 g EDTA; 0.8 g FeCl₃; 0.05 g ZnCl₂; 0.01 g CuSO₄; 0.01 g CoCl₂; 0.01 g H₃BO₃; 1.6 g MnCl₂ x 6 H₂O; 0.01 g Na₂MoO₄ x 2 H₂O; adjust to 1000 ml, pH 8.0; sterile filtration, dark kept

100x Glucose: 40 g Glucose/100 ml dH₂O; sterile filtration

100x¹³C-Glucose: Powder

1000x Thiamin: 50 mg Thiamin HCl/ml dH₂O; Freshly prepared, sterile filtration, freshly use

500x ¹⁵N-NH₄Cl: 0.25 g ¹⁵N-NH₄Cl/ml dH₂O

E. coli strain BL21 (DE3) was used for the expression of ¹⁵N-labelled thioredoxin-fusion VWC1. A single clone was inoculated into 2 ml LB medium containing ampicillin (100 mg/L) for 8 h at 37°C, 170rpm. After culture, the 2 ml LB medium was transferred to 120 ml ¹⁵N-labelled M9 minimal medium with ampicillin (100 mg/L), and cultures were grown at 37°C for 15-17 h. 40 ml bacteria from them was added to 800 ml ¹⁵N-labelled M9 minimal medium containing ampicillin (100 mg/L) and the cultures were shaken at 30°C, 150 rpm. When OD₆₀₀ reached 0.6, 0.8

Material and Methods

ml of 1 M IPTG was added to the medium to induce the protein expression. The culture was grown at 20°C, 120 rpm, for 15 h-17 h. Bacteria were harvested by centrifugation (10 min, 6000 rpm) and washed by resuspension in the wash buffer followed by centrifugation. The bacteria pellets were stored at -20°C until next step. The expression of ¹⁵N¹³C-labelled fusion protein Thr-CV2-VWC1 was performed similar to the expression of ¹⁵N-labelled protein, except that 0.8g ¹³C-Glucose was added to the ¹⁵N-labelled M9 minimal medium without Glucose 10 min later after the adding of 1M IPTG.

2.7.3 Selenomethionine labelled thioredoxin fusion CV2-VWC1 and mutants

Selenomethionine labelled thioredoxin fusion CV2-VWC1 and mutants were expressed in the *E. coli* strain BL21 (DE3). A single clone incubated in 2 ml LB medium containing ampicillin (100 mg/L) was grown at 37°C 170 rpm, for 6 h, and then transferred to 120 ml M9 minimal medium containing ampicillin (100 mg/L), which was shaken at 37°C, 120 rpm for 15-17 h. 40 ml medium from the cultures was added to 800 ml M9 minimal medium containing ampicillin (100 mg/L), shaken at 30°C, 150 rpm until its OD₆₀₀ reached to 0.4. At this point Selenomethionine (50 mg) along with lysinehydrochloride (100 mg), threonine (100 mg) phenylalanine (100 mg), leucine (50 mg) isoleucine (50 mg) and valine (50 mg) were added as solide. After about 1 h of shaking, 0.8 ml 1 M IPTG was added, and the cultures were grown with shaking at 20°C 120 rpm, for 15-17 h. The bacteria were harvested by centrifugation at 4°C for 10 min, 6000 rpm (JA-30), and washed by resuspension with wash buffer followed by centrifugation. The bacteria pellets were stored at -20°C until next step. The percentage of incorporation of selenomethionine was determined by mass spectrometry.

2.7.4 Expression of proteins in SF9 cells

The plasmid cDNA encoding target proteins was cotransfected into SF9 cells according to Co-transfection method. Then Plaque-assay was performed according to standard method to get single virus clone.

Single virus clones were picked up with 100 ul pipette tips, transferred into 1 ml cell culture medium and incubated at 27°C for 1h. Then the mediums containing virus were subjected to centrifugation at 1000 rpm for 5 min at RT to remove the agarose debris. The supernatants were planted to a 6-well plate with each well having 1.5×10^6 SF9 cells, then the plate was incubated at 27°C for 4 days for the first virus amplification.

The virus solution from the first virus amplification was centrifugated at 1000 rpm for 5 min at RT, and then the supernatant was planted to a 6-well plate with each well having 1.5×10^6 SF9 cells and 1 ml medium. The plate was incubated at 27°C for 4 days for the second virus amplification. 4 days later, 10 ul virus solution was taken from every well and subjected to western blot to test positive expression.

The positive virus solution from the secondary amplification was centrifugated at 1000 rpm for 5 min at RT, and then the 2 ml supernatant was added to flasks (175 cm²) with 80% SF9 cells confluence in 35 ml medium. Subsequently the flasks were incubated at 27°C for 4 days for the fourth virus amplification. 4 days later, the virus titers were determined by Plaque-assay to ensure that the titers were above 5×10^7 virus/ml.

After the fourth virus amplifications, 10-20 ml high titer virus solution containing at least 9×10^8 virus was added to roller-bottle having 200 ml medium with 1.5×10^6 cells/ml, which was incubated at 27°C for 4 days for protein expression.

Material and Methods

Co-transfection:

When grew to 90% confluence, the SF9 cells were suspended by hand-shake in new medium and adjusted to a cell density of 0.8×10^6 cells/ml. 1 ml cell-suspension was transferred to each well of a 6-well plate and supplemented with additional 1 ml SF9 medium. The plate was incubated for 1 h at 27°C to let cells attach to the surface of the plate. Afterwards, the medium was removed from the wells and 500 ul transfer buffer A was added to each wells. DNA mixture was prepared by mixing 1.5 ug recombinant plasmid with 2.5 ul Baculo-Gold DNA and incubating it at 20°C for 5 min, and then adding 500 ul transfer buffer B. The mixture was slowly pipetted to the cells, and was incubated for 4 h at 27°C. Then the cells was washed for 2 times with 1.5 ml SF9 cell medium, and then incubated cells for 4-5 days at 27°C.

Plaque-assay:

After grown to 90% confluence, the SF9 cells were suspended by hand-shake in new medium and adjusted to a density of 0.8×10^6 cells/ml. 1 ml cell suspension was added to every well of a 6-well plate and supplemented with additional 1 ml SF9 medium. Afterwards the plate was incubated for 1h at 27°C. During this period, the virus solution was collected from the co-transfection experiment and diluted stepwise into different concentrations: 10^{-1} , 10^{-2} , 10^{-3} , 10^{-4} , 10^{-5} , 10^{-6} , 10^{-7} , and 10^{-8} . Then the medium from the 6-well plate was removed and the virus dilution (10^{-3} , 10^{-4} , 10^{-5} and 10^{-6}) was added to each well of the plate and incubated at 27°C for 1h. After 1h, the medium was removed and 1.5 ml agarose mixture, which was freshly prepared by mixing 3.5 ml 2.7 % agarose with 700 ul fetal calf serum and 6.6 ml 2×Xpress medium, was added to every well of the plate. Following the solidification of the agarose, the plate was wrapped with parafilm and stored it on top of wet papers, and lay inside a box at 27°C for 5 days.

2.8 Purification of proteins

2.8.1 Bacteria sonication

Sonication buffer: 20 mM Tris/HCl; pH 7.9; 500 mM NaCl; 5 mM Imidazol
1 mM PMSF

Ultrasonic: System 585, Ultratransducer 512/1204 (KLM)

Super centrifuge: Super centrifuge L8-70M, 45Ti-Roter (Beckman)

8-12 g bacteria stored at -20°C was defrosted in 4°C and resuspended in 200 ml sonication buffer. Sonication was performed for 30 s at 300 W for 10 times in a glass cup with a 10 min-cooling interval. Afterwards solution was centrifugated at 30,000 for 30 min at 18°C. The resultant supernatant containing soluble thioredoxin fusion protein was collected for the Ni-chelating chromatography.

2.8.2 Nickel-chelating chromatography

Loading buffer: 20 mM Tris/HCl; pH 7.9, 500 mM NaCl, 5 mM Imidazole

Wash buffer: 20 mM Tris/HCl; pH 7.9, 500 mM NaCl, 60 mM Imidazole

Elution buffer: 20 mM Tris/HCl; pH 7.9, 500 mM NaCl, 500 mM Imidazole

Precolumn material: Sephacryl S-100 (Pharmacia)

Column material: Chelating Sepharose FF (Pharmacia)

Pump: Minipuls 3 (Gilson)

Detector: 2238 Uvicord II (LKB Bromma)

The Ni-chelating column was stored in 250 mM EDTA at 4 °C. Before use, the column was washed by 100 ml ddH₂O to remove the EDTA, and then 100 ml 50 mM NiCl₂-solution was loaded to it followed by an equilibration with 100 ml loading buffer. The supernatant was load through a connected precolumn to the Ni-chelating

Material and Methods

column. Afterwards the column was first washed with loading buffer, followed by wash buffer to remove the contaminated proteins from *E. coli*. Proteins bound to the column were eluted by elution buffer and collected every 7 min for 1 fraction in a collector. The Ni-chelating column was washed with 250 mM EDTA to remove the Nickel-ions. Proteins collected from every fraction were analysed in a SDS-PAGE and dialysed against 5 L buffer for Thrombin cleavage at 4 °C.

2.8.3 Ni-NTA chromatography

Loading and Wash buffer: 50 mM NaH₂PO₄, pH 8.3, 10 mM Imidazol, 300 mM NaCl

Elution buffer: 50 mM NaH₂PO₄, pH 8.3, 300 mM Imidazol, 300 mM NaCl

Cell suspension was centrifugated at 10000 rpm for 15 min (GSA-10a, 4 °C). The supernatant was dialysed for two times against 10-fold volumes of loading buffer at 4 °C for 6-8 h. The supernatant was centrifugated again after dialysis at 10000 rpm for 15 min (GSA-10a, 4 °C). 5 ml Ni-NTA resin was equilibrated by wash buffer, mixed with the supernatant and then stirred for 1h at 4 °C. Mixture was transferred to the column cartridge and washed with 5 beads volumes wash buffer. Proteins bound to the Ni-NTA column were eluted with about 50 ml elution buffer.

2.8.4 Anion and cation exchange chromatography

Loading buffer: 20 mM Tris/HCl, pH 7.4

Elution buffer: 20 mM Tris/HCl, pH 7.4; 1 M NaCl

Column material: Fractogel EMD TMAE 650 (S) (Merck, Darmstadt)
SP-sepharose (Merck, Darmstadt)

Column: Super performance 10 (Merck, Darmstadt)

Pump: L6200 intelligent pump (Merck/Hitachi)

Detector: L-4200 UV-VIS (Merck/Hitachi)

Collector: FC 203B (Gilson)

Material and Methods

Protein separation by ion exchange chromatography depends on the reversible adsorption of charged molecules to an immobilized ion exchange group of opposite charge. Various conditions such as ionic strength and pH could influence these interactions. To ensure electrostatic binding, the total ionic strength needs to be low.

The columns for anion exchange chromatography or cation exchange chromatography were equilibrated with 5 column volumes of loading buffer. Then the sample was loaded (flow rate 1.5 ml/min) and washed until baseline was reached in the recorder. The elution was performed with a linear gradient of NaCl concentration (flow rate 1 ml/min) as shown in Table 2.2. Proteins were collected in a way of tube/1.5 min. Eluted fractions containing the protein of interest were pooled. CV2-VWC1 was purified by TMAE column, and the other four VWC domains were purified by SP-sepharose column.

Table 2.2 Purification procedure of CV2-VWC domains by TMAE column or Sp-sepharose column.

CV2-VWC1		CV2-VWC2		CV2-VWC3		CV2-VWC4		CV2-VWC5	
T(min)	C _{NaCl} (mM)	T(min)	C _{NaCl} (mM)	T(min)	C _{NaCl} (mM)	T(min)	C _{NaCl} (mM)	T(min)	C _{NaCl} (mM)
0	0	0	0	0	0	0	0	0	0
40	250	20	300	10	150	10	150	60	350
50	1000	80	600	70	500	70	500	70	1000
60	1000	90	1000	80	1000	80	1000	80	1000
70	0	100	0	90	0	90	0	90	0

2.8.5 High Performance Liquid Chromatography (HPLC)

Loading buffer:	0.1 % (v/v) TFA in ddH ₂ O
Elution buffer:	100 % Acetonitrile (ACN)
Analytic column:	Vydac-214TP; C4; 10 μ M; 46 x 250 cm (MZ-Analysentechnik)
Semiprep column:	Vydac-214TP; C4; 10 μ M; 80 x 250 cm (MZ-Analysentechnik)
Pump:	L6200 intelligent pump (Merck/Hitachi)
Detector:	L-4200 UV-VIS (Merck/Hitachi)
Collector:	FC 203B (Gilson)

Material and Methods

The capacity of the analytic HPLC column is maximal 2 mg protein, and maximal 30 mg protein for the semiprep column. Columns were first washed with 100% Acetonitrile, and then equilibrated with 0.1 % TFA buffer. The sample was mixed in a ratio of 1:1 with 0.1% TFA to make the pH value less than 4.0. After loading the samples, the column was washed until baseline was reached in the recorder. The elution was performed with a linear gradient of ACN concentration (flow rate 0.7 ml/min for analytic column and 2 mg/ml for the semiprep column). VWC domains were eluted at 26% -27% Acetonitrile (Table 2.3).

Table 2.3 Gradients of reverse phase HPLC in analytic and semiprep column.

Analytic Flow rate 0.7 ml/min Fraction 1.4 ml		Semiprep Flow rate 2 ml/min Fraction 1.4 ml	
Time(min)	% Acetonitrile	Time(min)	% Acetonitrile
0	0	0	0
5	25	5	25
40	30	40	30
50	100	50	100
100	100	100	100

2.8.6 Gel filtration chromatography

Loading buffer: 10 mM HEPES, pH 7.4; 700 mM NaCl
Column material: Superdex 200 HR 10/30 (Pharmacia)
Pump: L6200 intelligent pump (Merck/Hitachi)
Detector: L-4200 UV-VIS (Merck/Hitachi)
Collector: FC 203B (Gilson)

On a gel filtration (or size exclusion) column the molecules are separated based on the differences of their sizes. Column was equilibrated with two column volumes (50 ml) loading buffer and the concentrated protein solution (less than 500 μ l) was injected

Material and Methods

into a 10 ml loop with an injection needle (Rothe). Flow rate was 0.5 ml/min and fractions were collected 1 tube/min. Small molecules that can diffuse into the pores of the gel beads are delayed in their passage through the column in contrast to the larger molecules, which cannot diffuse into the gel beads. The larger molecules thus leave the column first, followed by the smaller ones in order of their sizes. Gel filtration was performed with a Superdex 200 HR 10/30 column (Pharmacia).

2.8.7 Calibration of the superdex 200 column

Calibration of Superdex 200 HR 10/30 allows the estimation of protein molecular weights to obtain a calibration curve. The eluant was monitored by a UV detector at a wavelength of 280 nm. Bovine serum albumin (66.4 kDa), Ovalbumin (43 kDa) and Ribonuclease A (13.7 kDa) were used to calibrate the column.

The void volume of the column was determined using Blue Dextran 2000. The K_{av} for individual protein was calculated as follows:

$$K_{av} = (V_R - V_0)/(V_c - V_0)$$

V_0 = void volume of the column

V_R = retention volume of the protein

V_c = the geometric bed volume in ml.

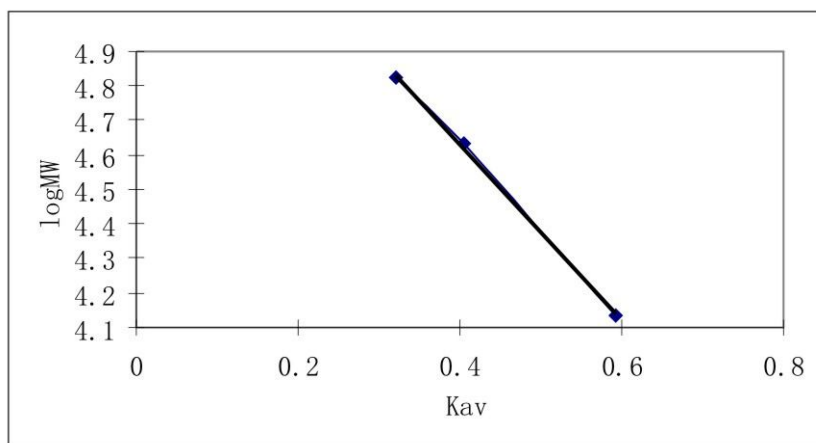


Figure 2.4 Calibration curve of superdex 200 HR 10/30 column.

A plot of K_{av} versus $\log MW$ for a standard run resulted in a straight line with a correlation coefficient $R^2 = 0.99$ (Fig 2.4). Linear regression gave the equation $\log MW = -2.5524 \times K_{av} + 5.6528$. This equation was used to calculate the apparent molecular weight of the proteins separated by the column.

2.8.8 BMP-2 affinity chromatography

Running buffer:	10 mM Hepes pH 7.5, 500 mM NaCl
Elution buffer:	4 M $MgCl_2$
Column keeping buffer:	10 mM Hepes pH 7.5, 150 mM NaCl
Column material:	20 mg BMP-2 bound to 10 mg Cyanbromid-activated Sepharose (Pharmingen)
Pump:	Minipuls 3 (Gilson)
Detector:	2238 Uvicord II (LKB Bromma)

The whole procedure was performed at 4 °C. Proteins were separated based on their interaction with BMP-2 proteins. Proteins that had no binding for BMP-2 flew through BMP-2 affinity column and were separated from proteins binding to the column. The BMP-2 column was first equilibrated with 5 column volumes loading buffer (HBS_{500}), then the sample was loaded and washed until baseline reached in the recorder to make sure proteins unspecifically bound to the column flew through it.

Material and Methods

Afterwards elution step was performed with 4 M MgCl₂ with a collected fraction of tube/6 min. After the elution, the BMP-2 affinity column was washed by 10 mM Hepes pH 7.5, 150 mM NaCl buffer to get rid of MgCl₂, and kept at 4°C.

2.9 Thrombin cleavage

Buffer for thrombin cleavage: 50 mM Tris/HCl pH 7.5; 150 mM NaCl, 2.5 mM CaCl₂

Thrombin solution: 8.0 g thrombin (Sigma), 600 ul buffer for thrombin-cleavage, 600 ul Glycerine

Thioredoxin-fusion proteins were dialysed against the thrombin cleavage buffer overnight and centrifuged at 4°C, 5000 rpm for 10 min. Thrombin was then added (2-4 ug of thrombin per mg fusion protein) and the cleavage was performed at 30°C for 3 h. Centrifugation was performed afterwards to remove the precipitant proteins.

2.10 Protein chemistry methods

2.10.1 Proteins marker (Biofermentas):

Protein name	Molecular Weight (in kDa)	[$\mu\text{g}/5\mu\text{l}$]
Phosphorylase b:	97	0,67
Albumin:	66	0,83
Ovalbumin:	45	1,47
Carbon Anhydrase:	30	0,83
Trypsin Inhibitor:	20.1	0,80
Lactalbumin:	14.4	1,16

2.10.2 SDS-Polyacrylamid-Gelelektrophorese (SDS-PAGE)

AA/BAA-solution:	30% Acrylamide; 1% N,N'-Methylenbisacrylamide
4X Lower Tris:	1.5 M Tris/HCl; pH 8.8; 0.4% SDS
4X Upper Tris:	0.5 M Tris/HCl; pH 6.8; 0.3% SDS
SDS-Running bufferr:	25 mM Tris/HCl; pH 8.6; 0.19 M Glycin; 0.15% SDS
SDS-Loading buffer:	62.5 mM Tris/HCl; pH 6.8; 2% SDS; 20% Glycerin; 2% Bromophenol blue in H ₂ O; (for reduced conditions: add 2% 2-Mercaptoethanol)

Table 2.4 is a summary of the solutions for one SDS-PAGE gel. After adding the separating gel, 1.5-2 cm space was filled with H₂O. When the separating gel was solid, the water was suck out and stacking gel was filled. Protein samples were diluted 1:1 with SDS-PAGE loading buffer, and heated for 3 min at 100 °C. Electrophoresis was carried out at 175 V and maximal 35 mA in SDS-PAGE running buffer.

Material and Methods

Table 2.4: Solutions for preparing SDS-PAGE gel.

	Separating gel 12%	Stacking gel 5%
AA/BAA	4.0 ml	0.2 ml
4 × Upper Tris		0.5 ml
4 × Lower Tris	2.5 ml	
H ₂ O	1.5 ml	1.3 ml
Glycerin	2.0 ml	
40%APS	12 ul	6 ul
TEMED	12 ul	6 ul

2.10.3 Coomassie Brilliant Blue staining

Coomassie Brilliant Blue staining solution:

6.25 g Coomassie Brilliant Blue R250; 0.25 L Acetic acid; 1L Methanol; 1.25L dH₂O

Destaining buffer: Isopropanol: Acetic acid: dH₂O 1:1:8

Protein fixing buffer: 30% methanol.

The gels were stained in Coomassie Brilliant Blue R250 solution for 20 min on a shaking platform. Next, the gels were destained in the destaining solution. For long time storage, the gels after destained were incubated in 30% methanol for a minimum of 20 min and sealed with 2 layers Cell membranes and kept at room temperature.

2.10.4 Silver staining

Solution 1: 50% (v/v) acetone in dH₂O; 0.75 ml 50% (w/v) TCA in dH₂O;
12.5 µl 37% Formaldehyde.

Solution 2: 30 ml 50% (v/v) Aceton in dH₂O

Solution 3: 50 µl 10% (w/v) Na₂S₂O₃ • 5 H₂O in dH₂O; 30 ml dH₂O

Solution 4: 0.4 ml 20% AgNO₃ in dH₂O; 0.3 ml 37% Formaldehyde; 30 ml dH₂O

Material and Methods

- Solution 5: 0.6 g Na_2CO_3 ; 12.5 μl 37 % Formaldehyd; 12.5 μl 10 % (w/v) $\text{Na}_2\text{S}_2\text{O}_3 \cdot 5 \text{H}_2\text{O}$; 30 ml dH_2O
- Solution 6: 1% (v/v) Glacial Acetic Acid

One gel was incubated in solution 1 for 5 min and washed 3 times with water, and then put to solution 2 for 5 min and then solution 3 for 1 min. Subsequently put the gel to solution 4 for 8 min after washed 3 times in H_2O . After washing, put gel to solution 5 for about 30 seconds for staining, and then transfer solution 6 to solution 5 to stop the staining. Wash the gel again with water and put to 30% methanol for keeping.

2.10.5 Concentrating the protein solution

The protein solutions were concentrated using the Amicon[®] Ultra-4 Centrifugal Filter Units (Millipore). In this device, a membrane with a molecular weight cut-off lower than that of the interested protein is placed at the bottom of a cell, which is filled with the protein solution. The cell is then placed in a 15 ml falcon tube and centrifuged at less than 4000 rpm. In this manner, the flow-through solution contains only lower molecular weight components, while the protein is concentrated in the chamber.

2.10.6 Determination of the protein concentration

We used measurement of UV absorbance at 280 nm to determine protein concentration. Quartz cuvetts or cuvettes that are known to be transparent to 280 nm, filled with a volume of solution sufficient to cover the aperture through which the light beam passes. The protein solution must be diluted in the buffer to a concentration that is well within the accurate range of the instrument. The protein solution to be measured can be in a wide range of buffers. At low concentrations, protein can be lost from solution by adsorption on the cuvette; the high ionic strength helps to prevent this. The value obtained will depend on the path length of the cuvet.

If not 1 cm, it must be adjusted by the appropriate factor. The Beer-Lambert law states that: A (Absorbance) = $\hat{E} \cdot c \cdot l$

where \hat{E} = extinction coefficient, c = concentration in mol/L and l = optical path length in cm. Therefore, if \hat{E} is known, measurement of A gives the concentration directly, e is normally quoted for a 1-cm path length.

2.10.7 Biosensor interaction analysis

System: Biosensor BIAcore 2000TM (BIAcore)

HBS –Puffer: 10 mM HEPES, pH 7.4; 500 mM NaCl; 3.4 mM EDTA, 0.05% P20

The BIAcore 2000 system (Amersham Biosciences) was used for all biosensor experiments in this thesis. A CM5 biosensor chip was first loaded with streptavidin in flow cells 1, 2, 3 and 4, and subsequently biotinylated proteins were immobilized at the streptavidin matrix of flow cell 2, 3 and 4 at a density of about 200 resonance units (RU) or 400-600 RU depending on the affinity of the interaction. The proteins for perfusion were diluted with HBS running buffer (10 mM HEPES, pH 7.4/500 mM NaCl/3.4 mM EDTA/0.005% surfactant P20) and applied at concentrations between 10 and 1000 nM. Flow rates were set to $10 \mu\text{l}\cdot\text{min}^{-1}$ at 25°C , flow path was 1-2-3-4, and data were recorded at 2.5 Hz. Sensorgrams were evaluated on the basis of a 1:1 association model according to fitting routines 2 or 3 provided by the BIA evaluation 2.1 software (Amersham Biosciences). For dissociation constants (K_D) < 50 nM, kinetic constants (k_{on} and k_{off}) were evaluated. For K_D values > 50 nM, dose-dependent equilibrium binding was evaluated. K_D values or rate constants $k_{\text{off}}/k_{\text{on}}$ was evaluated from one experiment determined for 6 to 9 different concentrations of the analytes. Mean values of K_D and their standard deviations (SD) were calculated from the values of at least three different experiments. Standard deviations for the obtained affinities were less than 50%. For the comparison of the wt CV2-VWC1 and mutants, differences between mean values of more than $2 \times \text{SD}$ were considered significant. All Biosensor interaction analysis was performed by Dr. Jinli Zhang.

2.10.8 Mass spectrometry

All mass spectrometry analysis of proteins performed with Electrospray Ionization Fourier Transform Ion Cyclotron Resonance Mass Spectrometry (ESI-FTICR-MS) by Dr. Werner Schmitz. Mass spectrometry analysis was used to determine the molecular weights of stable fragment of CV2-VWC1 and selenomethionine-labelled proteins.

2.10.9 Western blotting

Transfer buffer:	25 mM Tris/HCl, 200 mM Glycine, 10% methanol
Blocking and wash buffer:	3% milk, 10 mM Tris/HCl, 50 mM NaCl, 0.1% Tween-20
Luminol solution:	2.5 mM Luminol in 0.1 M Tris/HCl pH 8.5, 1% DMSO
Enhancer solution:	90 mM p-Cumarsäure in DMSO
H ₂ O ₂ solution:	5.4 mM in 0.1 M Tris/HCl pH 8.5

Transfer proteins to a membrane

(1) Run an SDS-PAGE, and then transfer the proteins from SDS-PAGE to the nitrocellulose membrane for 60 min at 150V.

Antibody incubation

(2) Incubate the blot with 10 ml blocking buffer for 1h at room temperature with gentle agitation. Dilute first antibody (1:1000-2000) in 10 ml of blocking buffer and incubate the blot with the primary antibody for 1h at room temperature.

(3) Wash the blot 3 times, 10 minutes each, in washing buffer with gentle agitation to get rid of the first antibody.

(4) Dilute second antibody (1:5000-10000) in 10 ml of blocking buffer and incubate the blot with second antibody for 1h at room temperature.

(5) Wash the blot 3 times, 10 minutes each, in washing buffer with gentle agitation.

Luminol detection

(6) Drain wash buffer, and then add mixture of 5 ml Luminol solution, 22 ul enhancer solution and 5ml H₂O₂ solution, incubate for 2-3 min in a dark room.

(7) Drain the fluid and cover the blot in plastic wrap and put 3 X-ray films on it. Expose the blot to X-ray film for 5 min in dark room.

2.11 Crystallization solutions and methods

2.11.1 Crystallization solutions

Crystallization screens purchased from Hampton Research:

Crystal screen 1	Additive screen 1
Crystal screen 2	Additive screen 2
Crystal screen Index	Additive screen 3
SaltRx screen	Crystal screen Lite

2.11.2 X-ray Crystallization of BMP-2 and CV2-VWC1 complex

Crystallization experiments were carried out with Sitting Drop Vapour Diffusion technique for crystal initial screening and Hanging Drop Vapor Diffusion method for crystal optimization. CrystalQuick 96 wells were used for Sitting Drop Vapour Diffusion technique and 24 wells reservoir plates were used for Hanging Drop Vapor diffusion method. The detailed procedure for Hanging Drop Vapor diffusion method is as follows: Using a clean pipet tip, pipet 1 ml of each crystal screen reagent into reservoirs, and took 1 µl buffer of the reagent and mixed with 1 µl of complex protein. Applied the 2 ul mixture to the thin bead of cover slide sealant to the upper edge of each of the reservoir. Regarding the Sitting Drop Vapor diffusion method, we pipeted 100 ul of each crystal screen reagent into wells, and the mixture of 1 ul of the complex protein and 1 ul buffer was set in the middle of the reservoir, finally sealed

the whole plate by tape. Crystallization setup was performed in duplicate and incubated at 20°C for several weeks in a stable temperature environment, free of vibration. The drops were observed under a stereo microscope (10 to 100 x magnification) once each day for the first week, then once a week for the following three weeks.

2.11.3 Cryoprotection of crystals

Cryocooling techniques are routinely used in macromolecular crystallography to preserve crystals and reduce radiation damage during X-ray data collection.

The high intensity of synchrotron radiation can lead to radiation damage of the protein crystals. The interaction between the beam and the crystal generates thermal disorder and may even break bonds within the protein. A common method to prevent this radiation damage was to freeze the crystals in a stream of cold nitrogen and collect the diffraction data at low temperature (93). But the high solvent content (~50%) of protein crystals can lead to ice crystal formation during freezing and these ice crystals will destroy the crystal integrity and disturb the protein diffraction. This problem can be overcome by soaking the crystal in a cryoprotectant solution that maintains the crystal quality and prevents the formation of ice crystals (93). Binary complex of BMP-2 and CV2-VWC1 crystals were soaked in different cryoprotecting agents like glycerol, sucrose and glucose and tested for the diffraction quality.

2.12 Biological Activity in Cell Lines

Alkaline phosphatase (ALP) activity was determined in serum-starved C2C12 cells. The promyoblast C2C12 cells (ATCC CRL-1772) were stimulated at a density of 3×10^4 cells/well in a 96-well microtitre plate for 3 days with 0.5–250 nM of each BMP-2 variant in 100 μ l of Dulbecco's modified Eagle's medium (DMEM) containing 2% calf

Material and Methods

serum and antibiotics (100 U/ml penicillin G and 100 ug/ml streptomycin) at 37°C in a humidified atmosphere at 5% CO₂. Cells were washed with phosphate-buffered saline (PBS) and then lysed for 1 h with 100 ul of 1% NP-40 in ALP buffer (0.1 M glycine, pH 9.6, 1 mM MgCl₂, 1 mM ZnCl₂). ALP activity was determined by incubating lysed cells for 15 min with 100 ul of ALP buffer plus 1 mg/ml *p*-nitrophenylphosphate, and measuring the extinction at 405 nm. One A₄₀₅ extinction unit corresponds to 1.5 nmol of *p*-nitrophenolate produced per min per 3 ×10⁴ cells. Inhibition of BMP-2-induced ALP activity by CV2, CV2-VWC1 and CV2-VWC1 mutants were assessed by incubating C2C12 cells with different concentrations of them plus 10 nM BMP-2. Relief of CV2 inhibition of BMP-2-induced ALP activity was assessed by incubating C2C12 cells with 10 nM BMP-2 plus CV2 and increasing concentrations (6.3-25 nM for CV2) of BMP-2 mutants. Results are given as mean values from six determinations done in parallel for each condition.

3. Results

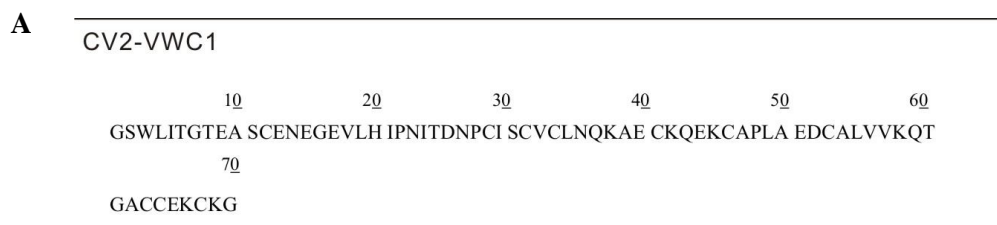
3.1 Preparation of VWC domains of CV2

3.1.1 Expression and purification of CV2-VWC1 domain

Cloning and expression of zCV2-VWC1 fusion protein

In a previous study the binding properties of zebrafish CV2 (zCV2) and its fragments to human BMP-2 have been investigated. Results showed that the zCV2 binds human BMP-2 with the same binding affinity as human CV2 (hCV2) (78). For further structural analysis, we initially expressed hCV2-VWC1 and zCV2-VWC1 in parallel. The hCV2-VWC1 could be induced as a thioredoxin fusion protein in *E. coli*, but no soluble hCV2-VWC1 could be isolated after removing thioredoxin by protease cleavage. In contrast, native zCV2-VWC1 could be easily isolated with very high yield (see below). Thus, the zCV2 was used in all the experiments in this thesis.

The cDNA encoding the residues 1-66 of mature zCV2 (Swiss-prot entry Q5D734) plus an N-terminal GSW extension was amplified by a recombinant PCR and cloned into a derivative of expression vector pET-32a (+) at the XbaI and Bpu1102I restriction enzyme sites. The expression plasmid pET32a [Trx-CV2-VWC1] (Fig. 3.1A) that contains VWC1, thioredoxin, 6x histidine-tag and a Thrombin cleavage site was transformed into *E. coli* strain Origami (DE3). The encoded protein was expressed as a soluble thioredoxin fusion protein.



Results

B

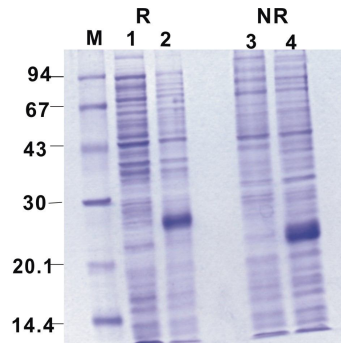


Figure 3.1A amino acids sequence of CV2-VWC1. B Induction of the fusion protein Thr-CV2-VWC1 under non-reducing (NR) and reducing conditions (R). Lane M, Protein marker; Lane 1 and 3, uninduced bacteria; Lane 2 and 4, induced bacteria

The calculated molecular weight of Trx-CV2-VWC1 was 21.15KD, but it migrates anomalously at about 26KD under reducing condition and about 23KD under non-reducing conditions, both of which were higher than its theoretical molecular weight (Fig. 3.1B). We could obtain 3.0-3.8 g bacteria per liter TB medium after fermentation.

Sonication, Ni-chelating chromatography and Thrombin cleavage

8-15 g cell pellet was suspended and sonicated in 200 ml sonication buffer. The soluble fusion protein Trx-CV2-VWC1 was in the supernatant after sonication and centrifugation. As an initial purification step, Immobilized Metal Affinity Chromatography (IMAC) with Ni-chelating agarose was used to purify the fusion protein. After the Ni-chelating chromatography, the majority of the unspecific proteins were removed and the target protein could be eluted with a high concentration of imidazole (Fig. 3.2, lane 5-7). Yields of the purified fusion proteins were usually in the range of 25-32 mg per gram-wet bacteria.

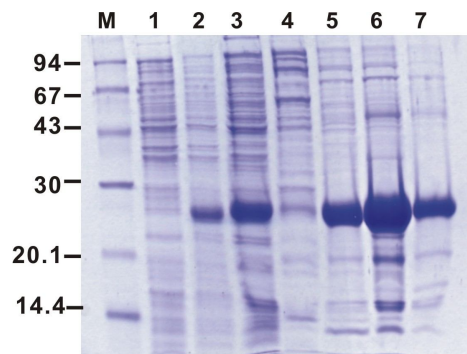


Figure 3.2 Expression and purification of thioresdoxin fused CV2-VWC1. SDS-PAGE under reducing conditions show the expression and Ni-chelating chromatography results: lane 1, uninduced bacteria; lane 2, induced bacteria; lane 3, supernatant after centrifugation of the sonicated bacteria, lane 4, flow-through of the column washed with a buffer containing 60 mM column; lane 5-7, fractions eluted by a buffer containing 500 mM imidazole.

Results

As shown in Fig. 3.2 lanes 5-7, the histidine-tag proteins could be purified by Ni-chelating chromatography. These proteins were then applied to subsequent Thrombin-cleavage. SDS-PAGE showed that CV2-VWC1 was efficiently cleaved from thioredoxin and the histidine-tag after thrombin treatment. The band of CV2-VWC1 protein migrates at 17 and 19 kDa in the SDS-PAGE under both reducing and non-reducing conditions, respectively, more than twice that computed from the protein sequence (7.3 kDa). There are still some uncut proteins which may represent incorrectly folded or multimer fusion proteins insensitive to thrombin (Fig. 3.3).

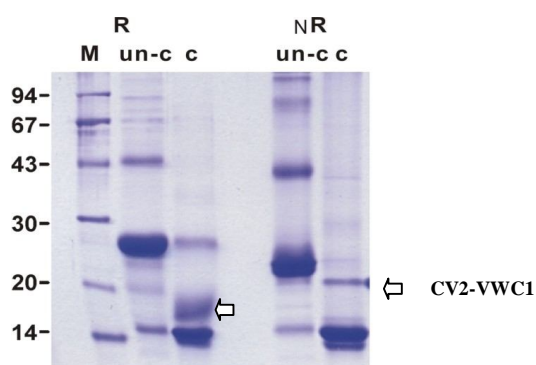


Figure 3.3 SDS-PAGE analysis of fusion protein Thr-CV2-VWC1 cleaved by thrombin under reducing (R) and non-reducing (NR) conditions. M, protein markers; un-c, uncleaved fusion protein; c, fusion protein cleaved by thrombin.

Anion exchange chromatography using TMAE column

After cleavage of the fusion protein by Thrombin, the separation of CV2-VWC1 from thioredoxin and the histidine-tag was achieved by anion exchange chromatography using a EMD-TMAE column. The column was equilibrated in 20 mM Tris/HCl, pH 7.4, and bound protein was eluted with a linear NaCl gradient from 0 to 1 M (Fig. 3.4A). Fractions eluted from 60 mM-260 mM NaCl were subjected to SDS-PAGE. Fractions eluted from 100 mM-120 mM NaCl were shown to contain thioredoxin and CV2-VWC1 according to their molecular weight. Later fractions contain little VWC1, but mainly thioredoxin protein multimers and unspecific proteins (Fig. 3.4B). The proteins eluted with 60-120 mM NaCl were collected for further purification.

Results

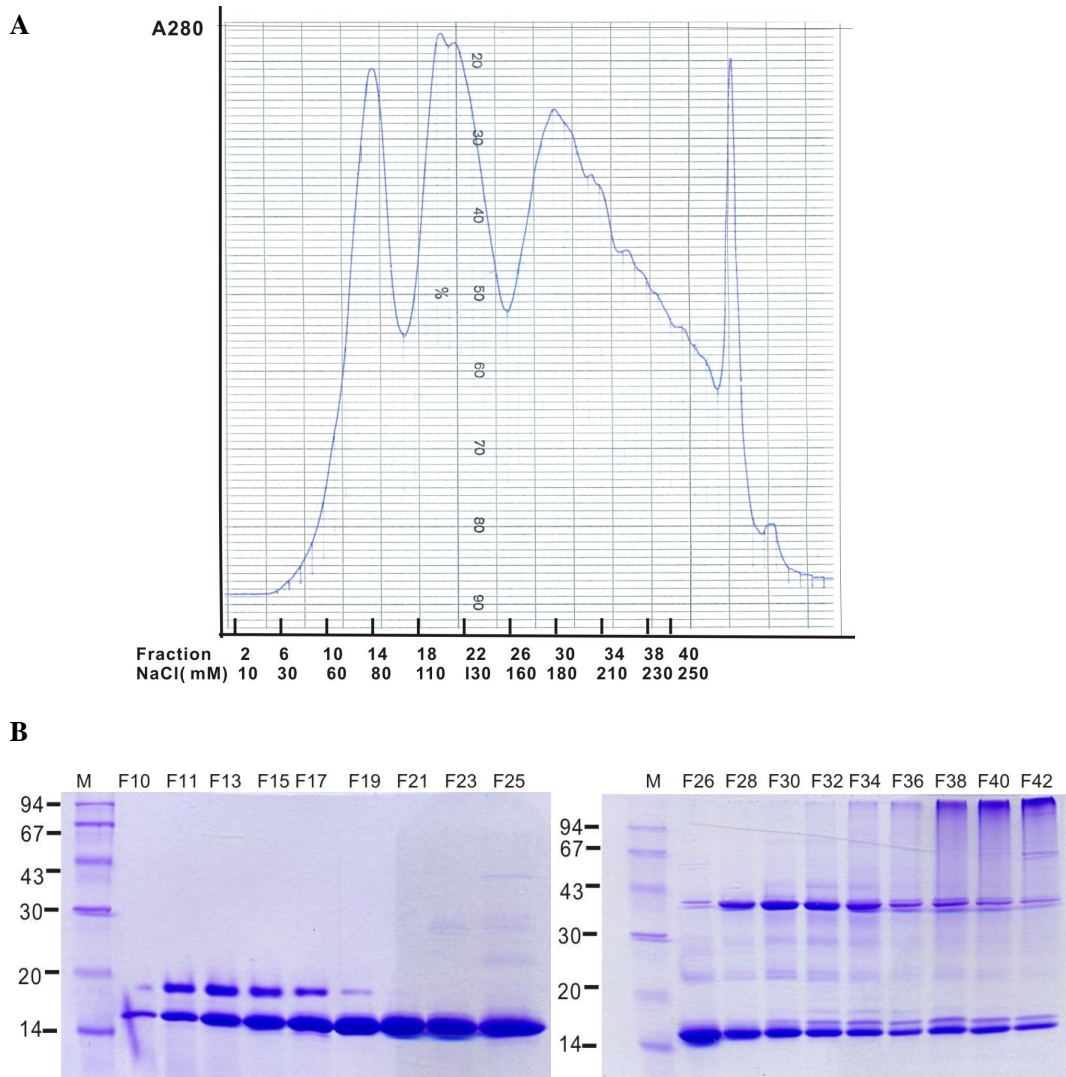


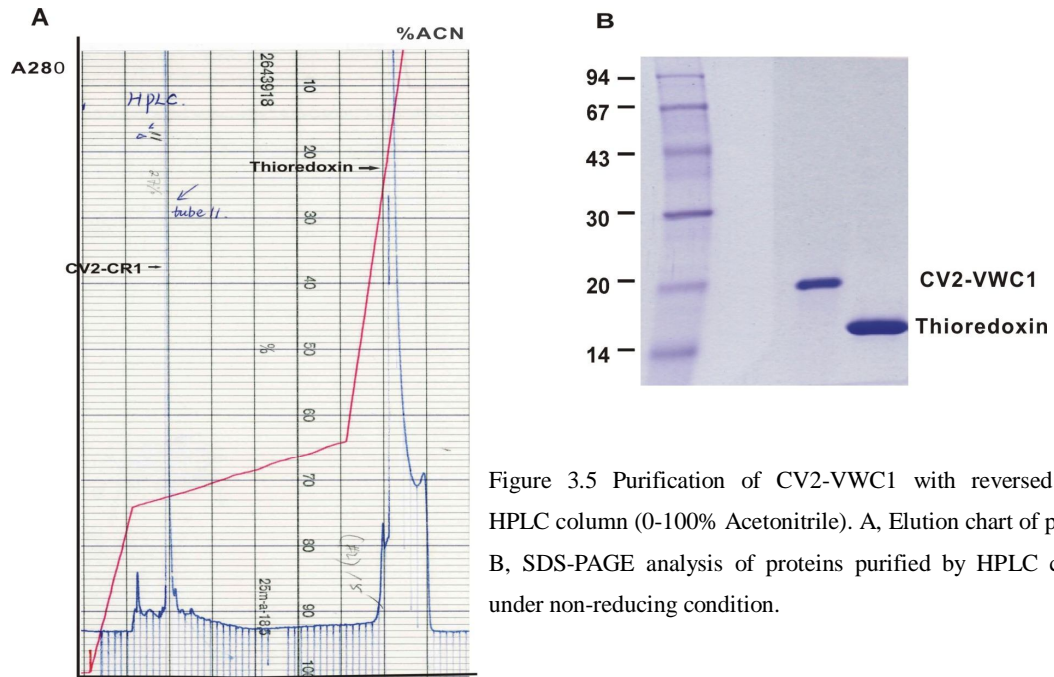
Figure 3.4 Purification of CV2-VWC1 after thrombin cleavage with TMAE column. The column was equilibrated with 20 mM Tris, pH 7.4 and eluted by the same buffer containing 0-1 M NaCl. A: Elution chart of proteins. B: SDS-PAGE analysis of proteins eluted with 60–260 mM NaCl under non-reducing conditions. F10-42 were collected as indicated in A.

Reversed -Phase HPLC

Reversed phase HPLC was sufficient to separate CV2-VWC1 from thioredoxin. CV2-VWC1 and thioredoxin were eluted separately with a linear Acetonitrile (ACN) gradient from 0-100%. There were 2 large peaks eluted by ACN on the chart, the first of which was very sharp and the corresponding proteins were eluted with 26% Acetonitrile, and the second with an ACN concentration higher than 80% (Fig. 3.5A). SDS-PAGE analysis showed that proteins from the second peak correspond to

Results

thioredoxin and the histidine-tag (14 KDa), while CV2-VWC1 was in the first sharp peak based on its low electrophoretic mobility. The CV2-VWC1 protein was very homogeneous on the SDS-PAGE gel (Fig. 3.5B). After thrombin cleavage of the thioredoxin fusion protein, anion exchange chromatography and reversed phase HPLC, we could routinely obtain about 2-2.67 mg CV2-VWC1 per gram wet bacteria.



Mass spectroscopy

The identity of CV2-VWC1 was established by mass spectroscopy. Our result showed that no post-translational modified CV2-VWC1 or other unspecific proteins were found. The molecular weight of 7319.328 KDa measured by mass spectroscopy fitted very well with its theoretical value of 7319.295 KDa (Fig. 3.6).

Results

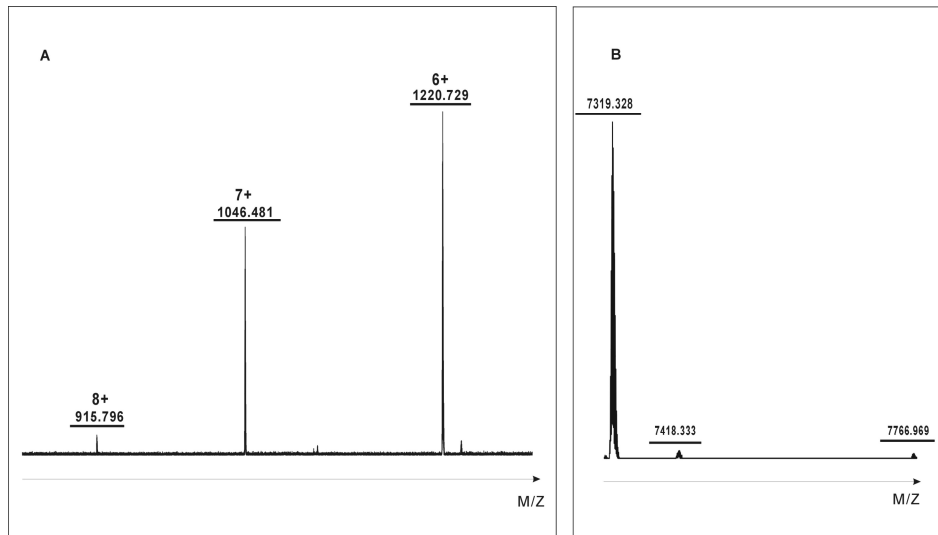


Figure 3.6 A. Mass spectrometry analysis of CV2-VWC1. B Deconvolution analysis of 6-fold-charged ions with corresponding molecular weight.

BMP-2 affinity chromatography

Although the CV2-VWC1 protein appears to be uniform on the SDS-PAGE after HPLC, the homogenous binding competent CV2-VWC1 could only be purified by means of BMP-2 affinity chromatography. The pure and active CV2-VWC1 could be used for the further NMR spectroscopy and crystallization. The BMP-2 affinity column was first equilibrated with 10 mM Hepes/500 mM NaCl, pH 7.4. Protein purified from the HPLC column was loaded and then the bound active VWC1 was eluted by 4M $MgCl_2$. Finally the eluted proteins were dialyzed against 10 times 10 mM Hepes/500 mM NaCl. SDS-PAGE showed that the CV2-VWC1 protein appears to be a smear under reducing condition and a sharp band under non-reducing condition (Fig. 3.7). There were about 10%-14% of proteins that might represent the not correctly folded CV2-VWC1 proteins could not bind to BMP-2 affinity column.

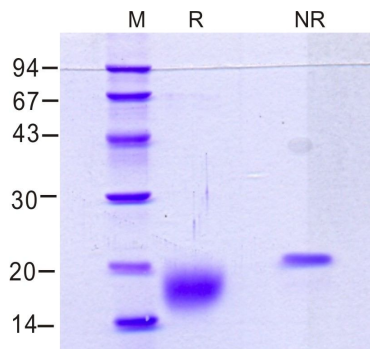


Figure 3.7 SDS-PAGE analysis of BMP-2 affinity column purified CV2-VWC1 under reducing (R) and non-reducing (NR) conditions.

Results

Table 3.1 Yields of CV2-VWC1 purification.

Purification step	Product	Yield
After fermentation	Induced bacteria	3-3.8 g /L TB culture medium
After Ni-chelating chromatography	CV2-VWC1 fusion protein	25-32 mg /g wet bacteria
After RE-HPLC	CV2-VWC1	2-2.67 mg /g wet bacteria
After BMP-2 column	Homogenous and active CV2-VWC1	1.8-2.4 mg /g wet bacteria

Results

3.1.2 Expression and purification of CV2-VWC2, VWC3, VWC4 and VWC5

Cloning and expression of CV2-VWC2, VWC3, VWC4 and VWC5 fusion proteins

The cDNAs encoding zebrafish CV2-VWC2, VWC3, VWC4 and VWC5 were cloned into the derivative of expression vector pET-32a (same as mentioned above) at the NcoI and Bpu1102I restriction enzyme sites (Fig. 3.8). The expression plasmid pET32a that contains one of the VWC domains (domains 2 to 5), thioredoxin, 6x histidine-tag and a Thrombin cleavage site was transformed into *E. coli* strain Origami (DE3) and expressed as a soluble thioredoxin fusion protein.

CV2-VWC2	10	20	30	40	50
	GSKGCLLKGT	SYNSSHHWIS	PVKPCVTYSC	QEGVITEAEM	RCVIHCKNPK
	60				
	IHPKKCCPTC	PG			
CV2-VWC3	10	20	30	40	50
	GSPGCIFEGN	LYKEDEEFHP	EGNPCIKVCV	TGGQSMCHKL	VCPVLSCPSH
	60	70			
	LHTPPGQCC	PRCRGQRRVF	DLSPGS		
CV2-VWC4	10	20	30	40	50
	GSRGQRRVFD	LSPGSLFHS	EVYENGSSIS	YDNCTTCTCV	DSTVLCRKRC
	60	70			
	SPPGSCHGTA	CCEACQSHLK	MEDVKY		
CV2-VWC5	10	20	30	40	50
	GSQSHLKMED	VKYCRVKSKI	YRDGDRWSSV	NCSLCTCVKG	NIQCQPKICV
	60	70			
	PITSCPSNKI	LNRTGCCPVC	TDKPGV		

Figure 3.8 Amino acids sequences of CV2-VWC2, -VWC3, -VWC4 and -VWC5.

The induction of the host *E. coli* cells with IPTG led to the production of the desired proteins (Fig. 3.9). The molecular weight of Trx-VWC2, VWC3, VWC4, and VWC5 are 20.95, 22.57, 22.39 and 22.63 KDa, respectively, and their electrophoretic mobility in the SDS-PAGE were very closed to their theoretical molecular weights. We could get about 3.5, 12, 5 and 12 g bacteria per liter TB medium, respectively.

Results

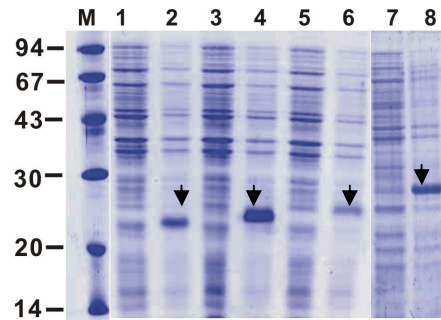


Figure 3.9 Induction of the thioredoxin fusion proteins of CV2-VWC2 (1, 2), CV2-VWC3 (3, 4), CV2-VWC4 (5, 6) and CV2-VWC5 (7, 8). Lanes 1,3,5,7 are samples of uninduced bacteria control. Lanes 2,4,6,8 are samples of bacteria induced by 1 mM IPTG.

Purification of fusion proteins Trx-CV2-VWC2, -VWC3, -VWC4 and -VWC5

The 4 fusion proteins expressed in Origami (DE3) were isolated by standard procedures involving Ni-chelating chromatography, digested with thrombin, purified by TMAE or SP-Sepharose ion-exchange chromatography, and reversed phase HPLC column to apparent homogeneity.

Ni-chelating chromatography was first used to roughly separate these four fusion proteins from endogenous *E. coli* proteins. The presence of disulfide bonds may sometimes cause improper folding in these products. Fig. 3.10 shows that most proteins purified after Ni-chelating chromatography were target proteins Thr-VWC2, -VWC3, and -VWC5 (with molecular weight between 20 kDa and 23 kDa). For Thr-CV2-VWC4, about 40% proteins migrated at 25 kDa which is close to the theoretical molecular weight. The other 60% migrated at 15 kDa which is similar to the molecular weight of thioredoxin plus 6x Histidine-tag. This is likely a truncated Thioredoxin-CV2-VWC4 which was processed in *E. coli* but still bound to Ni-chelating agarose (Fig. 3.10).

Thrombin digestion could efficiently cleave most part of the Thr-CV2-VWC3 and VWC5 proteins. Thr-CV2-VWC2 seems to be partially digested as the cleaved thioredoxin was visualized after thrombin treatment. However, no clear VWC2 band could be found (Fig. 3.10, compare lanes 1 and 2, and lanes 3 and 4). Similarly,

Results

Thr-CV2-VWC4 could be partially cleaved, but the single VWC4 band could not be clearly separated from that of thioredoxin, probably due to their similar mobilities in the SDS-PAGE. At this point, it was not clear whether VWC2 and VWC4 proteins could be isolated.

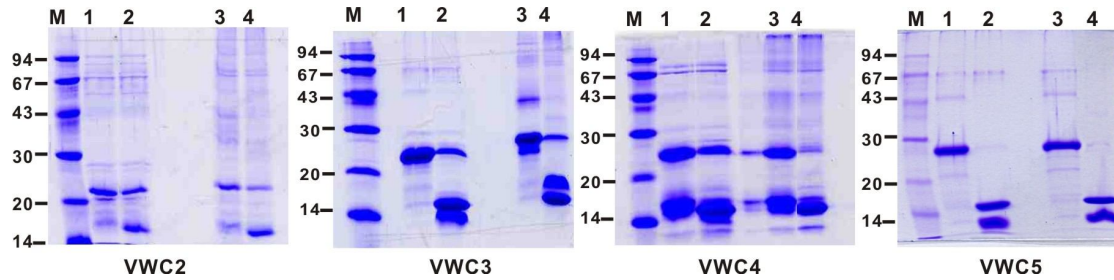


Figure 3.10 SDS-PAGE analysis of fusion protein Thr-CV2-VWC2, -VWC3, -VWC4, and -VWC5 cleaved by thrombin under reducing and non-reducing conditions. M, protein markers; 1 and 3, uncleaved fusion protein; 2 and 4, fusion protein cleaved by thrombin. 1 and 2 under reducing conditions; 3 and 4 under non-reducing conditions.

Following a cleavage reaction, the 4 positively charged VWC domains could be easily separated from thioredoxin by cation-exchange chromatography employing a SP-Sepharose column (Fig. 3.11). The pI of VWC1, VWC2, VWC3 and VWC4 is 8.87, 7.02, 6.95 and 9.02, respectively, and that of thioredoxin is 5.83. Therefore after loading of the protein mixture, thioredoxin was obtained in the flowthrough, while VWC domains bound and could be eluted by different NaCl concentrations. In the case of VWC3 and VWC5, very pure protein was obtained after SP-sepharose column, and the purity after such a separation usually exceeded 90%. In the case of VWC2 and VWC4, soluble proteins with similar apparent molecular weight can be detected. The target proteins were mixed with some unspecific proteins (dimers or multimers) that could not be easily separated by the SP-Sepharose column.

Results

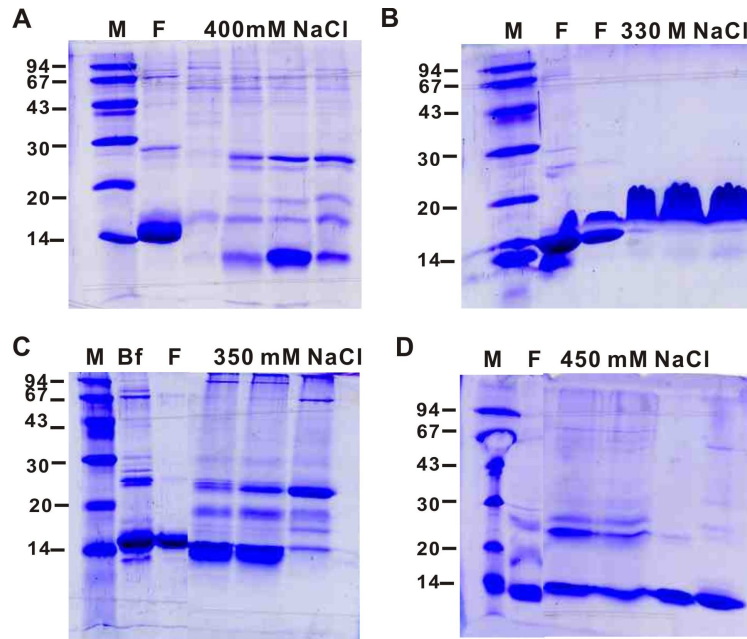


Figure 3.11 SDS-PAGE analysis of 4 VWC domains purified from the SP-sepharose column. M, protein markers; F, flow-through; Bf, samples before loading to the column. A, CV2-VWC2 eluted by 400 mM NaCl. B, CV2-VWC3 eluted by 330 mM NaCl. C, CV2-VWC4 eluted by 350 mM NaCl. D, CV2-VWC5 eluted by 450 mM NaCl.

Although the 4 VWC domains could be effectively separated from thioredoxin by SP-Sepharose column, there were still a few unspecific proteins which remained (Fig. 3.11). Reversed phase HPLC chromatography was then used to purify the proteins to apparent homogeneity (Fig. 3.12). The yield of the four VWC domains was not as high as that of VWC1. VWC2 and VWC4 yielded only 0.4 mg and 0.3 mg per liter TB medium, respectively. In contrast, the yields of VWC3 and VWC5 were quite high, 1.6 and 5.0 mg per liter TB medium, respectively.

Results

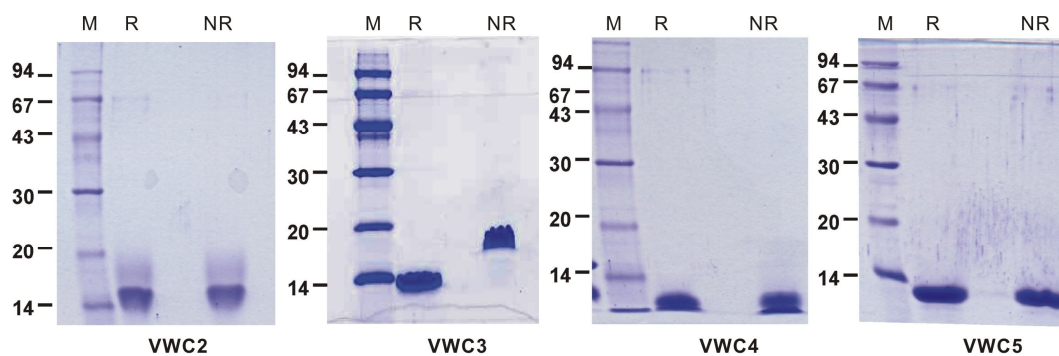


Figure 3.12 CV2-VWC domains purified by HPLC column. M, protein markers; R, proteins in reducing conditions; NR, proteins in non-reducing conditions.

Mass Spectroscopy results

The identity of the VWC domains were characterized and determined by mass spectroscopy. The measured Mass value of the 4 VWC domains matched very well with their calculated values (Table 3.2).

Table 3.2 Mass analysis of CV2-VWC2, 3, 4 and 5.

Domain	Mass measured	Mass calculated
VWC2	7097.400	7097.317
VWC3	8553.905	8553.806
VWC4	8460.678	8460.644
VWC5	8702.264	8702.115

3.1.3 Preparation of ^{15}N -labelled CV2-VWC1 and $^{15}\text{N}^{13}\text{C}$ -double labelled CV2-VWC1

The expression plasmid pET32a [Trx-CV2-VWC1] was transformed into *E. coli* strain BL21 (DE3) and expressed in M9 minimal medium. ^{15}N -VWC1 was generated using (^{15}N) ammonium sulfate as the sole nitrogen source. For $^{15}\text{N}^{13}\text{C}$ -VWC1, the carbon source was (^{13}C 6-D-UL) glucose in the M9 minimal medium. We could get about 3.7 g (^{15}N) and 2.91 g ($^{15}\text{N}^{13}\text{C}$) bacteria per liter M9 minimal medium. The labelled CV2-VWC1 was purified using the same methods as described above for the unlabelled protein.

Consistent with our previous experiments with unlabelled CV2-VWC1, the fusion protein was expressed (Fig. 3.13 lane 2) and found primarily in the supernatant after sonication (lane 3). The majority of non-target proteins were removed by Ni-chelating chromatography (lane 4). After thrombin cleavage of the fusion protein, CV2-VWC1 was efficiently disconnected from thioredoxin (lane 5). CV2-VWC1 was still mixed with thioredoxin after TMAE column (lane 6). Reverse phase HPLC can efficiently separate the CV2-VWC1 from thioredoxin (lane 7) and the active protein was purified with a BMP-2 affinity column (lane 8).

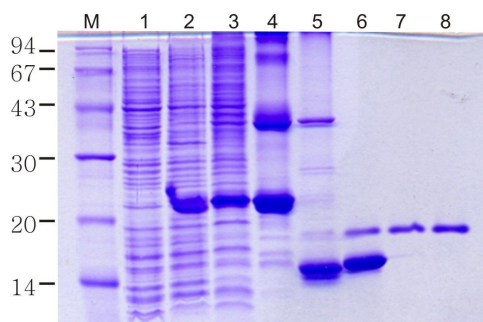


Figure 3.13 Expression and purification of labelled CV2-VWC1 subjected to SDS-PAGE. Lane M, marker; lane 1, uninduced bacteria; lane 2, induced bacteria; lane 3, supernatant after centrifugation of sonicated bacteria; lane 4, purified protein after Ni-chelating chromatography; lane 5, protein mixture after thrombin cleavage; lane 6, TMAE isolated Thioredoxin containing CV2-VWC1; lane 7, HPLC isolated CV2-VWC1; lane 8, BMP-2 affinity column separated CV2-VWC1.

Results

Mass spectroscopy

Labelled CV2-VWC1 was characterized by mass spectroscopy. The result showed that about 99% of the CV2-VWC1 protein was labelled. We found that labelled CV2-VWC1 was not posttranslational modified, and the measured mass value of 7702.205 KDa fitted very well with its theoretical value of 7702.055 KDa (Fig. 3.14).

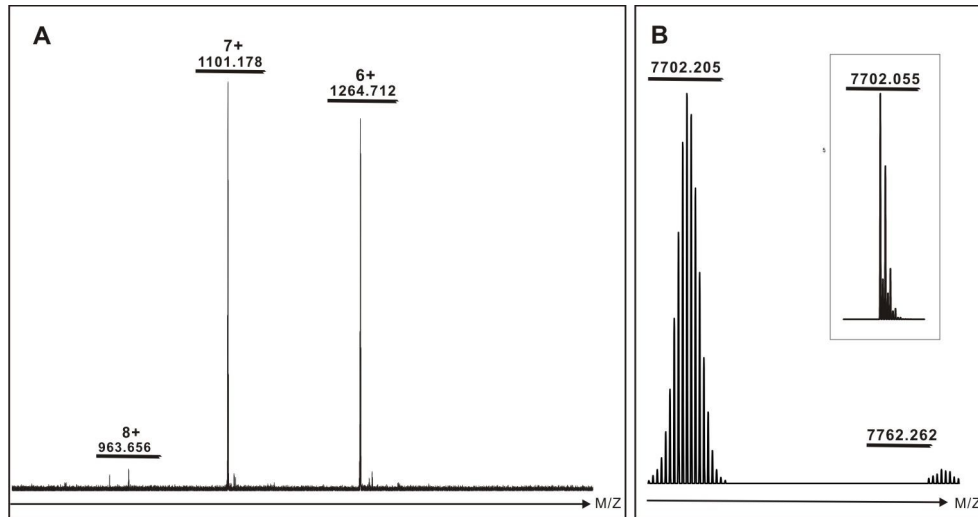


Figure 3.14 A: Mass spectroscopy analysis of $N^{15}C^{13}$ -labelled CV2-VWC1. B: Deconvolution analysis of 6-fold-charged ions with corresponding molecular weight.

The yield of the labelled VWC1 was lower than the unlabelled ones (Table 3.3), and was likely due to the different *E. coli* strains used for the expression of the two proteins. Origami (DE3) is a modified cell strain of BL21. It is more efficient in facilitating correct disulfide bond formation of a fusion protein than BL21 (DE3). Thus it was not unexpected that the yield of the active ^{15}N - or $^{15}N^{13}C$ -labelled CV2-VWC1 expressed in BL21 (DE3) was less than the unlabelled proteins, which were expressed in Origami (DE3) (Table 3.3). The labelled proteins were dialysed against 20 mM Na-phosphate, 20 mM NaCl, pH 6.6 plus 0.02% NaN_3 and concentrated to 14 mg/ml (about 1-2 mM) for NMR measurement.

Results

Table 3.3 Comparison of the yields of the labelled-VWC1 expressed in ¹³C-and ¹⁵N-containing M9 minimal medium and the unlabelled-VWC1 expressed in TB medium.

	Fermentation (g bacteria/L medium)	Ni-chelating chromatography (mg fusion protein/g bacteria)	Reversed phase HPLC (mg /g bacteria)	BMP-2 affinity chromatography (mg /g bacteria)
WT CV2-VWC1 (TB medium)	3.0-3.8	25.0-32.0	2.0-2.6	1.8-2.4
Labelled CV2-VWC1 (M9 medium)	3.5-3.7	24.5-26.4	0.7-0.9	0.6-0.7

3.1.4 Binding affinity and specificity of BMPs for CV2 and CV2-VWC domains

The binding of CV2 to BMP-2/-7 and GDF-5 occurs via its N-terminal segment containing VWC1-5 (CV2-N) (78). However, which of the individual domains was required for binding was unknown. Now the binding of the individual CV2-VWC domains to representatives of three subfamilies of BMPs, i.e., BMP-2, BMP-7 and GDF-5 was determined by biosensor-based interaction analysis. Surprisingly, we found that CV2-VWC1 was the only one of the five existing VWC domains that is involved in binding. CV2-VWC1 bound to BMP-2, BMP-7 and GDF-5 with affinities similar to those of full-length CV2 and CV2-N (VWC1-5) (Table 3.4). In contrast, the VWC domains 2, 3, 4 and 5 did not show any measurable binding affinity for these ligands. BMP-2 bound to CV2 and CV2-VWC1 with high affinities, which was similar to the high affinity of BMP-2 for its type I receptor (30).

A			
	CV2	CV2-N	CV2-VWC1
BMP-2	22 nM	25 nM	22 nM

B			
	CV2	CV2-N	CV2-VWC1
BMP-2	2.4 nM	2.2 nM	4.0 nM
BMP-7	7 nM	ND	20 nM
GDF-5	34 nM	ND	66 nM

ND, not determined. The data for CV2 and CV2-N are taken from Rentsch et al (72)

Table 3.4 A Apparent K_D of CV2 proteins to immobilized BMP-2. B Apparent K_D of BMP-2, BMP-7 and GDF-5 to immobilized CV2 proteins.

Results

When CV2-VWC1 was immobilized on the chip, the binding affinity of BMP-2 was about 4 nM, while binding affinity of CV2-VWC1 to immobilized BMP-2 was about 22 nM (Fig. 3.15B). The difference could be explained by a speculation that the solute BMP-2 dimer binds simultaneously to two immobilized CV2-VWC1 on the chip (1:2 interaction), which results in an enhanced affinity; while the separate VWC1 domains bind immobilized BMP-2 in a 1:1 interaction, leading to a lower affinity.

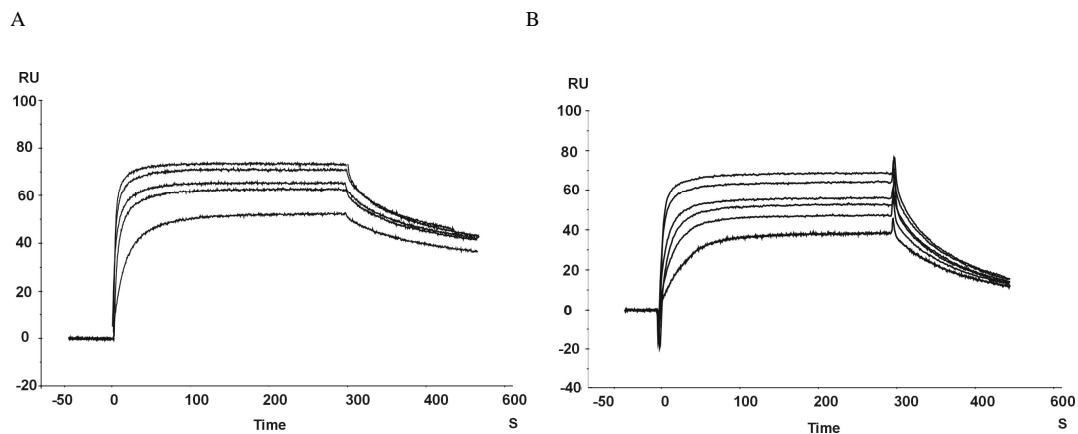


Figure 3.15 Binding affinity of BMP-2 for CV2-VWC1 was analyzed by Biacore. A, CV2-VWC1 was immobilized on the chip surface, with 25, 75, 100, 200 and 300 nM BMP-2 injected over the chip surface. B, BMP-2 was immobilized on the chip surface, with 20, 40, 60, 100, 200 and 300 nM CV2-VWC1 injected over the chip.

3.2 Identification of CV2 binding site for Chordin

We previously found that CV2 and CV2-N (VWC1-5) could bind Chordin with the same binding affinity (Zhang, personal communication), suggesting that the CV2-N of CV2 is responsible for the binding with Chordin. In order to identify the exact binding sites, we expressed several fragments of CV2-N in SF9 cells. Fragments VWC1-4, VWC1-3, VWC4-5, VWC2-4 and VWC3-4 were expressed with a C-terminal thrombin cleavage site (LVPRGS) plus a 6×Histidine-tag in SF9 insect cells.

Results

The 6 fragments of CV2-N were then purified with Ni²⁺/nitriloacetate/agarose and gel-filtration chromatography to more than 80% purity (Fig. 3.16) and used for the Biacore interaction analysis.

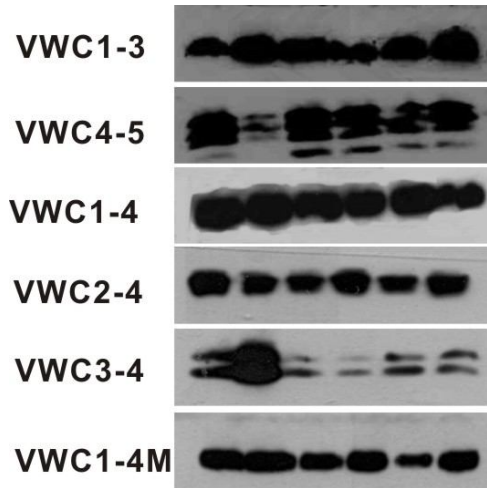


Figure 3.16 Western blot analysis of the protein fragments expressed in SF9 cells. Protein fragments were analysed using 15 μ l of supernatant samples from 6 virus clones. The first antibody was an anti-his tag antibody. It was applied at a dilution of 1:1000. The secondary antibody was horseradish peroxidase (HRP)-labelled goat anti-mouse immunoglobulin G and was applied at a dilution of 1:7000.

As expected, Biacore analysis showed that fragments VWC1-4 and VWC1-3, which contained the VWC1, could bind to BMP-2 (Fig. 3.17A) with the same affinity as that of VWC1 alone. Interestingly, while VWC1-4 binds Chordin with a similar affinity as VWC1-5 (Fig. 3.17), VWC1-3 and VWC2-4 did not show any binding to Chordin. Other fragments, VWC4-5 and VWC3-4, could bind neither BMP-2 nor Chordin (Table 3.5). These results suggest that for Chordin binding VWC1 and VWC4 are required. In addition, the results presented here indicate that the negative results of BMP-binding for *E. coli* expressed VWC2, 3, 4 and 5 were not likely caused by incorrect folding of the proteins.

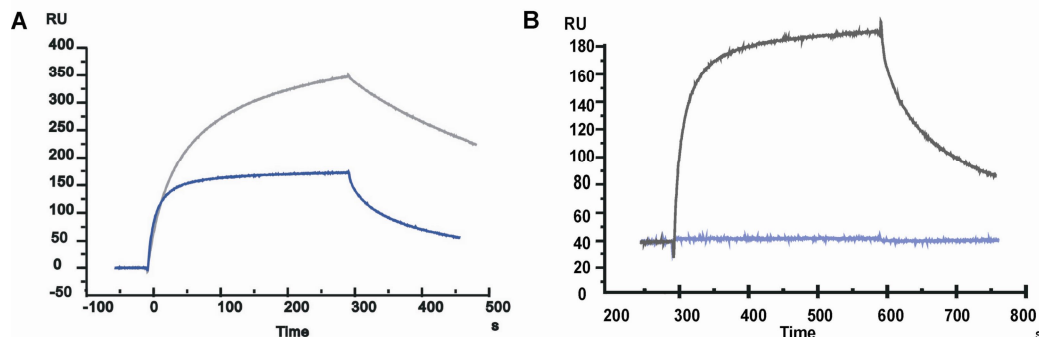


Figure 3.17 Biacore analysis of VWC1-4 (A) and VWC1-4M (B) to immobilized BMP-2 and chordin. Sensorgram showing overlay of the VWC/BMP-2 (grey) and VWC/Chordin (blue) interactions.

Results

All these results confirmed that only CV2-VWC1 could bind to BMPs and suggested that the VWC1 domain is not only involved in BMP-2 binding, but also participates in binding with Chordin. Furthermore, it is unknown whether VWC1 and VWC4 are sufficient for Chordin binding, since these results show that the contribution of VWC2 and VWC3 can not be excluded. It is likely that the VWC4 domain forms a composite interface with VWC1 or VWC1-3 for Chordin binding. To test this idea, we generated a VWC1-4 insertion mutant (VWC1-4M) in which 12 random residues GSLVPRGSMLSG were inserted between VWC3 and VWC4.

Table 3.5 Comparison of the binding of CV2 proteins for BMP-2 and Chordin.

CV2 fragments	BMP-2	Chordin
CV2 (full length)	Yes	Yes
CV2N (VWC1-5)	Yes	Yes
VWC1-4	Yes	Yes
VWC1-3	Yes	No
VWC2-4	No	No
VWC3-4	No	No
VWC4-5	No	No
VWC1-4M	Yes	No

As expected, VWC1-4M could no longer bind to Chordin, whereas its BMP binding activity was retained (Table 3.5), indicating that the composite interface of CV2 for Chordin is successfully destroyed. Future experiments will be required to demonstrate the *in vivo* biological relevance of the CV2/Chordin interaction. This may offer a clue for the complicated pro- and anti-BMP activity of CV2. The Chordin binding-deficient mutant VWC1-4M will be a good candidate for such an experiment.

3.3 Crystallization of the BMP-2 /CV2-VWC1 binary complex

3.3.1 Preparation of BMP-2 and CV2-VWC1 complex

Our functional analysis of the CV2-VWC1/BMP-2 interaction indicated that CV2-VWC1 bound mainly to the knuckle epitope of BMP-2 (see later results). As two knuckle epitopes exist in the BMP-2 dimer, the binding stoichiometry of CV2-VWC1 and BMP-2 is very likely 2:1. We therefore mixed CV2-VWC1 and BMP-2 at a molar ratio of 2.4: 1 for the complex formation. More CV2-VWC1 was added to make sure that all the BMP dimers were occupied by the VWC1 molecules. BMP-2 was dissolved in H₂O and diluted to 10 μM to ensure that BMP-2 would not precipitate in the final concentration under 5 μM during the mixture process. In parallel, CV2-VWC1 was dissolved in 10 mM HEPES, pH 7.4, and 1400 mM NaCl. After quickly mixing the two samples, the binary complex of BMP-2 and CV2-VWC1 in the buffer of 10 mM HEPES, pH 7.4, 700 mM NaCl was applied for gel-filtration chromatography.

Gel filtration chromatography

As shown in Fig. 3.18A, the binary complex of BMP-2/CV2-VWC1 (peak 1) could be efficiently separated from the excess VWC1 (peak 2). The purity and identity of the proteins from the two peaks were characterized and determined by SDS-PAGE analysis (Fig. 3.18B). We noted that the VWC1 protein in fraction 26 and 27 showed 3 bands, similar to what we usually saw in the VWC1 protein purified by the BMP-2 affinity column. These VWC1 isomers have different mobility in the SDS-PAGE. They are unmodified proteins with the same molecular weight as characterized by Mass spectroscopy (see 3.1.1).

Results

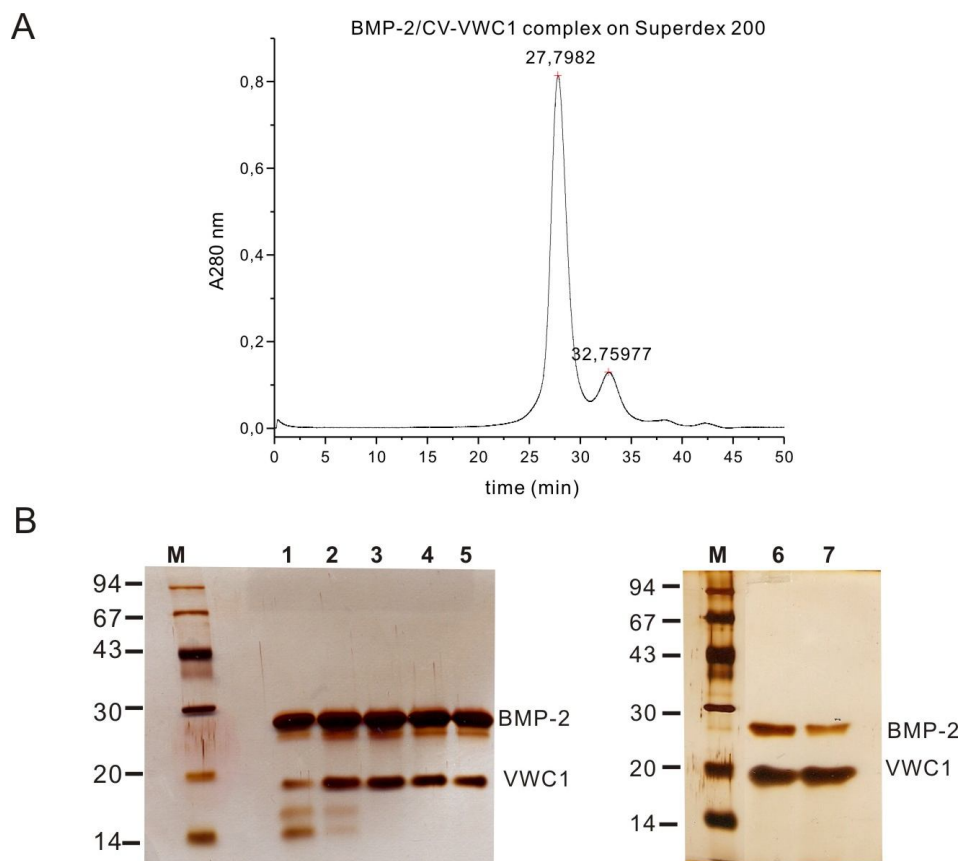


Figure 3.18 A Gel filtration chromatography of the binary complex of BMP-2 and CV2-VWC1. B SDS-PAGE analysis of the two peaks from FPLC. Lane 1-5: protein from fractions 26, 27, 28, 29 and 30; lane 6-7: protein from fractions 31 and 32.

3.3.2 Crystallization of the binary complex of wt BMP-2/CV2-VWC1 and preliminary analysis of the native data

Crystallization was performed according to the sitting and hanging Drop Vapor Diffusion method. The concentration of the complex BMP-2/CV2-VWC1 was 5-10 mg/ml in 10 mM Hepes, pH 7.4 and 700 mM NaCl. 1 ul of protein sample was mixed with 1 ul of the screening reagents.

Initial screening of the complex

Initial crystallization trials were performed by the sitting drop vapor diffusion technique in Crystal Quick 96 well sitting drop plates. Hampton crystal screen kits Crystal screen 1, Crystal screen 2, SaltRx, Lite and Index of the Hampton research company (about 350 conditions) were used. 1 μ l of protein (10 mg/ml) was mixed

Results

with 1 μ l of reservoir solution and this mixture was equilibrated against 100 μ l of reservoir solution. The conditions with crystal formation were further optimized using 24 well VDX plates. Conditions that gave rise to crystals are summarized in table 3.6.

Table 3.6 Summary of conditions giving crystals for the BMP-2/CV2-VWC1 complex using Kits of Structure-Screen HR-I, Structure-Screen HR-II, Salt Screen, Index Screen and Lite Screen.

Screen kit	Salt	Buffer	Precipitant	Days
HR-I # 9	0.2 M NH ₄ OAc	0.1 M Na Citrate pH 5.6	30% PEG 4000	2 days
HR-I # 15	0.2 M (NH ₄) ₂ SO ₄	0.1 M Na Cacodylate pH 6.5	30% PEG 8000	1 day
HR-I # 22	0.2 M NaOAc	0.1 M Tris HCl pH 8.5	30% PEG 4000	7 days
HR-I # 28	0.2 M NaOAc	0.1 M Na Cacodylate pH 6.5	30% PEG 8000	1 day
HR-I # 30	0.2 M (NH ₄) ₂ SO ₄	None	30% PEG 8000	1 day
HR-I # 40	None	0.1 M Na Citrate pH 5.6	20% PEG 4000 20% Isopropanol	4 days
HR-I # 41	None	0.1 M Na Hepes pH 7.5	20% PEG 4000 10% Isopropanol	4 days
HR-I # 43	None	None	30% PEG 1500	1 day
HR-I # 47	None	NaOAc pH 4.6	2.0 M (NH ₄) ₂ SO ₄	1 day
HR-I # 50	0.5 M Li ₂ SO ₄	None	15% PEG 8000	1 day
HR-II # 13	0.2 M (NH ₄) ₂ SO ₄	0.1 M NaOAc pH 4.6	30% PEG 2000	7 days
HR-II # 40	None	0.1 M Tris pH 8.5	25% tert-Butanol	1 day
HR-Salt # 52	None	0.1 M Tris pH 8.5 pH 8.5	2.4 M (NH ₄) ₂ HPO ₄	1 day
HR-Index # 7	None	0.1 M Citric Acid pH 3.5	3.0 M NaCl	5 days
HR-Index # 23	None	2.1 M DL-Malic acid pH 7.0	None	2 days
HR-Lite # 28	0.2 M NaOAc	0.1 M Na Cacodylate pH 6.5	15% PEG 8000	4 days
HR-Lite # 41	None	0.1 M NaHepes	10% PEG 4000 5% Isopropanol	4 days

Crystal screen 1 and Crystal screen 2

There were 12 conditions that could give rise to crystals from Crystal screen 1 and 2. Crystals growing in conditions of these two screening kits were small and needle-shaped or formed clusters composed of small needle crystals (Fig. 3.19). The 12 crystallization conditions generating crystals were very similar. As shown in table 3.6, the precipitant in most of the conditions contained different concentrations of PEG, explaining why crystals of BMP-2 and CV2-VWC1 complex from these crystallization conditions were similar in morphology. Crystals usually appeared in one to two days after the setting.

Crystal screen Lite, Crystal Screen Salt, and Crystal screen Index

Crystal screen Lite is similar to Crystal Screen I, but with the precipitant concentration halved. Only two conditions, #28 and #41, of the crystal screen Lite resulted in crystals. The shape of the crystals from # 28 and # 41 were also similar to that from Crystal Screen I.

#52 of Crystal Screen Salt was the only condition that gave crystals with different shapes. The crystals are needle-shaped, but larger than those from the other conditions (Fig. 3.19L). Precipitant of this condition was 2.4 M $(\text{NH}_4)_2\text{HPO}_4$, instead of PEG solutions. Small needle shaped crystals could also be obtained from two crystallization conditions of Index screen.

In summary, binary complex of BMP-2 /CV2-VWC1 could easily form needle-shaped crystals or clusters in different concentrations of PEG. Furthermore, one condition with 2.4 M $(\text{NH}_4)_2\text{HPO}_4$ resulted in larger needle-shaped crystal without cluster formation.

Results

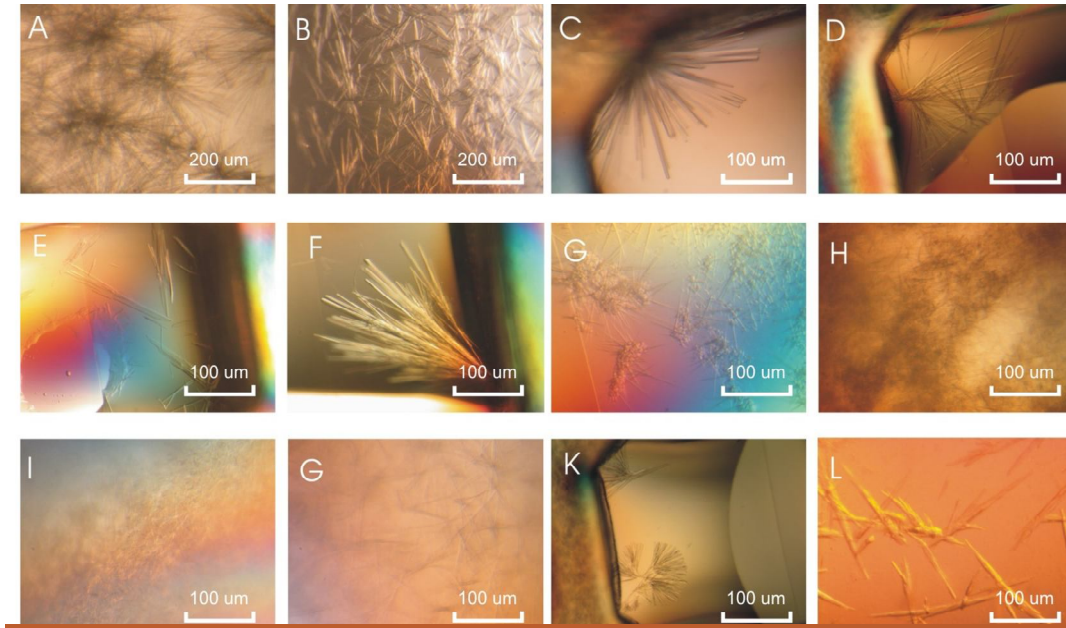


Figure 3.19 Crystals of the CV2-VWC1/ BMP-2 binary complex obtained from initial screening. Crystallization conditions were

- A: 30% PEG 4000, 0.1 M Na Citrate, pH 5.6, 0.2 M NH_4OAc (HR-I # 9)
- B: 30% PEG 8000, 0.1 M Na Cacodylate, pH 6.5, 0.2 M $(\text{NH}_4)_2\text{SO}_4$ (HR-I # 15)
- C: 30% PEG 4000, 0.1 M Tris/HCl pH 8.5, 0.2 M NaOAc (HR-I # 22)
- D: 30% PEG 8000, 0.1 M Na Cacodylate, pH 6.5, 0.2 M NaOAc (HR-I # 28)
- E: 20% PEG 4000, 20% Isopropanol, 0.1 M Na Citrate, pH 5.6 (HR-I # 40)
- F: 20% PEG 4000, 10% Isopropanol, 0.1 M Na Hepes, pH 7.5 (HR-I # 41)
- G: 30% PEG 8000, 0.2 M $(\text{NH}_4)_2\text{SO}_4$ (HR-I 30)
- H: 30% PEG 1500 (HR-I # 43)
- I: 2.0 M $(\text{NH}_4)_2\text{SO}_4$, NaOAc pH 4.6 (HR-I # 47)
- J: 15% PEG 8000, 0.5 M Lithium Sulfate (HR-I # 50)
- K: 30% PEG2000, 0.1 M Na Acetate pH 4.6, 0.2 M $(\text{NH}_4)_2\text{SO}_4$ (HR-II 13)
- L: 2.4 M $(\text{NH}_4)_2\text{HPO}_4$, 0.1 M Tris/HCl, pH 8.5 (HR-Salt # 52)

Crystal optimization

Optimization of crystallization conditions was performed according to the hanging Drop Vapor Diffusion method using 24 well VDX Plates. 1 ul of the protein samples was mixed with 1 ul of the screening reagents. Crystallization was performed according to the initial screening results. Protein concentration, precipitant concentration, pH, salt concentration, and temperature were taken into account for optimization.

Results

Crystal screening I # 9, # 15, # 22, # 28, # 40, crystal screening-index # 23 and Salt # 52 from the 17 conditions that gave rise to crystals in initial screening, were chosen to be further optimized by the hanging drop diffusion method. Unfortunately, after optimization the crystals were still needle or silk shaped and the resolution of crystals from all these conditions was only about 8-10 Å (Fig. 3.20). One exception was the optimization of HR-Salt # 52 whose crystals were bigger than that in the initial screen and had a diffraction resolution of 5-6 Å. This condition was thus selected for further optimization.

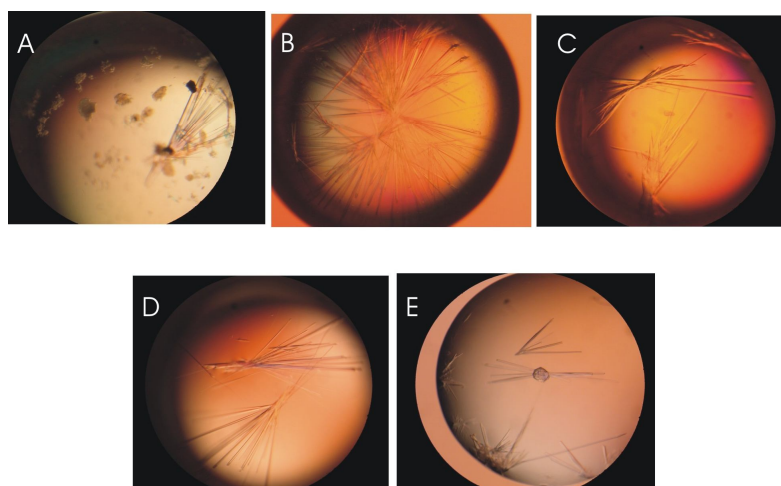


Figure 3.20 Crystals of BMP-2/CV2-VWC1 complex in the conditions of:

A: 30% PEG4000, 0.1 M Tris/HCl pH 8.5, 0.2 M NaOAc, 10% Glucose (HR-I # 22)

B: 25% PEG 8000, 0.1 M NaCacodylate pH 6.0, 0.2 M NaOAc, 10% Sucrose (HR-I # 28)

C: 30% PEG 4000, 0.1 M Nacitrate pH 5.6, 0.2 M (NH₄)OAc (HR-I 9)

D: 20% PEG 8000, 0.1 M NaCacodylate, pH 6.5, 0.2 M (NH₄)₂SO₄ (HR-I 15)

E: 25% PEG 4000, 20% Isopropanol, 0.2 M Nacitrate, 0.2 M (NH₄)OAc, 12% Sucrose (HR-I 40)

Optimization of HR-Salt # 52

2.4 M (NH₄)₂HPO₄, 0.1 M Tris/HCl, pH 8.5 was the basic composition of HR-Salt # 52. In order to optimize the conditions for crystallization, protein concentration, precipitant concentration, pH, additives, cryoprotectants, buffer and temperature were considered. We could observe the difference between the crystal images when the concentration of precipitant (NH₄)₂HPO₄ of HR-Salt # 52 varied from 2.4 M to 2.0 M. Rod-shaped crystals were obtained at room temperature in pH 8.5 when the

Results

$(\text{NH}_4)_2\text{HPO}_4$ concentration was between 2.2 -2.4 M. However, the third dimension of the crystals was very thin when the precipitant concentration was 2.4 M, and the crystals were silk-shaped when with a precipitant concentration of 2.0 M (Fig. 3.21 B and D). Interestingly, the crystals grow in 2.2 M $(\text{NH}_4)_2\text{HPO}_4$ were mainly rod-shaped and the third dimension was relatively larger (Fig. 3.21 C).

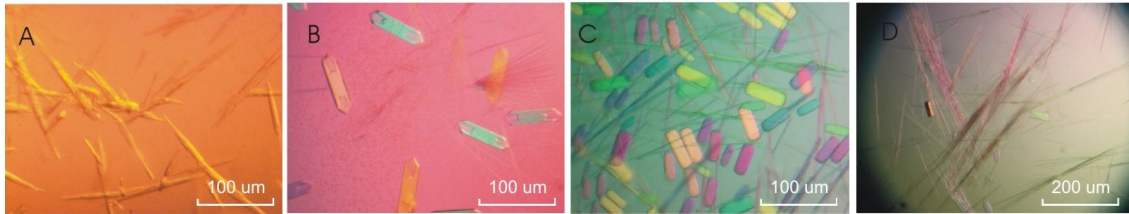


Figure 3.21 Crystal images of CV2-VWC1/BMP-2 complex at different precipitant concentrations. The conditions are as follows:

A: Initial screening of CV2-VWC1/BMP-2 complex in 2.4 M $(\text{NH}_4)_2\text{HPO}_4$, 0.1 M Tris/HCl, pH 8.5

B: 2.4 M $(\text{NH}_4)_2\text{HPO}_4$, 0.1 M Tris/HCl, pH 8.5

C: 2.2 M $(\text{NH}_4)_2\text{HPO}_4$, 0.1 M Tris/HCl, pH 8.5

D: 2.0 M $(\text{NH}_4)_2\text{HPO}_4$, 0.1 M Tris/HCl, pH 8.5

Protein concentrations of 5, 8 and 10 mg/ml were then tested at room temperature. 5 mg/ml appeared to be too low, since the crystals were small needle shaped at this protein concentration (Fig. 3.22A). In contrast, protein concentrations of 8 and 10 mg/ml gave similar rod-shaped crystals mixed with needle-shaped crystals (Fig. 3.22B and C). Considering most of the crystals were formed in 24 hours, which seems to be too fast, we selected the relatively lower protein concentration (8mg/ml) for further optimization.

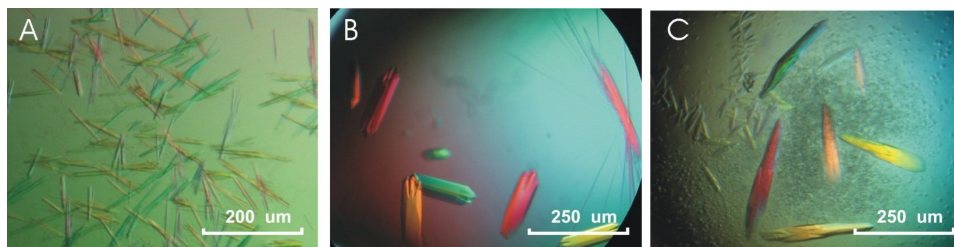


Figure 3.22 Crystal images of CV2-VWC1/BMP-2 complex from different protein concentrations of 5 (A), 8 (B) and 10 mg/ml(C) in 2.2 M $(\text{NH}_4)_2\text{HPO}_4$, 0.1 M Tris/HCl pH 8.5, 10 % Glycerol reservoir solution.

Results

When temperature was tested, we found that crystals grown at 4°C were very small and needle-shaped, and no further growth was observed after 3 weeks.

For pH optimization, using pH 8.5, 7.5 and 7.0, no significant differences for the shape of crystals was found. However, there were bigger club-shaped crystals at pH 7.5.

5-15 % of generally used cryoprotectants, Glucose, Sucrose and Glycerol were tested in the crystallization of the binary complex BMP-2/CV2-VWC1. We found that crystals were much smaller than in the original conditions without cryoprotectant when Glucose was added. The largest crystals were grown in conditions with sucrose added (Fig. 3.23C). Several other cryoprotectants from a Hampton Kit (HR2-122) were also tested, but without significant improvement in crystal formation or their diffraction patterns. Finally, larger rod-shaped crystals with better diffraction were obtained in 5-10% glycerol and sucrose.

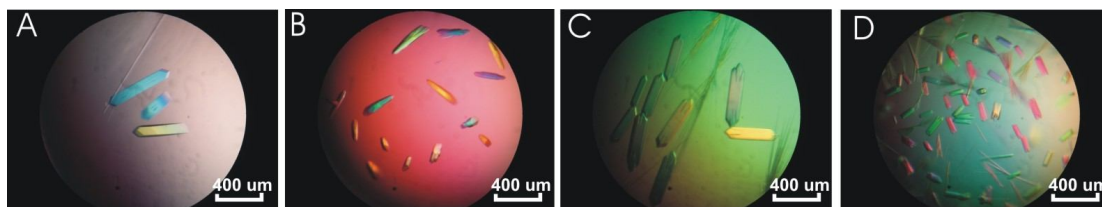


Figure 3.23 Images of crystals of CV2-VWC1 /BMP-2 complex growing in different cryoprotectants in 2.2 M $(\text{NH}_4)_2\text{HPO}_4$, 0.1 M Tris/HCl pH 7.5. (A) no cryoprotectant, (B) with 5 % Glycerol, (C) with 5 % Sucrose, (D) with 5 % Glucose.

Data collection

After optimization, crystals of native protein complex of BMP-2 and CV2-VWC1 grew by mixing 1 ul of protein complex solution (8 mg/ml) with 1 ul 2.2 M $(\text{NH}_4)_2\text{HPO}_4$, 0.1 M Tris pH7.5, 5-15% Sucrose or Glycerol and placing this mix over reservoir solution consisting of 2.2 M $(\text{NH}_4)_2\text{HPO}_4$, 0.1 M Tris pH7.5, 5-15% Sucrose or Glycerol at room temperature. Crystals grew to final size within two weeks. About 10% of the protein crystals could diffract to 3-4 Å, while the other crystals diffracted

Results

to 4-6 Å.

A complete native data set was acquired from wild-type BMP-2 and CV2-VWC1 on beamline X06SA at the SLS (Villigen, Switzerland). The data set from 180 1° frames consists of 17 136 unique reflections. The overall Rmerge was 10.5% in the resolution range 41.3–3.1 Å and the completeness was 100% (Table 3.7). The crystal belonged to the tetragonal space group P41 (or P43), with unit-cell parameters $a = b = 82.4$, $c = 140.9$ Å. To solve the structure of the complex, molecular replacement was employed using the software Phaser (94) with the BMP-2 dimer (23) as the search template. A clear molecular- replacement solution (LLG = 2292 for both BMP-2 dimers, with RFZ = 10.5 and 4.7 and TFZ = 25.0 and 36.2 for the first and second BMP-2 molecule, respectively) allowed the placement of two BMP-2 dimers in the asymmetric unit and thus confirmed the tetragonal space group P41 as the correct enantiomer. However, electron density for the CV2-VWC1 domains was vastly incomplete and did not allow the building of a model of the full complex (Fig. 3.24). Using the NMR structures of a distantly related VWC domain of Procollagen IIA (90) as an additional search template was unsuccessful.

Table 3.7 Data-collection and processing statistics for the native crystal (complex of BMP-2/CV2-VWC1).

Values in parentheses are for the highest resolution shell.

Beamline	PXI, X06SA,SLS
Detector	MAR 225 mosaic
Space group	$P4_1$
Temperature (K)	100
Unit-cell parameters (Å, °)	$a = b = 82.44$, $c = 140.88$, $\alpha = \beta = \gamma = 90$
Wavelength (°)	1.1048
Resolution range (Å)	41.33–3.10 (3.27–3.10)
No. of reflections (total/unique)	126906/17136
Completeness (%)	100.0 (100.0)
Multiplicity	7.4 (7.4)
R_{merge}^\dagger	0.105 (0.334)
$\langle I/\sigma(I) \rangle$	18.2 (5.7)

$^\dagger R_{\text{merge}}$ is defined as in Table 3.8

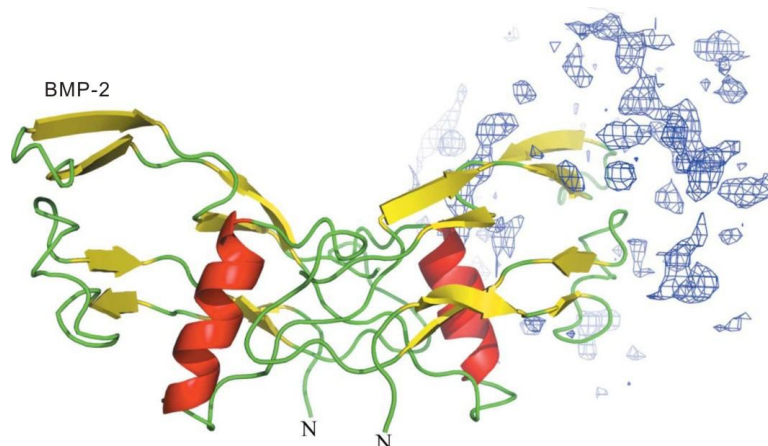


Figure 3.24 Molecular replacement was initially used to perform phasing of the BMP-2/CV2-VWC1 complex. Although two BMP-2 dimers could be unambiguously placed in the asymmetric unit (only one is shown), only residual electron density was observed for the CV2-VWC1 molecule at the putative binding site as determined from mutagenesis data (54). One BMP-2 dimer is shown in ribbon representation, with part of an $F_{obs} - F_{calc}$ electron-density map contoured at 1.5σ shown around 15 \AA of the putative CV2-VWC1-binding site.

Additive screening

Three Hampton Additive screening kits (72 conditions) were tested to improve the crystal quality. The basic composition of the buffer was 2.2 M $(\text{NH}_4)_2\text{HPO}_4$, 0.1 M Tris, pH 7.5. 10% Sucrose was also added to keep the crystals in Cryoprotection. 1 ul of additive solution was first mixed with 4 ul reservoir solution, and then 1 ul of the 5 ul mixture was mixed with 1 ul of protein sample. This 2 ul mixture was equilibrated against 1 ml of reservoir solution. In most conditions, proteins precipitated or gave rise to very thin needle-shaped crystals. However, larger rod-shaped crystals were obtained at room temperature in conditions with several additives. These include 3% w/v 1,6 Hexanediol, 0.01 M L-Cysteine, 0.01 M Spermidine, 0.01 M Hexaminecobalt Trichloride, 0.01 M Betaine monohydrate, 0.01 M Ammonium sulfate and 4% 2,2,2-Trifluoroethanol (TFE). The diffraction resolution from these crystals was about 3-4 Å in conditions with additives of 0.01 M L-Cysteine and 0.01 M Ammonium Sulfate (Fig. 3.25). Generally, crystal quality was improved and about 40%-50% crystals with the two additives could diffract to 3-4 Å. The other 5 additives that resulted in larger crystals did not make any improvement on the diffraction resolution.

Results

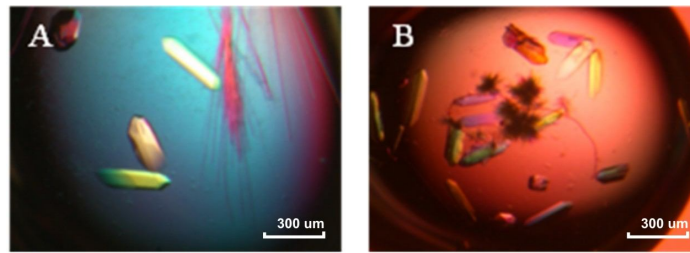


Figure 3.25 Crystal images of CV2-VWC1 /BMP-2 complex in 2.2 M $(\text{NH}_4)_2\text{HPO}_4$, 0.1 M Tris/HCl, 10% Sucrose pH 7.5 with (A) 0.1 M $(\text{NH}_4)_2\text{SO}_4$ and (B) 0.01 M L-Cystein.

3.3.3 Crystallization of the Selenomethionine-labelled complex of BMP-2 and CV2-VWC1

As the collected data from crystals of wild type BMP-2 and CV2-VWC1 did not allow building a model of the complex, the SeMet-driven MAD approach was therefore applied for experimental phasing. Since the number of native methionine residues was rather low when using the wild-type proteins (four methionines per BMP-2 dimer and none in CV2-VWC1), several residues in BMP-2 and CV2-VWC1 were substituted in order to increase the number of methionines. In BMP-2 the substitutions Y41M and F91M were chosen owing to their position outside the BMP type I and type II receptor-binding epitopes (30). Interaction analysis using BIAcore showed that the binding affinity of BMP-2 (F41M,Y91M) to CV2-VWC1 is unaltered.

As an alternative approach, SeMet labelling of CV2-VWC1 was also planned. However, since the wild-type sequence of CV2-VWC1 lacks methionines and no structural data for CV2-VWC1 were available, four polar residues were selected for exchange to methionine (Fig. 3.26). The single CV2-VWC1 mutants S28M, N33M, K39M and E41M could be expressed and purified in a similar manner as described for the wild-type protein. Their binding characteristics to BMP-2 were analysed by BIAcore, showing that all mutants exhibited wild-type binding affinity.

Results

CV2-VWC1 S28M N33M K39M E41M

10 20 30 40 50
GSLWITGTEA SCENEGEVLH IPNITDNPIC **MCVCLMQKAE** **CMQM**KCAPLA EDCALVVVKQT
60
GACCEKCKG

Figure 3.26 Amino acids sequence of CV2-VWC1 S28M, N33M, K39M and E41M. 4 amino acids were replaced with Methionines that were marked in red.

Additionally, the CV2-VWC1 double mutants S28MN33M, N33ME41M and N33MK39M were prepared in order to further increase the number of methionines or to enable the use of unlabelled BMP-2 in the complex; however, only the variant CV2-VWC1 (N33M,K39M) could be prepared and isolated. Yield of CV2-VWC1 (N33M,K39M) was very low, producing only 100-120 ug/g wet bacteria. The incorporation of SeMet was checked by Mass spectrometry, which suggested that the labelling efficiency was about 90%-98% for the N33MK39M double mutant and the S28M single mutant (Fig. 3.27).

Results

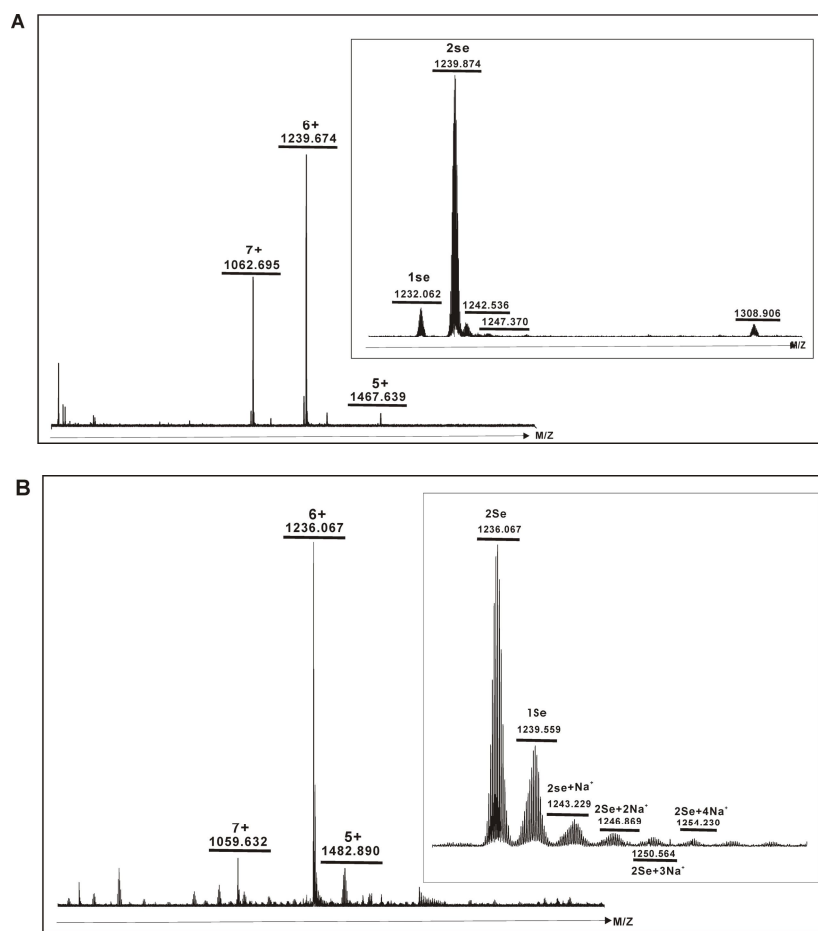


Figure 3.27 Mass spectrometry analysis of CV2-VWC1 mutants. A: CV2-VWC1 (N33M,K39M); B: CV2-VWC1 (S28M).

The SeMet-labelled variants CV2-VWC1 (N33M,K39M) and SeMet CV2-VWC1(S28M) were used for complex preparation with SeMet BMP-2; however, only the complex SeMet BMP-2/SeMet CV2-VWC1(S28M) yielded diffracting crystals. The complexes SeMet BMP-2(Y41M,F91M)/CV2-VWC1 and SeMet BMP-2/SeMet CV2-VWC1(S28M) formed crystals similar to those of the wild-type proteins (Fig. 3.28).

For data acquisition, SeMet BMP-2 (Y41M,F91M)/CV2-VWC1 crystals were grown at 294 K from 2.0 M $(\text{NH}_4)_2\text{HPO}_4$, 0.1 M Tris/HCl pH 7.5, 8%(v/v) glycerol, 5%(w/v) sucrose, whereas SeMet BMP-2/SeMet CV2-VWC1(S28M) crystals were grown at 294 K from 2.2 M $(\text{NH}_4)_2\text{HPO}_4$, 0.1 M Tris/HCl pH 7.5, 10%(v/v) glycerol. Crystallization experiments were performed at a protein concentration of 8 mg/ml. Crystals grew reproducibly within 10 d to approximate dimensions of $200 \times 500 \times$

Results

500 μm (Fig.3.28).

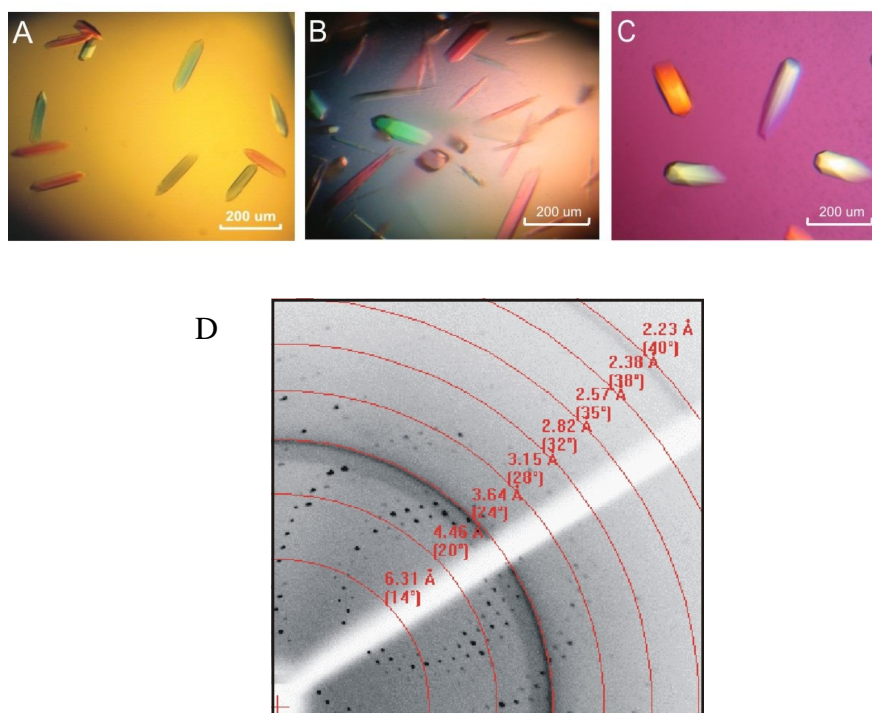


Figure 3.28 Crystal images of the complex of SeMet BMP-2 and SeMet CV2-VWC1. A: Complex of SeMet BMP-2 (Y41M, Y91M) and wt CV2-VWC1. B: Complex of SeMet wt BMP-2 and SeMet VWC1(28M). C: Complex of SeMet wt BMP-2 and SeMet VWC1(33M39M). D: X-ray diffraction pattern from a crystal of SeMet BMP-2 (F41M, Y91M)/CV2-VWC1 complex. The diffraction limit of these crystals was about 2.7 Å.

Three-wavelength data sets (inflection, peak and remote) were recorded from both crystals and processed using the software HKL-2000 (95) and CrystalClear (Rigaku) (Table 3.8). Despite the fact that crystals of the two complexes grew under identical conditions, crystals of the complex SeMet BMP-2 (Y41M, F91M)/CV2-VWC1 belonged to space group $I4_1$, while crystals of the complex SeMet BMP-2/SeMet CV2-VWC1 (S28M) belonged to space group $P4_22_12$ (or $P4_32_12$). Trials to index the diffraction data of either SeMet BMP-2 (F41M, Y91M)/CV2-VWC1 or SeMet BMP-2/SeMet CV2-VWC1 (S28M) in the ‘wrong’ space group failed, showing that two clear crystal forms exist despite the almost identical unit-cell parameters (Table 3.9). Analysis of the data using the software SHARP/_{auto}SHARP (96) showed the presence of seven out of eight Se sites in the asymmetric unit for crystals of the

Results

complex SeMet BMP-2 (Y41M,F91M)/CV2-VWC1 and six out of six Se sites for crystals of the complex SeMet BMP-2/SeMet CV2-VWC1 (S28M).

Table 3.8 Data collection and processing statistics for SeMet-labelled crystals. Values in parentheses are for the highest resolution shell.

	SeMet BMP-2 (Y41MY91M)/CV2-VWC1			SeMet BMP-2/SeMet CV2-VWC1 (S28M)		
	Infection	Peak	Remote	Infection	Peak	Remote
Beamline	BL141,BESSY					
Detector	MAR 225 mosaic					
Space group	$I4_1$			$P4_12_12$		
Temperature (K)	100			100		
Unit-cell parameters (\AA , °)	$a = b = 83.70$, $c = 139.63$, $\alpha = \beta = \gamma = 90$			$a = b = 86.71$, $c = 139.19$, $\alpha = \beta = \gamma = 90$		
V_M ($\text{\AA}^3 \text{Da}^{-1}$)	3.32			3.58		
Solvent content (%)	62.7			65.3		
Wilson B factor (\AA^2)	57.2			51.1		
Wavelength (\AA)	0.9799			0.9799		
Resolution range (\AA)	36.20–2.70 (2.80–2.70)	40.68–2.70 (2.80–2.70)	36.16–2.70 (2.80–2.70)	37.36–3.00 (3.11–3.00)	41.39–3.00 (3.11–3.00)	33.90–3.00 (3.11–3.00)
No. of reflections (total/unique)	43616/13191	43563/13146	43969/13165	59992/11181	60048/11176	39023/9668
Completeness (%)	99.7 (99.7)	99.7 (99.8)	99.7 (100.0)	100.0 (100.0)	99.9 (100.0)	86.4 (90.6)
Multiplicity	3.31 (3.23)	3.31 (3.27)	3.34 (3.27)	5.37 (5.51)	5.37 (5.50)	4.04 (3.97)
R_{merge}^\dagger	0.090 (0.342)	0.100 (0.342)	0.099 (0.381)	0.086 (0.311)	0.094 (0.312)	0.099 (0.350)
R_{anom}^\ddagger	0.059	0.074	0.071	0.043	0.067	0.069
$\langle I/\sigma(I) \rangle$	8.9 (3.3)	7.7 (3.1)	8.0 (2.7)	11.0 (4.4)	9.9 (4.5)	9.0 (3.5)
Phasing	7 out of 8 Se sites identified, two-wavelength MAD (SHARP)			6 out of 6 Se sites identified, three-wavelength MAD (SHARP)		
R_{cullis}	0.84	0.72	0.84	0.83	0.71	0.83
R.m.s. lack of closure	0.76	0.92	0.75	0.86	0.93	0.82
Phasing power	1.01	1.38	1.09	1.18	1.41	1.13
Mean figure of merit	0.57			0.57		
Figure of merit after DM	0.74			0.81		

$\dagger R_{\text{merge}} = \sum_{hk} \sum_i |I_i(hkl) - \langle I(hkl) \rangle| / \sum_{hk} \sum_i I_i(hkl)$, where $I_i(hkl)$ is the intensity of the i th observation of the unique reflection hkl , $\langle I(hkl) \rangle$ being the mean of the intensities of all observations of reflection hkl . $\ddagger R_{\text{anom}} = \sum_{hk} (I^+ - I^-) / \sum_{hk} (I^+ + I^-)$.

Table 3.9 Comparison of R_{merge} values for the three data sets. Values in parentheses are for the highest resolution shell. All R_{merge} values were obtained for the same resolution range of the peak data set and native data set. The respective resolution ranges are shown in Tables 3.8 and 3.9. The values in bold designate the data used for structure solution. R_{merge} is defined as in Table 3.9.

	$I4_1$	$P4_1$	$P4_12_12$
SeMet BMP-2 (Y41MY91M)/CV2-VWC1	0.10 (0.342)	†	†
SeMet BMP-2/SeMet CV2-VWC1 (S28M)	†	0.111 (0.364)	0.094 (0.312)
BMP-2/CV2-VWC1	†	0.096 (0.383)	0.267 (0.526)

† Indexing not possible in this space group.

In both cases almost all or all the expected Se positions were identified, confirming the presence of a binary complex consisting of a BMP-2 dimer and two CV2-VWC1 domains in the asymmetric unit (Fig. 3.29), which is appropriate for a solvent content of around 63–65% ($V_M = 3.3\text{--}3.6 \text{ \AA}^3 \text{Da}^{-1}$) (97). The complex structure of BMP-2 and CV2-VWC1 was elucidated by Dr. Thomas D. Mueller.

Results

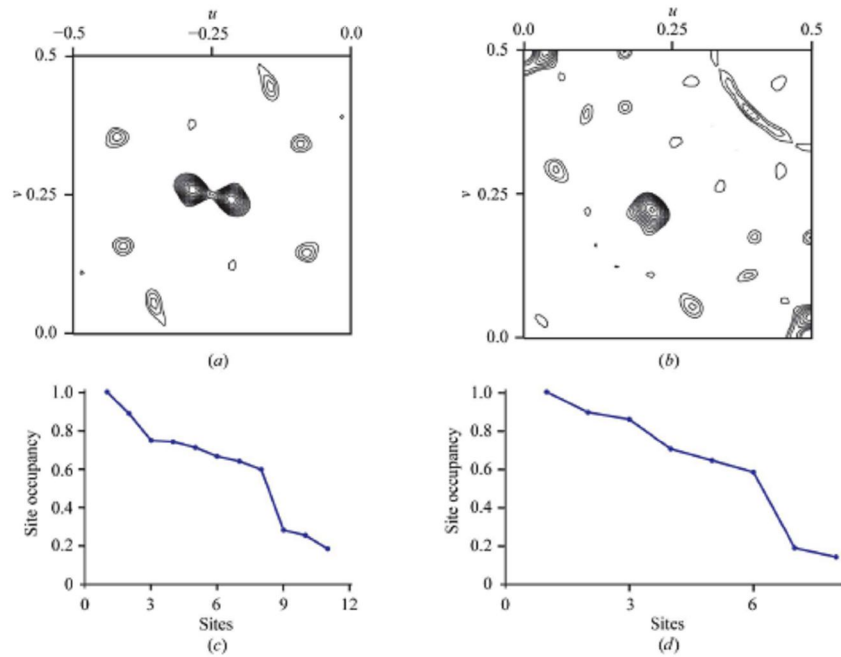


Figure 3.29 Harker sections of anomalous Patterson maps of the complexes (a) BMP-2(F41M,Y91M)/CV2-VWC1 (only $z = 0.5$ shown) and (b) BMP-2/CV2-VWC1(S28M) (only $z = 0.5$ shown). The anomalous Patterson maps were produced with CNS, illustrating the data quality for phasing. SHELXD analysis of the data derived at peak wavelength suggest the presence of eight (c) and six (d) Se sites in the complexes BMP-2(F41M,Y91M)/CV2-VWC1 and BMP-2/CV2-VWC1(S28M), respectively, of which seven in BMP-2(F41M,Y91M)/CV2-VWC1 and all six in BMP-2/CV2-VWC1(S28M) could be refined with SHARP.

The structures of the mutant proteins are now being determined in order to determine the molecular basis of the formation of different space groups by the two complexes. The final structures of the complexes of CV2-VWC1 bound to BMP-2 will provide the first insights into how BMP ligands are recognized by modulator proteins of the chordin family, of which CV2 is a member.

3.3.4 NMR analysis of CV2-VWC1

We also analyzed the solution structure of CV2-VWC1. Preliminary analysis provided a nice NMR signal (Fig. 3.30). We would like to see how it is in the solution structure of CV2-VWC1, and to compare the structure of this domain alone in solution and that in complex and to see whether they have differences. The data sets for ^{15}N single and $^{15}\text{N}^{13}\text{C}$ double-labelled proteins have been collected. The NMR analysis of labelled CV2-VWC1 is underway.

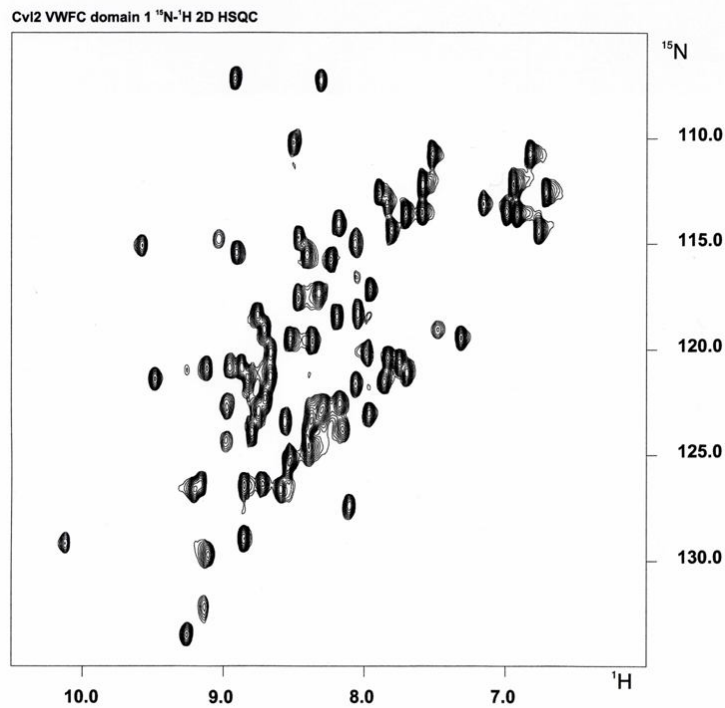


Figure 3.30 Preliminary analysis of ^{15}N -labelled CV2-VWC1 by NMR.

3.4 Structure of the binary complex of BMP-2 and CV2-VWC1

3.4.1 Binding epitopes of BMP-2 for CV2-VWC1

General description of the structure

The complex consists of a single BMP-2 dimer and two molecules of the CV2-VWC1 (Fig. 3.31). For BMP-2, every monomer contains residues Lys11-Arg114. The residues Leu1-Gly66 were included in the CV2-VWC1 structures.

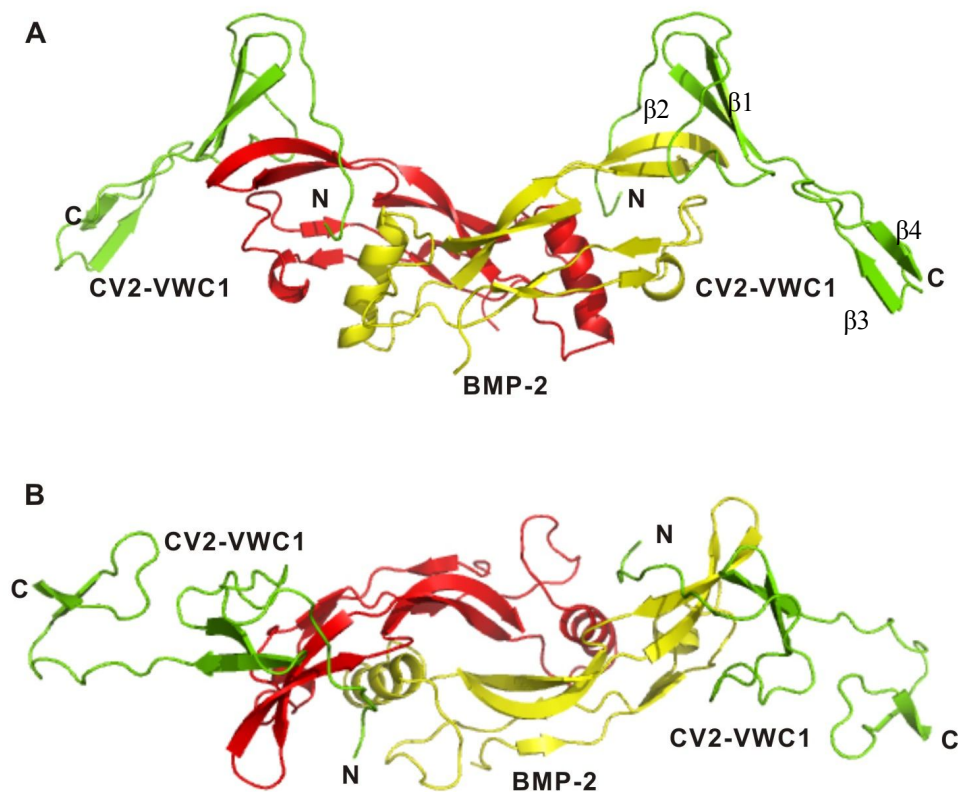


Figure 3.31 The structure of the BMP-2 and CV2-VWC1 complex. A, side view of the structure. BMP-2 dimer is shown in yellow and red, displaying the butterfly conformation. The two CV2-VWC1 domains are shown in green. B, a top view of the complex. The colour scheme is the same as in A.

The butterfly-shaped BMP-2 homodimer in this structure has the same overall structure as that in the binary complex of BMP-2/BMPR-IAecd and the ternary complex of BMP-2/BMPR-IAecd/ActR-IIB (30, 32). Two CV2-VWC1 domains are located on two sides of the BMP-2 dimer and each VWC1 domain interacts with one

Results

monomer of BMP-2. There are no contacts between the VWC1 domains. The VWC1 domain manifests an N-terminal segment (residues Leu1 to Ser8), which we refer to as a clip, an N-terminal subdomain SD1 (Cys9–Lys42) and a C-terminal subdomain SD2 (Cys43–Gly66). Two disulfide-bonds within each subdomain maintain their rigidity, while a fifth disulfide-bond links the two subdomains. The N- and C-terminal subdomains are predominantly composed of a β -sheet configuration. Strands β 1, β 2, and β 3, β 4, respectively, form the N- and C-terminal antiparallel sheets (Fig. 3.31A). The disulfide bonds of VWC1 are constructed as C1-C4, C2-C8, C3-C5, C6-C9 and C7-C10, which are consistent with that of Collagen IIA VWC domain (Fig. 3.32). The concave surface formed by the N-terminal β -sheets contacts the convex surface of the BMP-2 fingers (knuckle epitope), while the C-terminal subdomain displays no contact with BMP-2 (Fig. 3.31). Notably, the N-terminal clip of VWC1, contacts the concave surface of the BMP-2 wrist epitope, constituted by residues from α 3-helix of the BMP-2 monomer A, and the fingers of the monomer B, and the edge between the wrist and knuckle epitopes.

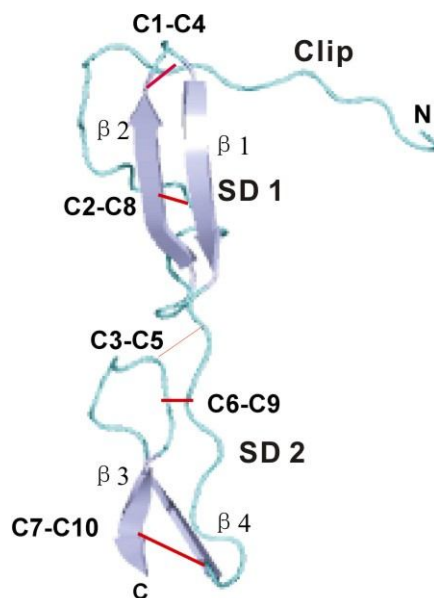


Figure 3.32 Structure of the CV2-VWC1 domain, the 4 β strands are colored in lightblue and 5 disulfide bonds are marked.

Two distinct contact interfaces

The total buried interface between VWC1 and BMP-2 is 1578 Å², including 618 Å² (2 x 309 Å²) in the wrist epitopes and 960 Å² (2 x 480 Å²) in the knuckle regions. These are not comparable to the type I and type II receptor interfaces, 2 x 1130 Å² for BMP-2/BMPR-IA_{ecd}, 2 x 660 Å² for BMP-7/ActR-II_{ecd} and 2 x 774 Å² for Act/ActR-IIB_{ecd} (30, 22).

The binding sites for the CV2-VWC1 SD1 and clip overlap with both type I and type II receptor binding sites. The first binding contacts are formed by the clip that is bound predominantly through hydrophobic interactions. The hydrophobic side chain of Ile 2 of VWC1 inserts into a hydrophobic pocket on BMP-2 formed by Trp 28, Trp 31, Val 63, Tyr 103 and Met 106 (Fig. 3.33A), mimicking a similar insertion of Phe 85 of BMP receptors BMPR-IA into the hydrophobic cleft on BMP-2 (Fig. 3.33B) (30). This residue is thought to be a key determinant of all type I receptors. Although site 1 overlaps only partially with type I receptor binding site, VWC1 is able to inhibit the binding of BMPR-IA to BMP-2, probably due to the abolishment of the Phe 85 insertion.

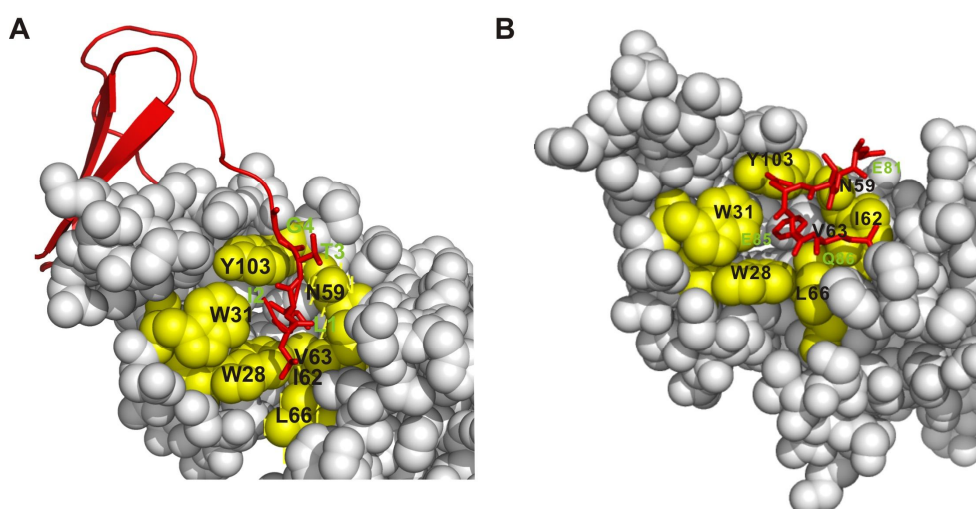


Figure 3.33 First ligand-binding interface of BMP-2 and CV2-VWC1 domain. A. part of the VWC1 clip binds to the wrist epitope of BMP-2. B. Phe 85 of BR1A inserts into the hydrophobic cleft of BMP-2.

Results

The second binding site is formed by hydrophobic residues on the concave surface of VWC1 (Ala 7, Ile 18, Ile 21, Ile 27, Ala 36) that pack with hydrophobic BMP-2 residues (Val 33, Ala 34, Pro 35 on finger 1, and Leu 90, Val 98, and Leu 90 on finger 2) (Fig. 3.34A). In addition, the amide and carbonyl of Thr 5 and the amide of Ala 7 of VWC1 form three hydrogen bonds with Asn 102 and Leu 100 of BMP-2, respectively (Fig. 3.34B). Although the buried surface in this binding site is smaller than those of type II receptor interfaces (480 \AA^2 versus $660\text{-}774 \text{ \AA}^2$), it overlaps almost perfectly with the core region of the type II receptor-binding sites, as seen in previous structures.

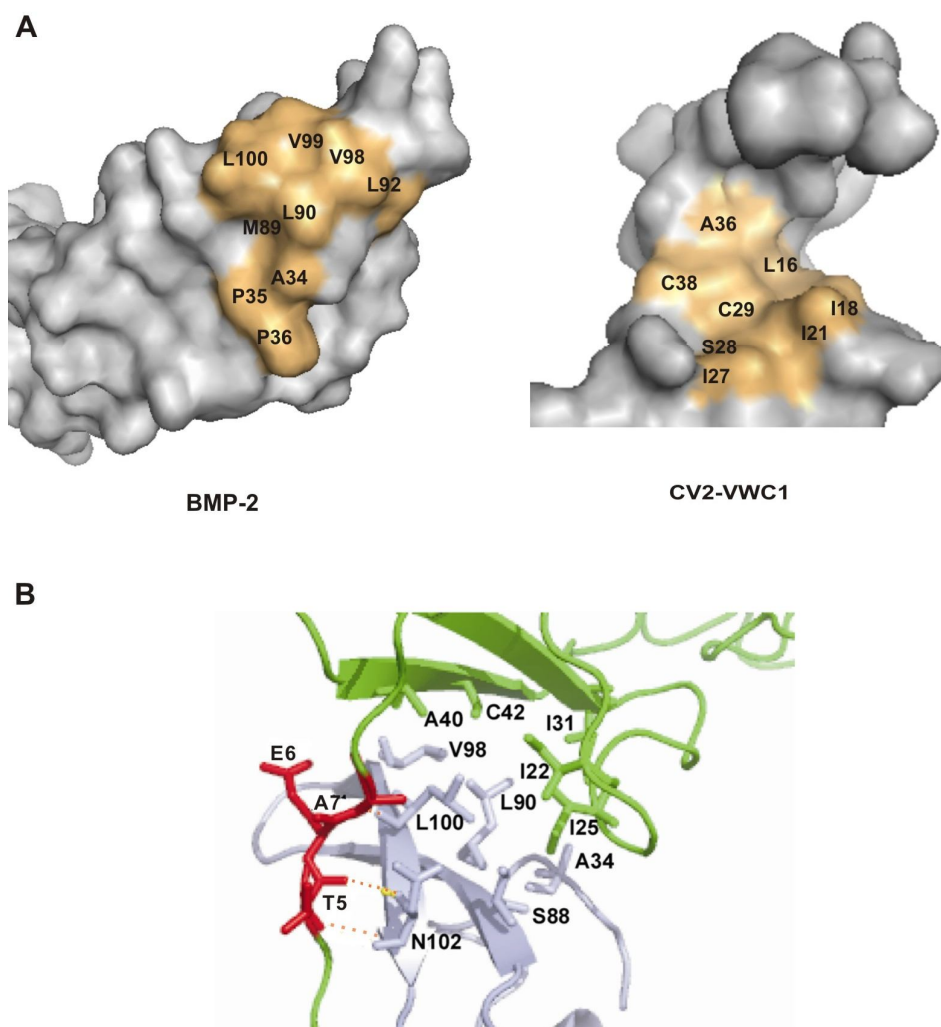


Figure 3.34 Second Ligand-binding interface of BMP-2 and CV2-VWC1 domain. A. Open-book view of the hydrophobic interface of BMP-2 and CV2-VWC1 domain. B. The hydrogen bonds between BMP-2 Leu 100, Asn 102 and CV2-VWC1 Ala 7, Thr 5 are shown by dashed lines.

Because of these two interaction sites, CV2-VWC1 can inhibit BMP-2 from binding

Results

to both type I and type II receptors. However, the functional epitopes and determinants, i.e., the sites and residues important for binding, are more sufficiently determined by mutagenesis (see below).

3.4.2 Key interactions between CV2-VWC1 and BMP-2

We generated an array of BMP-2 mutants in the wrist and knuckle epitope for type I and type II receptors to delimit binding epitopes for CV2 and CV2-VWC1 (Table 3.7).

Table 3.7 Mutational analysis of BMP-2 interaction with CV2 and CV2-VWC1. The binding affinities of wild-type BMP-2 (WT) for full-length CV2 and VWC domains are set to 1. Relative affinities show the influence of the mutations on binding.

Variant	Epitope	CV2	VWC1
		Relative K_D (Apparent K_D nM)	
F49A	Wrist	1.0	1.1
P50A	Wrist	1.3	1.8
L51P	Wrist	1.1	1.3
A52R	Wrist	1.2	1.8
S69R	Wrist	1.4	1.6
M106A	Wrist	4.1	3.3
A34D	Knuckle	13	9
H39D	Knuckle	1.6	3.3
S88P	Knuckle	1.3	1.9
L90A	Knuckle	3.4	3.3
V98P	Knuckle	1.0	2.0
L100P	Knuckle	4.5	11
L100K	Knuckle	119	135
L100P/N102D	Knuckle	275	300

According to the structure of the ternary complex of BMP-2/BMPRII/ActRII (32), six variants mutated in the wrist epitope and seven variants mutated in the knuckle

Results

epitope (Table 3.7) were selected for analyzing the interaction of BMP-2 with CV2 and CV2-VWC1 by Biacore analysis. The binding characteristics of the five wrist and three knuckle epitope mutants for different receptor ectodomains have been described elsewhere (34, 35). The additional mutants S88P, V98P and L100P bound to type II receptors with reduced affinities. The M106A mutant exhibited a reduced affinity for type I receptors. It has been shown that the corresponding mutant of M108A in activin behaved as an activin antagonist, possibly owing to its disrupted binding to type I receptor ActR-IB. The decrease in binding affinities between BMP-2 mutants and CV2/CV2-VWC1 reflect the influences of the amino acid substitutions in the wrist and knuckle epitope for binding.

CV2-VWC1 showed similar decreased affinities to some of the BMP-2 variants like those for full-length CV2, suggesting that the epitopes of BMP-2 for the VWC1 domain of CV2 are same to those of BMP-2 for the whole CV2 protein (Table 3.7). This result is consistent with the observation that CV2-VWC1 governs all binding affinity in CV2 (Table 3.4).

Remarkably, the variant L100K exhibited a dramatic decreased affinity for CV2/CV2-VWC1 compared to that of L100P. This effect was even more pronounced for a L100K/N102D double mutant. When variants L100K and L100K/N102D were immobilized on the chip, the binding of CV2/CV2-VWC1 to these mutants was too weak to be measured. Taken together, these results demonstrate that CV2/CV2-VWC1 binds to the BMP-2 knuckle epitope mainly by hydrophobic interactions and Leu 100 of BMP-2 is a hot spot for CV2/CV2-VWC1 binding. The results of the mutational analysis are consistent with the crystal structure analysis showing that the two sites of BMP-2 are involved in binding.

Our mutational analysis indicated that the binding epitope of BMP-2 for CV2 not only overlaps with the knuckle epitope, but also partially overlaps with the wrist epitope, as the wrist epitope mutant M106A exhibited 4.1- and 3.3-fold lower affinities to CV2

Results

and CV2-VWC1, respectively (Table 3.7). These results fit perfectly with the structure of the BMP-2/VWC1 complex, which demonstrates that the clip and SD1 of VWC1 bind to the knuckle and wrist epitopes respectively. Previous studies showed that the M106A mutant bound to the wrist epitope binding protein CHL2-VWC3 with reduced binding affinity, but bound to the knuckle epitope binding protein CHL2-VWC1 normally. Interestingly, the affinity of M106A for Chordin VWC1 and VWC3 are also 100- and 11-fold lower than the wt protein, respectively, even though the results of the mutational analysis clearly indicated that these two domains bind to the knuckle epitope of BMP-2 (54). These results suggest that besides CV2-VWC1, other VWC domains can also simultaneously bind both the knuckle and wrist epitopes of BMP-2.

To define the contribution of the two subdomains for binding, we expressed the N-terminal subdomain with Cys 26 mutated to Serine, and thus no free cysteine remained in the protein. This construct (VWC1- Δ SD2) has a similar affinity for BMP-2 to that of the wt CV2-VWC1. This result suggests that the binding region of CV2-VWC1 is located in the N-terminal subdomain SD1. Similarly, to check the contribution of clip in binding, two truncation mutants were generated. The mutants VWC1- Δ clip1 and VWC1- Δ clip2 showed a 135- and 2400-fold lower affinity respectively than wt VWC1, indicating that the clip plays an important role in binding (Table 3.8).

Results

Table 3.8 Binding affinities of different CV2-VWC1 constructs with BMP-2

	K_D (equ) ^a (nM)	$k_{on} \times 10^6$ ($M^{-1}s^{-1}$)	$k_{off} \times 10^{-2}$ (s^{-1})	K_D (k_{on}/k_{off}) (nM)	V/W
VWC1	-	1.2	2.4	20	1
VWC1-Δclip1	2700	0.012 ^b	3.2		135
VWC1-Δclip2	48000	0.0005	2,4		2400
VWC1-ΔSD2	-	1.2	4	33	1.6

^c: VWC1: GSWLITGTEAS-----G
 VWC1- Δ clip1: GSEAS-----G
 VWC1- Δ clip2: GS-----G
 VWC1W- Δ SD2: GSWLITGTEAS---C26S---K

a: equilibrium binding

b: Calculated by equation $k_{on} = k_{off} \times K_D$ (equ)

c: N-terminal residues, point mutation and ends of the constructs

Table 3.9 Geometry of hydrogen bonds in the BMP-2 and CV2-VWC1 interface.

CV2-VWC1	BMP-2	Distance(Å)	Hydrogen bond	Variant
T3 (O)	N59 (ND2)	3. 21	MC-SC	a T3P
T3 (N)	N59 (OD1)	3. 16	MC-SC	a T3P
T5 (O)	N102 (N)	2. 29	MC-MC	a T5P
T5 (N)	N102 (O)	3. 23	MC-MC	a T5P
A7 (N)	L100 (O)	2. 95	MC-MC	b L100P/L100K

MC, main chain; SC, side chain.

a CV2-VWC1 variants

b BMP-2 variants

Results

In order to define the binding determinants of CV2-VWC1 for BMP-2, an array of CV2-VWC1 mutants were constructed according to the crystal structure (Fig. 3.35). The expression and purification procedure of the mutant proteins was the same as that for wt CV2-VWC1.

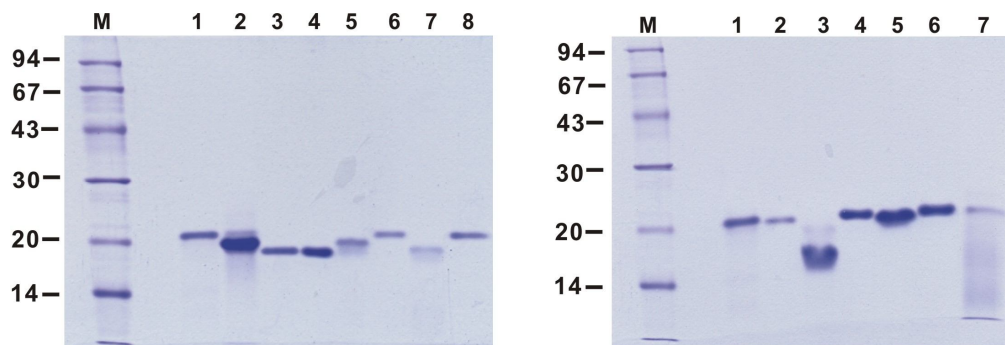


Figure 3.35 SDS-PAGE analysis of purified CV2-VWC1 mutants. A: Lane 1 wt VWC1, lane 2 VWC1- Δ clip1, lane 3 I18A, lane 4 I18E, lane 5 I18R, lane 6 I27A, lane 7 I27R and lane 8 36R under non-reducing conditions. B: lane 1 wt VWC1, lane 2 I21A, lane 3 I21R, lane 4 L1A, lane 5 L1R, lane 6 I2A and lane 7 I2R under non-reducing conditions.

The binding affinities of the CV2-VWC1 mutants for BMP-2 were analyzed by Biacore. As the SD1 binds to the BMP-2 knuckle epitope by hydrophobic bonds, which are formed mainly by Ile 18, Ile 21, Ile 27, Ala 36 of CV2-VWC1, these residues were thus mutated to Ala or Arg. The clip of CV2-VWC1 binds to the wrist epitope of BMP-2 by hydrogen bonds and hydrophobic interactions, in which Leu 1, Ile 2, Thr 3 and Thr 5 were mutated. Table 3.10 shows that no “hot” spot in the clip and SD1 was found for the binding. Most of the mutants have decreased affinities for BMP-2, particularly the mutants I21A and I21R, which showed 10- and 40-fold decreased affinities, respectively, compared with wt CV2-VWC1. In the clip region, the I2A mutant showed a 6-fold lower affinity, highlighting the importance of the “knob-into-hole” interaction for binding. Thr3 contributes only marginally to binding, as the T3P mutant demonstrated only a 2.5-fold lower affinity. In contrast, Thr5 contributes strongly to binding, since the clip mutant T5P in which the main chain hydrogen bonds were broken, exhibited about 21-fold lower affinity. The contribution

Results

of the hydrogen-bond between the Ala7 amide and the BMP-2 Leu100 carbonyl could be estimated from the 20-fold difference in the binding affinities of the two truncation mutants Δ clip1 and Δ clip2, whose interaction only differs in this Hydrogen-bond. In summary, the binding in the SD1 involves several weak hydrophobic binding, and the residues Ile2, Thr 5 and Ala 7 of the clip contribute strongly to the binding to BMP-2. The clip residues and N-terminal β -sheets that form a concave surface work cooperatively for the binding, CV2-VWC1 thus binds to BMP-2 through both hydrogen bonds and hydrophobic interactions (Table 3.10).

Table 3.10 Binding affinities of CV2-VWC1 mutants for BMP-2.

	K_D (equ) ^a (nM)	$k_{on} \times 10^6$ ($M^{-1}s^{-1}$)	$k_{off} \times 10^{-2}$ (s^{-1})	K_D (k_{on}/k_{off}) (nM)	V/W
VWC1	-	1.2	2.4	20	1
VWC1-L1A	-	1.3	2.8	22	1
VWC1-L1R	-	1.2	2.8	23	1
VWC1-I2A	127	-	-	-	6.4
VWC1-I2R	66	-	-	-	3.3
VWC1-T3P	-	0.95	4.8	50	2.5
VWC1-T5P	417	0.18 ^b	7.5		21
VWC1-I18A	-	0.88	4.4	50	2.5
VWC1-I18R	-	2	8.9	45	2.3
VWC1-I21A	200	-	-	-	10
VWC1-I21R	790	-	-	-	40
VWC1-I27A	185	-	-	-	9.3
VWC1-I27R	160	-	-	-	8
VWC1-A36R	227	-	-	-	11

a: equilibrium binding

b: Calculated by the equation $k_{on} = k_{off} \times K_D(\text{equ})$

Results

As shown in Fig. 3.36, 200 nM CV2-VWC1 was able to completely inhibit the binding of 50 nM BMP-2 to immobilized BMPER-IA and ActR-IIB, similar to that of the complete CV2 protein. This result indicates that CV2 and CV2-VWC1 inhibit the binding of BMP-2 to both type I and type II receptors.

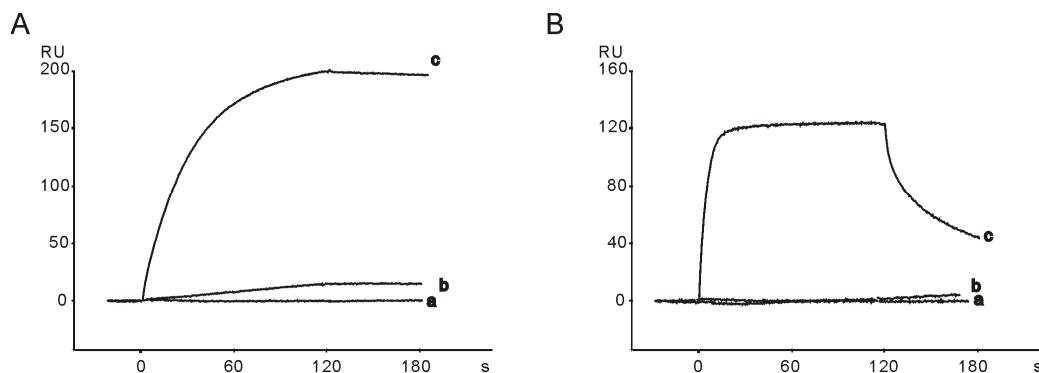


Figure 3.36 Inhibition of the binding of BMP-2 to type I and with type II receptors by CV2 and CV2-VWC1 in Biacore. BMPER-IA (A) and ActR-IIBecd (B) were immobilized on the chip surface. 50 nM BMP-2 plus 150 nM CV2 (a) and 200 nM CV2-VWC1 (b) respectively, and 50 nM BMP-2 alone (c) were injected over the chip surface.

3.5 Biological activity of CV2 and CV2-VWC1 in cell assay and *in vivo*

3.5.1 Inhibition of BMP-2 signaling by CV2 and CV2-VWC1

The inhibitory capability of CV2 and CV2-VWC1 was assayed in C2C12 cells. CV2 inhibited alkaline phosphatase (ALP) activity induced by 10 nM BMP-2 with an IC_{50} of 11 nM, in the same range as chordin (68). CV2-VWC1 was also able to inhibit BMP-2 signaling, but with a four times higher IC_{50} value (40 nM) (Fig. 3.37B). Using the Biacore interaction analysis, CV2-VWC1 bound to BMP-2 with the same affinity as CV2, and showed similar inhibitory activity with an *in vitro* receptor competition experiment (Fig. 3.36). Therefore, the different inhibitory capabilities of the CV2-VWC1 domain and full-length CV2, suggest that other parts of the CV2 molecule play an inhibition role in the cell culture assay.

Results

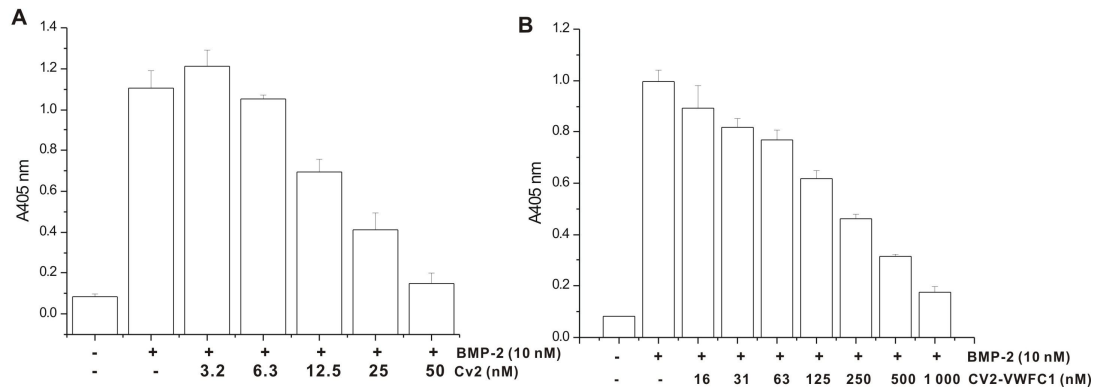


Figure 3.37 Inhibitory properties of CV2 and CV2-VWC1. Increasing doses of (A) CV2 and (B) CV2-VWC1 were applied to inhibit BMP-2 (10 nM)-induced alkaline phosphatase (ALP) activity in serum-starved C2C12 cells assay.

The mutants of CV2-VWC1 show different inhibition activity to BMP-2, basically consistent with their binding affinity results to BMP-2. Wild-type CV2-VWC1 exhibits an IC_{50} of 50 nM. VWC1 Δ SD2 that has only 1.6 fold lower affinity to BMP-2 than wt CV2-VWC1 shows a four-fold lower IC_{50} . All other variants, which have a reduced binding affinity for BMP-2 *in vitro*, can not (such as VWC1- Δ clip1 and A36R) or only partially (such as I2A) inhibit BMP-2 induced ALP induction (Fig. 3.38).

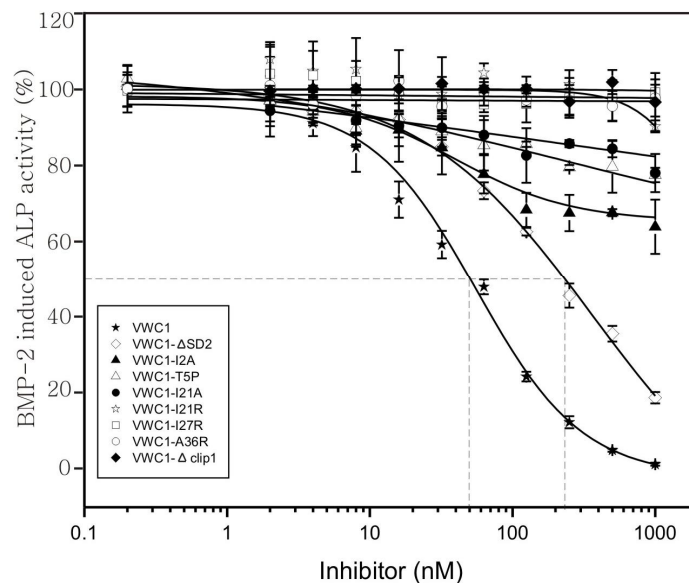


Figure 3.38 Biological activity of CV2-VWC1 in C2C12 cells. Alkaline phosphatase expression was induced by 10 nM BMP-2. Inhibition efficiency of CV2-VWC1 was determined by increasing doses of CV2-VWC1 protein added to the BMP-2.

3.5.2 BMP-2 variants that inhibit CV2 and CV2-VWC1

In a previous study, a BMP-2 “receptor dead” mutant L51P was generated, which does not bind BMPR-IA but binds to type II receptors normally (35). It does not induce measurable ALP activity in C2C12 or ADTC5 cells and has no dominant-negative inhibitory effect. The L51P mutant binds normally to Noggin (35), chordin, CHL2 as well as CV2 (50). It can release inhibition of BMP-2-induced ALP activity by Noggin (33) and also by CV2 in a dose-dependent manner as shown in Fig. 3.39. In the current study, five double or triple mutants of BMP-2 were generated, in which the knuckle epitope mutants A34D, L90A, V98P, L100P and L100K/N102D were introduced in addition to the L51P mutation. These mutants showed a dramatically reduced affinity for BMPR-IA, decreased affinities for BMPR-II, ActR-II, ActR-IIB, and normal or decreased affinities for CV2. The inhibition of BMP-2 activity by CV2 could be partially reversed to different extents by the five tested mutants. Fig. 3.39 shows that 25 nM L51P could completely relieve the inhibition of 10 nM BMP-2-induced ALP activity by CV2, and was also complete for the L51P/V98P double mutant, slightly weaker for L51P/L90A, significantly weaker for L51P/L100P and L51P/A34D, and completely lost for the L51P/L100P/K102D mutant. The release of the inhibition of BMP-2 activity by CV2 basically correlates with the binding affinities of the mutants to CV2 (Fig. 3.39). Taken together, these results open the perspective that BMP-2 mutants can be constructed, which specifically block single BMP modulator proteins.

Results

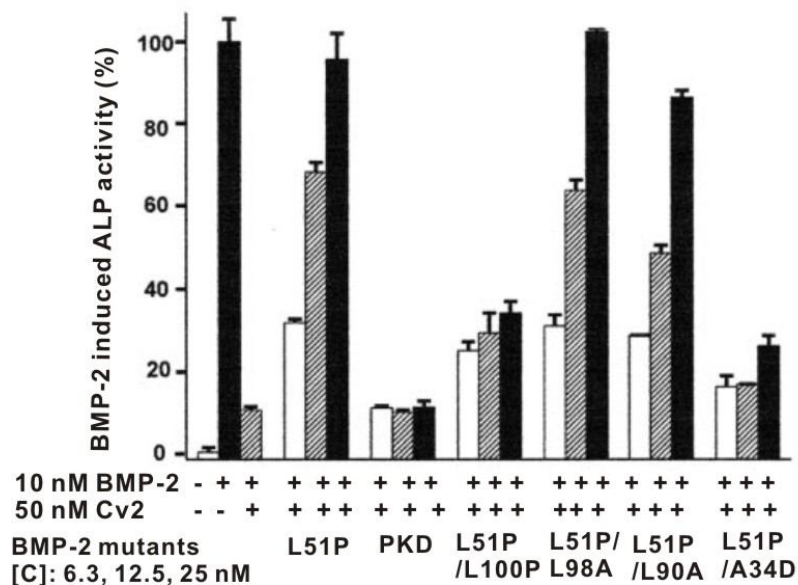


Figure 3.39 Release of CV2-inhibited BMP-2 activities by BMP-2 mutants. Induction of alkaline phosphatase (ALP) by 10 nM BMP-2 in C2C12 cells was inhibited to 10% by 50 nM CV2. L51P and the combined double mutants do not induce ALP activity. The release of CV2-inhibited BMP-2 activity was determined at the indicated mutant concentrations. PKD, L51P/L100K/N102D-BMP-2.

3.5.3 Biological activity of CV2-VWC1/CV2 *in vivo*

In order to analyze the effects of CV2 on BMP signaling *in vivo*, 2 mutant constructs of CV2 were generated: a full length construct in which I21 was mutated to R and a construct based on CV2-CM in which I21 was mutated to R (78). These two constructs were injected into the zebrafish embryos. In contrast to wild type CV2, which can both dorsalize and ventralize (Fig. 3.40b,c,g,h), injection of CV2-I21R mRNA into the zebrafish embryos only led to a weakly ventralized phenotype (Fig. 3.40d,g,h). This suggests that the BMP-2 antagonizing properties of CV2-VWC1 correspond to the anti-BMP activity in the context of the whole CV2 protein. When we additionally introduced the mutation I21R, which strongly attenuates BMP-2 binding of VWC1, into CV2-CM, a full rescue from dorsalization could be observed. Thus, the BMP-binding of VWC1 seems to be solely responsible for the anti-BMP activity of overexpressed CV2 *in vivo*, whereas the weak ventralizing activity (pro-BMP activity) of wt CV2 is very likely to be independent of BMP binding. One important conclusion of the *in vivo* experiments in zebrafish is therefore that the two contrary anti- and pro-BMP activities can be structurally separated to different

Results

regions/domains of the full-length CV2. All CV2 *in vivo* experiments were performed in collaboration with the group of Dr. Matthias Hammerschmidt at the University of Freiburg.

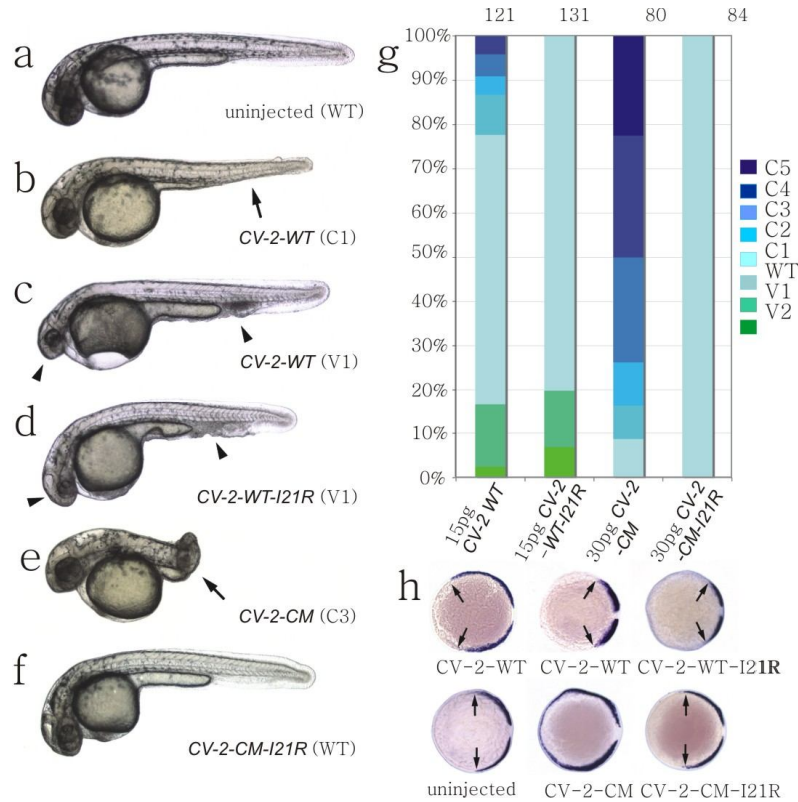


Figure 3.40 **(a-h)** Phenotypes of zebrafish embryos after mRNA injections. **(a-f)** Lateral views of 32 hpf embryos; arrows indicate dorsalized traits (loss of ventral tail fin/tail); arrowheads indicate ventralized traits (smaller head, expansion of ventral-most tissues). Injection of *cv2*-wt mRNA leads to both weakly dorsalized (C1 in **b**) or weakly ventralized (V1 in **c**) embryos, whereas injection of cleavage resistant construct *cv2*-CM mRNA causes strong dorsalization (C3 in **e**). Injections of mRNA of the mutants *cv2*-WT-I21R or *cv2*-CM-I21R result in weakly ventralized (**d**) or normal (**f**) embryos similar to those in **c** and **a**, respectively. **(g)** Graphical illustration of proportions of phenotypes generated on injection of different CV2 constructs. For classification, C5 (strong dorsalization) to V2 (strong ventralization) (78). **(h)** In situ hybridization of whole-mount 80% epiboly-stage embryos; animal pole views; dorsal, right. Arrows indicate the limits of dorso-lateral mesoderm marker *tbx24* (dark blue), which is expanded in dorsalized and reduced in ventralized embryos.

4. Discussion

More and more Chordin-like proteins are found to play important roles in development. The abundance of von Willebrand factor type C domain in extracellular matrix proteins and their ability to bind a variety of TGF- β superfamily members suggests a conserved function for these repeats in regulating growth factor signaling in the extracellular matrix (52). The primary objective of this study was to determine the complex structure of VWC repeats and TGF- β superfamily members. We solved the first structure of a complex between a BMP and a VWC domain, and analyzed in detail their binding affinities and specificities. The structure determined for BMP-2 bound to the VWC1 domain of CV2 provides new and interesting data, which in the future will augment an understanding of the cooperation of BMP-2 and CV2 during animal development. The methods for expression and purification of VWC domains provide a good example for the preparation of other VWC domain-containing proteins.

4.1 Expression and purification of VWC domains

VWC domains were prepared in insect cells or yeast cells in the previous studies (73, 85). Our studies here showed that VWC domains with 4-5 disulfide bonds could be expressed in *E. coli* in an active form. Some of the VWC domains could be obtained with very high yield. For instance, we can get ~ 2 mg CV2-VWC1 and ~ 1 mg CV2-VWC5/g wet bacteria. CV2-VWC1 was very stable, which could keep in active at 30 °C for up to 4 weeks, thus this makes it suitable for the NMR solution structure analysis. However, for other VWC domains, i.e., CV2-VWC2 and VWC4, which could be isolated only in low yields from *E. coli*, their expression methods still need to be explored. Protein renaturation from inclusion bodies can be a choice, because VWC3 of CHL-2 has been expressed in this way with higher yield than that as native fusion proteins (Huang and Zhang, unpublished). However, the appropriate buffers for

renaturation of VWC domains still need to be investigated.

Reverse phase HPLC was shown to be a good method for the VWC domains purification. During the purification, VWC domains are usually eluted by 26-27% acetonitrile, thus make them easily separated by reverse HPLC from other proteins such as thioredoxin, their dimer and multimer. Because of the common protein chemical features, reverse phase HPLC could be used as a good purification way for all VWC domains.

4.2 Binding affinity and specificity of VWC domains

BMP signaling is inhibited by modulator proteins through blocking type I and type II receptors. VWC domains are also able to prevent the binding of these two receptors to BMPs, which like Noggin that binds to the dimeric BMP-7 with very high affinity, occluding all four binding sites of the BMPs for the type I and type II receptors (45). Most of tested VWC domains such as Chordin VWC1, Chordin VWC3 and CHL-2 VWC1 bind mainly to knuckle epitope of BMP-2, but CHL2-VWC3 was found to bind preferentially to the wrist epitope of BMP-2 (54). For CV2-VWC1, its N-terminal SD1 binds to knuckle epitope of BMP-2, but its clip binds to the wrist epitope of BMP-2. Moreover, even for the same epitope of BMP-2, different determinants are found for different VWC domains.

The CV2-VWC1 domain is distinguished by the highest binding affinity for BMP-2 among the few analyzed VWC domains of the Chordin family (54). Our data showed that CV2 recognize BMP-2 in a mechanism that differs from that of other Chordin family members such as Chordin and CHL2 in two aspects. First, CV2 binds to BMP-2 via VWC1 with high affinity, which is comparable with the cooperative binding of two VWC domains in complete Chordin or CHL2. Second, Tsg that participate both Chordin/BMP-2 and CHL-2/BMP-2 interaction does not participate in

Discussion

CV2/BMP-2 interaction. Similar to full-length CV2, CV2-VWC1 alone could simultaneously block the binding of BMP-2 to both type I and type II receptors. The 4-fold lower inhibitory capacity of CV2-VWC1 in cell assay compared to complete CV2 is probably caused by the lack of the steric hindrance from other parts of CV2.

CV2-VWC1 binds to both knuckle and wrist epitopes of BMP-2 with an affinity of 20 nM, which was similar to the high affinity of BMP-2 for its type I receptor (30). It is reported that other tested VWC domains bind to either BMPs knuckle or wrist epitope and their affinity for BMPs are only 100 nM-2000 nM (54). However, upon removal of the clip, the affinity of CV2-VWC1 for BMP-2 reduced more than 2000-fold. This suggests that the clip help to stabilize the binding of VWC1 to BMP-2. It also indicates that the other VWC domains without clip might bind BMPs weakly, and the high affinity binding could be generated by cooperating with other parts. For instance, VWC1 and VWC3 of CHL-2 cooperatively form a 10 nM high affinity for BMP-2 (54).

It will be interesting to know how the epitopes of other VWC domains for BMP binding are constructed, because there are more than 500 VWC domain-containing proteins and no clear homology is found for these domains in alignment beside the cysteine pattern. It is tempting to speculate that the numerous disulfide bonds of VWC domains provide a scaffold for the attachments of a diversity of loops that can generate different binding specificities similar to an immunoglobulin. In the conotoxin superfamily comprising many hundreds of members with a disulfide-rich core, a similar principle has been established (48, 98).

Not all VWC domains have direct interaction with TGF- β superfamily members. Some of them are “silent” domains. The one VWC domain-containing protein CTGF can interact with BMPs, but only three of the four VWC domains of Chordin, two of the three VWCs of CHL2 and one of the five VWCs of CV2 can bind to BMPs (54, 55,, 90). The binding affinities of VWC domains for ligands vary. For instance, CV2

Discussion

binds to BMP-2 with high affinity and VWC1 governs all the binding of CV2 for BMPs. However, the VWC domains of Chordin and CHL-2 bind separately to BMPs with a low binding affinity and a high affinity could be only generated when they cooperate.

The VWC domains are highly diverse except the conserved cysteine sequence according to the alignment results (Fig. 4.1). Therefore, it is difficult to predict anything about why VWC domains have different binding features to TGF- β superfamily numbers from the amino acid sequence.

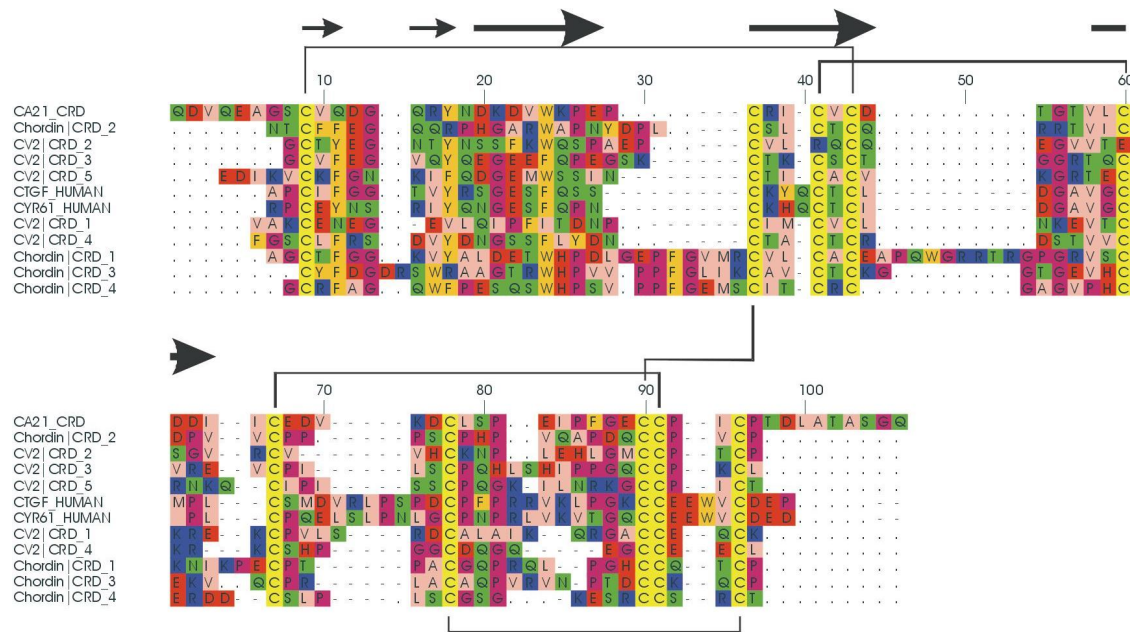


Figure 4.1 Alignment of the amino acid sequences of the VWC domains (CRD) of human Procollagen a2, mouse Chordin 1 to 4, zebrafish CV2 1 to 5, human CTGF and CYR61. Arrows indicate β -strands and lines indicate disulfide bonds as observed for the structure of the procollagen a2 VWC domain (from Prof. Sebald).

The binding affinity and specificity of CV2-VWC1 domain for BMPs also open the perspective to generate BMP-2 mutants as specific antagonists for VWC domains (Fig. 3.39). Studies showed that some of the VWC-containing proteins are involved in pathological process. For example, CTGF, which inhibits BMP signaling and promotes TGF- β activity via the binding of its VWC domain to BMP-4/TGF- β , has been shown playing a very important role in fibrotic disease (55). The multi-VWC

Discussion

domain-containing protein Kielin could attenuate the pathology of renal fibrotic disease by enhancing BMP signaling while suppressing TGF- β activation (57, 58). The functions of the VWC-containing proteins in these processes must be properly regulated. The antagonist specifically for the defined VWCs might be used in the therapeutic intervention of the VWC-containing protein-related diseases.

In this study, we found that the structure of CV2-VWC1 shares similarity with the VWC domain of Collagen IIA. They both contain two subdomains and the disulfide bond patterns are also identical. This implies that the structure of Collagen IIA VWC domain could be correctly folded. The reason for the absence of biological function for the Col IIA VWC is still not clear. Based on our structure of CV2-VWC1, the corresponding binding region of Col IIA to BMPs is largely inaccessible. BMP could bind only after a major rearrangement of the Col IIA VWC protein. This of course, would likely result in a low affinity. Study showed that the trimeric full-length Col IIA binds BMP-2 *in vivo* and *in vitro* (52, 91). These observations suggest that the intrinsic BMP affinity of single Col IIA VWC is low, and only when multiple VWC domains cooperate in full-length Col IIA, a high affinity is generated.

The binding and receptor blocking mechanisms of Noggin, Follistatin, and CV2 share some clear analogies, although their overall structures are completely unrelated (45, 50, 49). Noggin, Follistatin, and CV2-VWC1 differ vastly in size and architecture (Fig. 1.7 and Fig. 1.8), but all three modulator proteins and domains seem to interact with the ligand mainly via the type II receptor binding epitope. About 730 \AA^2 of surface area per molecule is buried in the knuckle epitope upon binding of Noggin to BMP-7, twice as much compared to the CV2-VWC1 SD1 binding to BMP-2. For Follistatin the complete type II receptor-binding site of Activin-A (Act-A) is covered by the domains FSD1 and FSD2 burying about 820 \AA^2 per molecule in the knuckle epitope.

Additionally, all structurally known modulator proteins block not only the type II receptor epitope but also the type I receptor epitope. The N-terminal domain of Follistatin binds in the wrist epitope of Activin-A, thereby inhibiting type I receptor binding (49). However, binding of Follistatin to BMPs might be different, as type I receptors and Follistatin were reported to bind simultaneously to BMP-4 (98). A clip in the N-terminal of Noggin, which is similar to the clip of CV2-VWC1, folds over finger 2 and binds in the BMP wrist epitope (45). The backbone Pro35–Ser38 of Noggin superimposes almost perfectly on the backbone of the corresponding residues Ile2–Thr5 in the clip of CV2-VWC1. Pro35 of Noggin makes a similar knob-into-hole interaction with BMP-7 as Ile2 of CV2-VWC1 with BMP-2. Noggin Ala36 and Ser38 form hydrogen bonds to Asn83 and Lys127 of BMP-7, similar to those of Thr3 and Thr5 of the CV2-VWC1 clip in the interaction with BMP-2. Mutagenesis showed that substitution of Pro35 by Arg leads to a 7-fold lower affinity for BMP-7 (45). Furthermore, familiar Symphalangism (48) results from the heterozygous mutation P35S, confirming the importance of the N terminus of Noggin in vivo.

4.3 VWC domains are multifunctional binding modules that exert multiple binding characteristics

Current reports indicate that the VWC domains are versatile binding modules which exhibit multiple binding characteristics. They bind not only to BMPs, but also to other VWC domains, for instance, CV2-VWC1 binds to VWC2 of Chordin, and CHL2-VWC1 and VWC3 bind to Tsg, which does not contain the VWC domain but participates in the regulation of BMP functions by Chordin-like proteins (54). Recently, drosophila CV2 was found to associate with the BMP receptor Tkv, one BMP type I receptor (Mihaela Serpe et al. unpublished). These reports also confirm that VWC domain-containing proteins such as CV2 regulate BMPs signaling in multiple levels. They modify BMP signaling through interacting with ligands, and also contacting with other BMPs regulating proteins and the receptors. Therefore the

isolated BMP regulators may integrate into a network in extracellular levels. To date, it is still unclear if those “silent” VWC domains exert a purely structural role or if they interact with other not yet identified proteins.

The binding epitope of CV2 for Chordin does not exist in one single domain, but is composed of two or more VWC domains that formed a composite interface. CV2-VWC1-4M could not bind to Chordin any more through successfully destroying this interface. It is interesting to see the *in vivo* effect of the Chordin binding deficiency mutant in which the same insertion as in CV2-VWC1-4M was introduced. The experiment is underway and the results might provide a clue for the pro-BMP activity of CV2.

The structure of CV2-VWC1 domain manifests a two subdomain architecture tethered by a flexible linkage. This makes it possible that the N-terminal subdomain clip and SD1 bind to BMPs and SD2 contributes to the binding for Chordin.

4.4 Mechanism of CV2 and CV2-VWC1 modulating BMP signaling

Previous studies showed that CV2 could be a pro- or anti-BMP factor, depending on different contexts (78, 79, 81, 82). CV2 at excessive doses inhibits the BMP-dependent differentiation of osteoblast and chondrocyte in cell culture system (82). The transfection of 293T cells with a CV2 cDNA-containing plasmid reduced cellular response to BMP-4 in a BMP-responding luciferase reporter assay (81). These results are consistent with our observation that excessive doses of CV2 and CV2-VWC1 inhibited BMP-2-induced ALP activity, and the CV2-VWC1 variants that have reduced binding affinity to BMP-2 can not or only partially inhibit the BMP-2 induced ALP induction. Our results showed that variant CV2-I21R only cause weakly zebrafish embryos ventralization, which is consistent with *in vivo* anti-BMP activity of CV2. However, *In vivo* studies showed that CV2 is an essential pro-BMP

Discussion

regulator during zebrafish gastrulation (78) and in mouse organogenesis (79).

Loss-of-function analysis of CV2 in *Xenopus* embryos and knock-out mice yielded controversial results with that of gain-of-function studies in cell culture systems (78, 79, 82). Loss-of-function basically showed CV2 play a promoting activity on BMP signaling, but gain-of-function studies showed both pro- and anti-BMP signaling activity. Although the mechanism of the *in vivo* pro-BMP activity of CV2 remains uncertain, our results in this study clearly showed that the anti- and pro-BMP activity is structurally separated to different regions/domains of the full-length CV2. The CV2-VWC1 alone, full-length CV2 and the uncleavable mutant CV2-CM exhibit the same binding affinity for BMP-2, which is competent with BMP receptors, result in their anti-BMP activity when they are at excessive doses. All the *in vitro* and *in vivo* anti-BMP activity of CV2 can be explained with this mechanism. To CV2-CM, it can bind to the proteoglycans in the extracellular matrix more effeciently than the cleaved wt CV2 (78). Therefore the anti-BMP signaling activity of uncleaved CV2 was increased compares to that of the wt CV2. Future study will have to determine if and how the uncleaved wt CV2 functions *in vivo*.

As shown in our *in vivo* zebrafish experiment, the pro-BMP activity (weak ventralizing activity) of wt CV2 is very likely to be independent of BMP binding. The physical interaction of Chordin and CV2 is one of the biggest possibilities for its pro-BMP activity. Chordin mainly acts as an antagonist of BMP signaling by binding to BMPs via its VWC domains, but CV2 can inhibit its interaction with BMPs through binding to Chordin-VWC2 domain. Thus, CV2 acquires a pro-BMP activity in this way. It is possible that the cleaved wt CV2, which only weakly binds to the proteoglycans in the extracellular matrix, binds to chordin *in vivo*. Rentzsch et al. also reported that embryological epistasis analyses revealed a significant dependence of CV2 activity on Chordin function (78). They found that CV2 promotes BMP signaling by antagonizing Chordin, otherwise CV2 cannot display its full pro-BMP effect. This notion of CV2-Chordin competition was further supported by CV2 overexpression

Discussion

studies, showing that application of CV2-N can rescue the dorsalization caused by Chordin, whereas it cannot compensate for the loss of BMP signaling caused by knockdown of BMPs (78). It remains to be established whether the binding of CV2 to Chordin is relevant to its pro-BMP activity and how the stimulation of BMP signaling is achieved.

According to previous results, CV2 functions as both a BMP antagonist and agonist depending on a number of factors, which include CV2 concentration, cell extracellular matrix, BMP modulator proteins that can interact with CV2 such as Chordin, and proteolytic processing and so on. In *Drosophila*, the cleavage is not required to affect the CV2 function on BMP signaling, but dCV2 was found to interact with Tkv type I BMP receptor (Mihaela Serpe et al. unpublished), which has not been confirmed in vertebrate. The mechanisms that explain the function of CV2 still need to be explored. Additionally, the functions of the four other VWC domains and the long C-terminal of the large CV2 molecule are still unknown. Elucidation of their functions may help to explain the complicated anti- and pro-BMP activities of CV2 in early embryogenesis. In general, the mechanism of CV2 regulating BMP activity should not be explained simply by one or two factors.

In this thesis, I described the expression of CV2-VWC domains. The interaction and biological analysis showed that CV2-VWC1 was responsible for binding of CV2 to BMPs. According to this result, VWC1 was used for preparation of the binary complex with BMP-2. After crystal structural analysis, we identified the binding determinants of CV2-VWC1 and BMP-2 by mutagenesis and interaction analysis. We provide the first structure of a complex between a VWC domain and a BMP ligand. Our results explain the mechanism by which CV2-VWC inhibit both the type I and type II receptor binding to BMP-2 and provide a paradigm for the large protein family which contains more than 80 VWC-containing proteins. Interestingly, CV2 binds to BMPs as well as BMP regulator Chordin. We found that the binding is not from one VWC domain, but a composite interface from at least two VWC domains. These

Discussion

findings are helpful in elucidating the biological function of CV2 and other BMPs modulators in regulating BMP activity.

5. References

1. Newfeld SJ, Wisotzkey RG, Kumar S. (1999) Molecular evolution of a developmental pathway: phylogenetic analyses of transforming growth factor-beta family ligands, receptors and Smad signal transducers. *Genetics*. **152**(2):783-95
2. Massagué J, Blain SW, Lo RS. (2000) TGF-beta signaling in growth control, cancer, and heritable disorders. *Cell*. **103**(2):295-309
3. DeRobertis EM, Kuroda H (2004) Dorsal-ventral patterning and neural induction in *Xenopus* embryos. *Annu Rev Cell Dev Biol* 20:285-308
4. Senn. (1889) Senn on the Healing of Aseptic Bone Cavities by Implantation of Antiseptic Decalcified Bone. *Ann Surg*. **10** (5):352-68
5. Canalis E, Economides AN, Gazzerro E. (2003) Bone morphogenetic proteins, their antagonists, and the skeleton. *Endocr Rev*. **24**(2):218-35
6. Gazzerro E, Canalis E. (2006) Bone morphogenetic proteins and their antagonists. *Rev Endocr Metab Disord*. **7**(1-2):51-65
7. Chen C, Grzegorzewski KJ, Barash S, Zhao Q, Schneider H, Wang Q, Singh M, Pukac L, Bell AC, Duan R, Coleman T, Duttaroy A, Cheng S, Hirsch J, Zhang L, Lazard Y, Fischer C, Barber MC, Ma ZD, Zhang YQ, Reavey P, Zhong L, Teng B, Sanyal I, Ruben SM, Blondel O, Birse CE. (2003) An integrated functional genomics screening program reveals a role for BMP-9 in glucose homeostasis. *Nat Biotechnol*. **21**(3):294-301
8. Hogan, B. L. (1996) Bone morphogenetic proteins in development. *Curr Opin Genet Dev*. **6**, 432-438
9. Schmierer B, Hill CS. (2007) TGF beta-SMAD signal transduction: molecular specificity and functional flexibility. *Nat Rev Mol Cell Biol*. **8**(12):970-82

References

10. Sebald, W., Nickel, J., Zhang, J. L., and Mueller, T. D. (2004) Molecular recognition in bone morphogenetic protein (BMP)/receptor interaction. *Biol Chem*, **385**, 697-710
11. Shi, Y., and Massague, J. (2003) Mechanisms of TGF-beta signaling from cell membrane to the nucleus. *Cell*, **113**, 685-700
12. Ducy P, Karsenty G. (2000) The family of bone morphogenetic proteins, *Kidney Int.* **57**(6):2207-14
13. Massague, J., Attisano, L., and Wrana, J. L. The TGF-beta family and its composite receptors (1994) *Trends Cell Biol.* **4**(5) 172-178
14. Miyazono, K., ten Dijke, P., Yamashita, H., and Heldin, C.-H. Signal transduction via serine/threonine kinase receptors (1994) *Semin Cell Biol.* **5**, 389 – 398
15. Attisano, L., Wrana, J. L., López-Casillas, F., and Massagué, J. (1994) TGF-beta receptors and actions. *Biochim. Biophys. Acta*, **1222**, 71-80
16. Kingsley, D. M. Identification and characterization of the infectious laryngotracheitis virus glycoprotein C gene. (1994) *Genes & Dev.* **8**, 133-146
17. Ventura, F., Doody, J., Liu, F., Wrana, J. L., and Massagué, J. (1994) Reconstitution and transphosphorylation of TGF-beta receptor complexes. *EMBO J*, **13**, 5581-5589
18. Wrana, J. L., Attisano, L., Wieser, R., Ventura, F., and Massagué, J. (1994) Mechanism of activation of the TGF-beta receptor. *Nature*. **370**, 341-347
19. Balemans, W. and Van Hul, W. (2002) Extracellular regulation of BMP signaling in vertebrates: a cocktail of modulators, *Dev Biol*, **250**, 231-250
20. Nickel J, Kotsch A, Sebald W, Mueller TD. (2005) A single residue of GDF-5 defines binding specificity to BMP receptor IB. *J Mol Biol.* **349**(5):933-47
21. Greenwald J, Groppe J, Gray P, Wiater E, Kwiatkowski W, Vale W, Choe S.

References

- (2003) The BMP7/ActRII extracellular domain complex provides new insights into the cooperative nature of receptor assembly, *Mol Cell*. **11**(3):605-17
22. Rebbapragada A, Benchabane H, Wrana JL, Celeste AJ, Attisano L. (2003) Myostatin signals through a transforming growth factor beta-like signaling pathway to block adipogenesis, *Mol Cell Biol*. **23**(20):7230-42
23. Scheufler, C., Sebald, W., and Hulsmeyer, M. J. (1999) Crystal structure of human bone morphogenetic protein-2 at 2.7 Å resolution, *Mol. Biol.* **287**, 103-115
24. McDonald, N. Q; Hendrickson, W. A., (1993) A structural superfamily of growth factors containing a cystine knot motif. *Cell*, **73**, 421-424
25. Eigenbrot C, Gerber N. (1997) X-ray structure of glial cell-derived neurotrophic factor at 1.9 Å resolution and implications for receptor binding. *Nat Struct Biol*. **4**(6):435-8.
26. Monica A. Brown, Qinghai Zhao, Kent A. Baker, Chethana Naik, Cecil Chen, Laurie Pukac, Mallika Singh, Tatiana Tsareva, Yanick Parice, Angela Mahoney, Viktor Roschke, Indra Sanyal, and Senyon Choe. (2005) Crystal Structure of BMP-9 and Functional Interactions with Pro-region and Receptors. *J. Biol. Chem.*, **280** (26): 25111-25118
27. Muller Y. A., Li B., Christinger H.W., Wekks J.A., Cunningham B. C., and de Vos A.M. (1997) Vascular endothelial growth factor: crystal structure and functional mapping of the kinase domain receptor binding site. *Proc. Natl. Acad. Sci*, **94m**: 7192-7197
28. McDonald , N. Q., Lapatto,R., Murray-Rust, J., Gunning, J., Wlodawer, A., and Blundell, T. L. (1991) New protein fold revealed by a 2.3-Å resolution crystal structure of nerve growth factor. *Nature*, **354**, 411-414
29. Kirsch, T., Sebald, W., and Dreyer, M. K. (2000) Crystal structure of the BMP-2-BRIA ectodomain complex. *Nat Struct Biol*, **7**, 492-496

References

30. Weber, D., Kotsch, A., Nickel, J., Harth, S., Seher, A., Mueller, U., Sebald, W., and Mueller, T. D. (2007) A silent H-bond can be mutationally activated for high-affinity interaction of BMP-2 and activin type IIB receptor. *BMC Struct Biol*, **7**, 6
31. Allendorph GP, Vale WW, Choe S. (2006) Structure of the ternary signaling complex of a TGF-beta superfamily member. *Proc Natl Acad Sci*, **103**(20):7643-8.
32. Kirsch, T., Sebald, W., and Dreyer, M. K. (2000) Crystal structure of the BMP-2-BRIA ectodomain complex. *Nat Struct Biol*, **7**, 492-496
33. Kirsch, T., Nickel, J., and Sebald, W. (2000) BMP-2 antagonists emerge from alterations in the low-affinity binding epitope for receptor BMPR-II. *Embo J*, **19**, 3314-3324
34. Keller, S., Nickel, J., Zhang, J. L., Sebald, W., and Mueller, T. D. (2004) Molecular recognition of BMP-2 and BMP receptor IA. *Nat Struct Mol Biol*, **11**, 481-488
35. Huang SS, Liu Q, Johnson FE, Konish Y, Huang JS. (1997) Transforming growth factor beta peptide antagonists and their conversion to partial agonists. *J Biol Chem*. **272**(43):27155-9
36. Wuytens G, Verschueren K, de Winter JP, Gajendran N, Beek L, Devos K, Bosman F, de Waele P, Andries M, van den Eijnden-van Raaij AJ, Smith JC, Huylebroeck D (1999) Identification of two amino acids in activin A that are important for biological activity and binding to the activin type II receptors. *J Biol Chem*. **274**(14):9821-7
37. Hatta T, Konishi H, Katoh E, Natsume T, Ueno N, Kobayashi Y, Yamazaki T. (2000) Identification of the ligand-binding site of the BMP type IA receptor for BMP-4. *Biopolymers*. **55**(5):399-406.
38. Wills, A., Harland, R. M., and Khokha, M. K. (2006) Twisted gastrulation is

References

required for forebrain specification and cooperates with Chordin to inhibit BMP signaling during *X. tropicalis* gastrulation *Dev Biol*, **289**, 166-178

39. Itoh F, Asao H, Sugamura K, Heldin CH, ten Dijke P, Itoh S, (2001) Promoting bone morphogenetic protein signaling through negative regulation of inhibitory Smads, *EMBO J*. **20**(15):4132-42

40. Nakao A, Imamura T, Souchelnytskyi S, Kawabata M, Ishisaki A, Oeda E, Tamaki K, Hanai J, Heldin CH, Miyazono K, ten Dijke P. (1997) TGF-beta receptor-mediated signaling through Smad2, Smad3 and Smad4, *EMBO J*. **16**(17):5353-62

41. Onichtchouk D, Chen YG, Dosch R, Gawantka V, Delius H, Massagué J, Niehrs C., (1999) Silencing of TGF-beta signalling by the pseudoreceptor BAMBI. *Nature*. **401**(6752):480-5

42. Grotewold L, Plum M, Dildrop R, Peters T, Rütger U.. (2001) Bambi is coexpressed with Bmp-4 during mouse embryogenesis. *Mech Dev.*, **100**(2):327-30

43. McMahon JA, Takada S, Zimmerman LB, Fan CM, Harland RM, McMahon AP. (1998) Noggin-mediated antagonism of BMP signaling is required for growth and patterning of the neural tube and somite, *Genes Dev.*, **12**(10):1438-52

44. Fürthauer M, Thisse B, Thisse C. (1999) Three different noggin genes antagonize the activity of bone morphogenetic proteins in the zebrafish embryo. *Dev Biol.*, **214**(1):181-96

45. Groppe, J., Greenwald, J., Wiater, E., Rodriguez-Leon, J., Economides, A. N., Kwiatkowski, W., Affolter, M., Vale, W. W., Belmonte, J. C., and Choe, S. (2002) Structural basis of BMP signalling inhibition by the cystine knot protein Noggin. *Nature*, **420**, 636-642

46. Zimmerman LB, De Jesús-Escobar JM, Harland RM. (1996) The Spemann organizer signal noggin binds and inactivates bone morphogenetic protein 4. *Cell*. **86**(4):599-606

References

47. Canalis E, Economides AN, Gazzerro E. (2003) Bone morphogenetic proteins, their antagonists, and the skeleton. *Endocr Rev.* **24**(2):218-35
48. Mangino, M., Flex, E., Digilio, M.C., Giannotti, A., and Dallapiccola, B. (2002). Identification of a novel NOG gene mutation (P35S) in an Italian family with symphalangism. *Hum. Mutat.* **19**, 308
49. Thompson TB, Lerch TF, Cook RW, Woodruff TK, Jardetzky TS. (2005) The structure of the follistatin:activin complex reveals antagonism of both type I and type II receptor binding. *Dev Cell*, **9**(4):535-43.
50. Harrington AE, Morris-Triggs SA, Ruotolo BT, Robinson CV, Ohnuma S, Hyvönen M. (2006) Structural basis for the inhibition of activin signaling by follistatin. *EMBO J.* **25**(5):1035-45.
51. Harrison CA, Chan KL, Robertson DM. (2006) Activin-A binds follistatin and type II receptors through overlapping binding sites: generation of mutants with isolated binding activities. *Endocrinology.* **147**(6):2744-53.
52. Larrain, J., Bachiller, D., Lu, B., Agius, E., Piccolo, S., and De Robertis, E. M. (2000) BMP-binding modules in chordin: a model for signaling regulation in the extracellular space. *Development*, **127**, 821-830
53. Garcia Abreu J, Coffinier C, Larraín J, Oelgeschläger M, De Robertis EM. (2002) Chordin-like CR domains and the regulation of evolutionarily conserved extracellular signaling systems. *Gene*, **287**(1-2):39-47
54. Zhang JL, Huang Y, Qiu LY, Nickel J, Sebald W. (2007) von Willebrand factor type C domain-containing proteins regulate bone morphogenetic protein signaling through different recognition mechanisms. *J Biol Chem.* **282**(27):20002-14
55. Abreu, J. G., N. I. Ketpura, B. Reversade, and E. M. De Robertis. 2002. Connective-tissue growth factor (CTGF) modulates cell signaling by BMP and TGF-beta. *Nat. Cell Biol.*, **4**:599-604.

References

56. Matsui M, Mizuseki K, Nakatani J, Nakanishi S, Sasai Y. (2000) Xenopus kielin: A dorsalizing factor containing multiple chordin-type repeats secreted from the embryonic midline. *Proc Natl Acad Sci.*, **97**(10):5291-6
57. Lin, J., Patel, S. R., Cheng, X., Cho, E. A., Levitan, I., Ullenbruch, M., Phan, S. H., Park, J. M., and Dressler, G. R. (2005) Kielin/chordin-like protein, a novel enhancer of BMP signaling, attenuates renal fibrotic disease. *Nat Med*, **11**:387-393
58. Lin J, Patel SR, Wang M, Dressler GR. (2006) The cysteine-rich domain protein KCP is a suppressor of transforming growth factor beta/activin signaling in renal epithelia. *Mol Cell Biol.* **12**:4577-85.
59. Kolle G, Georgas K, Holmes GP, Little MH, Yamada T, CRIM1. (2000) A novel gene encoding a cysteine-rich repeat protein, is developmentally regulated and implicated in vertebrate CNS development and organogenesis, *Mech Dev.* **90**(2):181-93
60. Matsui M, Mizuseki K, Nakatani J, Nakanishi S, Sasai Y. (2000) Xenopus kielin: A dorsalizing factor containing multiple chordin-type repeats secreted from the embryonic midline. *Proc Natl Acad Sci.* **97**(10):5291-6
61. Conley CA, Silburn R, Singer MA, Ralston A, Rohwer-Nutter D, Olson DJ, Gelbart W, Blair SS. (2000) Crossveinless 2 contains cysteine-rich domains and is required for high levels of BMP-like activity during the formation of the cross veins in *Drosophila*, *Development.* **127**(18):3947-59
62. Coffinier C, Tran U, Larraín J, De Robertis EM. (2001) Neuralin-1 is a novel Chordin-related molecule expressed in the mouse neural plate, *Mech Dev.* **100**(1):119-22
63. Nakayama N, Han CE, Scully S, Nishinakamura R, He C, Zeni L, Yamane H, Chang D, Yu D, Yokota T, Wen D. (2001) A novel chordin-like protein inhibitor for bone morphogenetic proteins expressed preferentially in mesenchymal cell lineages.

References

Dev Biol. 232(2):372-87

64. De Robertis EM, Sasai Y. (1996) A common plan for dorsoventral patterning in Bilateria. *Nature*. **380** (6569):37-40

65. Piccolo S, Sasai Y, Lu B, De Robertis EM. (1996) Dorsoventral patterning in *Xenopus*: inhibition of ventral signals by direct binding of chordin to BMP-4. *Cell*. **86**(4):589-98

66. De Robertis, E. M., and Kuroda, H. (2004) Dorsal-ventral patterning and neural induction in *Xenopus* embryos. *Annu Rev Cell Dev Biol*, **20**, 285-308

67. Marqués G, Musacchio M, Shimell MJ, Wünnenberg-Stapleton K, Cho KW, O'Connor MB. (1997) Production of a DPP activity gradient in the early *Drosophila* embryo through the opposing actions of the SOG and TLD proteins, *Cell*. **91**(3):417-26

68. Blader P, Rastegar S, Fischer N, Strähle U. (1997) Cleavage of the BMP-4 antagonist chordin by zebrafish tolloid. *Science*, **278**(5345):1937-40

69. Scott IC, Blitz IL, Pappano WN, Imamura Y, Clark TG, Steiglitz BM, Thomas CL, Maas SA, Takahara K, Cho KW, Greenspan DS. (1999) Mammalian BMP-1/Tolloid-related metalloproteinases, including novel family member mammalian Tolloid-like 2, have differential enzymatic activities and distributions of expression relevant to patterning and skeletogenesis. *Dev Biol.*, **213**(2):283-300

70. Oelgeschläger M, Larraín J, Geissert D, De Robertis EM. (2000) The evolutionarily conserved BMP-binding protein Twisted gastrulation promotes BMP signaling. *Nature*. **405**(6788):757-63

71. Chang C, Holtzman DA, Chau S, Chickering T, Woolf EA, Holmgren LM, Bodorova J, Gearing DP, Holmes WE, Brivanlou AH. Twisted gastrulation can function as a BMP antagonist. *Nature*. 410(6827):483-7, 2001

72. Ross JJ, Shimmi O, Vilmos P, Petryk A, Kim H, Gaudenz K, Hermanson S, Ekker

References

- SC, O'Connor MB, Marsh JL. (2001) Twisted gastrulation is a conserved extracellular BMP antagonist. *Nature*. **410**(6827):479-83
73. Scott IC, Blitz IL, Pappano WN, Maas SA, Cho KW. (2001) Greenspan DS, Homologues of Twisted gastrulation are extracellular cofactors in antagonism of BMP signaling. *Nature*. **410**(6827):475-8
74. Shimmi O, Umulis D, Othmer H, O'Connor MB. (2005) Facilitated transport of a Dpp/Scw heterodimer by Sog/Tsg leads to robust patterning of the Drosophila blastoderm embryo. *Cell*. **120**(6):873-86.
75. Nakayama, N., Han, C. Y., Cam, L., Lee, J. I., Pretorius, J., Fisher, S., Rosenfeld, R., Scully, S., Nishinakamura, R., Duryea, D., Van, G., Bolon, B., Yokota, T., and Zhang, K. (2004) A novel chordin-like BMP inhibitor, CHL2, expressed preferentially in chondrocytes of developing cartilage and osteoarthritic joint cartilage, *Development* **131**, 229-24
76. Garcia-Bellido and de Celis. (1992) Developmental genetics of the venation pattern of Drosophila, *Annu Rev Genet*. **26**:277-304
77. Coles E, Christiansen J, Economou A, Bronner-Fraser M, Wilkinson DG. (2004) A vertebrate crossveinless 2 homologue modulates BMP activity and neural crest cell migration. *Development*. **131**(21):5309-17
78. Rentzsch, F., Zhang, J., Kramer, C., Sebald, W., and Hammerschmidt, M. (2006) Crossveinless 2 is an essential positive feedback regulator of Bmp signaling during zebrafish gastrulation, *Development*, **133**: 801-811
79. Ikeya, M., Kawada, M., Kiyonari, H., Sasai, N., Nakao, K., Furuta, Y., and Sasai, Y. (2006) Essential pro-Bmp roles of crossveinless 2 in mouse organogenesis, *Development*. **133**:4463-447362.
80. O'Connor, M. B., Umulis, D., Othmer, H. G., and Blair, S. S. (2006) Shaping BMP morphogen gradients in the Drosophila embryo and pupal wing. *Development*. **133**:

References

183-193

81. Moser, M., Binder, O., Wu, Y., Aitsebaomo, J., Ren, R., Bode, C., Bautch, V. L., Conlon, F. L., and Patterson, C. (2003) BMPER, a novel endothelial cell precursor-derived protein, antagonizes bone morphogenetic protein signaling and endothelial cell differentiation. *Mol Cell Biol.* **23**:5664-5679
82. Binnerts ME, Wen X, Canté-Barrett K, Bright J, Chen HT, Asundi V, Sattari P, Tang T, Boyle B, Funk W, Rupp F. (2004) Human Crossveinless-2 is a novel inhibitor of bone morphogenetic proteins, *Biochem Biophys Res Commun.* **315**(2):272-80
83. Coffinier C, Ketpura N, Tran U, Geissert D, De Robertis EM. (2002) Mouse Crossveinless-2 is the vertebrate homolog of a Drosophila extracellular regulator of BMP signaling. *Mech Dev.* **119** Suppl 1:S179-84
84. Kamimura, M., Matsumoto, K., Koshiba-Takeuchi, K., and Ogura, T. (2004) Vertebrate crossveinless 2 is secreted and acts as an extracellular modulator of the BMP signaling cascade. *Dev Dyn*, 230:434-445
85. Lin, J., Patel, S. R., Cheng, X., Cho, E. A., Levitan, I., Ullenbruch, M., Phan, S. H., Park, J. M., and Dressler, G. R. (2005) Kielin/chordin-like protein, a novel enhancer of BMP signaling, attenuates renal fibrotic disease. *Nat Med*, **11**:387-393
86. Thuveson and Fries. (2000) The low pH in trans-Golgi triggers autocatalytic cleavage of pre- α -inhibitor heavy chain precursor. *J Biol Chem.* **275**(40):30996-1000
87. Ruppert R, Hoffmann E, Sebald W. (1996) Human bone morphogenetic protein 2 contains a heparin-binding site which modifies its biological activity, *Eur J Biochem.* **237**(1):295-302
88. Paine-Saunders S, Viviano BL, Economides AN, Saunders S. (2002) Heparan sulfate proteoglycans retain Noggin at the cell surface: a potential mechanism for shaping bone morphogenetic protein gradients. *J Biol Chem.* **277**(3):2089-96

References

89. Jasuja R, Allen BL, Pappano WN, Rapraeger AC, Greenspan DS. (2004) Cell-surface heparan sulfate proteoglycans potentiate chordin antagonism of bone morphogenetic protein signaling and are necessary for cellular uptake of chordin. *J Biol Chem.* **279**(49):51289-97
90. O'Leary JM, Hamilton JM, Deane CM, Valeyev NV, Sandell LJ, Downing AK. (2004) Solution structure and dynamics of a prototypical chordin-like cysteine-rich repeat (von Willebrand Factor type C module) from collagen IIA. *J Biol Chem* , **279**(51):53857-66
91. Zhu Y, Oganessian A, Keene DR, Sandell LJ. (1999) Type IIA procollagen containing the cysteine-rich amino propeptide is deposited in the extracellular matrix of prechondrogenic tissue and binds to TGF-beta1 and BMP-2. *J Cell Biol.* **144**(5):1069-80
92. Kirsch T, Nickel J, Sebald W. (2000) Isolation of recombinant BMP receptor IA ectodomain and its 2:1 complex with BMP-2. *FEBS Lett.*; **468**(2-3):215-9
93. Garman EF, Schneider TR. (1997) Macromolecular Cryocrystallography. *J. Appl. Cryst.* **30**:211-237
94. McCoy, A.J., Grosse-Kunstleve, R.W., Adams, P.,D., Winn, M.D., Storoni, L.C. & Read, R.J. (2007) Phaser crystallographic software, *J. Mol. Biol.* **33**, 491-497
95. Otwinowski, Z. & Minor, W. (1997) Processing of X-ray diffraction data collected in oscillation mode, *Methods Enzymol.* **276**, 307-326
96. Vonrhein, C., Blanc, E., Roversi, P. & Bricogne, G. (2007) Automated structure solution with autoSHARP. *Methods Mol. Biol.* **364**, 215-230
97. Matthews, B. W. (1968) The Solvent Content of Protein Crystals. *J. Mol. Biol.* **33** 491-497
98. Iemura, S., Yamamoto, T.S., Takagi, C., Uchiyama, H., Natsume, T., Shimasaki, S.,

References

Sugino, H., and Ueno, N. (1998) Direct binding of follistatin to a complex of bone-morphogenetic protein and its receptor inhibits ventral and epidermal cell fates in early *Xenopus* embryo. *Proc. Natl. Acad. Sci.* **95**, 9337-9342

Abbreviations

Abbreviations

ActR-I	Activin Type I Receptor
ActR-IB	Activin Type IB Receptor
ActR-II	Activin Type II Receptor
ActR-IIB	Activin Type IIB Receptor
Alk	Activin receptor-like kinase
ALP	Alkaline phosphatase
ACN	Acetonitrile
Amp	Ampicillin
Å	Angstrom
BMP	Bone Morphogenetic Protein
BMPR-IA	Bone Morphogenetic Protein Receptor Type IA
BMPR-IB	Bone Morphogenetic Protein Receptor Type IB
BMPR-II	Bone Morphogenetic Protein Receptor Type II
bp	Basepair
β-ME	β-Mercaptoethanol
CV2	Crossveinless 2
CHD	Chordin
CHL	Chordin like protein
CR	Cysteine-rich
Col IIA	Collagen IIA
cDNA	complementary DNA
Da	Dalton
DNA	Deoxyribonucleic acid
ddH ₂ O	Double Distilled H ₂ O
DMEM	Dulbecco's modified Eagle's medium
ecd	extracellular domain
<i>E.coli</i>	<i>Escherichia coli</i>

Abbreviations

FPLC	Fast Protein Liquid Chromatography
GDF	Growth and Differentiation Factor
HPLC	High Performance Liquid Chromatography
KCP	Kielin/Chordin like protein
K _D	Dissociation constant
LB	Luria Broth
Mw	Molecular weight
NMR	Nuclear magnetic resonance
OD	Optical density
PAGE	Polyacrylamid-Gelelektrophorese
PCR	Polymerase chain reaction
PDB	Protein Datebank
PEG	Polyethyleneglycol
RT	Room temperature
red.	reduced
rpm	Revolutions Per Minute
SF9	Spodoptera frugiperda
SDS	Sodium dodecyl sulphate
SDS	Polyacrylamid-Gelelektrophorese SDS-PAGE
TB	Terrific Broth
TβR-I	TGF-β Type I Receptor
TβR-II	TGF-β Type II Receptor
TFA	Trifluoroacetic acid
TGF-β	Transforming Growth Factor β
Trx	Thioredoxin
VWC	von Willebrand factor type C domain
wt	wild type

Abstracts

Bone morphogenetic proteins (BMPs) signaling regulates numerous processes of embryogenesis and organogenesis during vertebrate and invertebrate development. BMP function is regulated in the extracellular space by many modulator proteins, including those containing a von Willebrand factor type C (VWFC) domain. Crossveinless 2 is one of BMP extracellular modulator protein that contains 5 VWC domains. To date, the structural basis and the mechanism by which BMP is regulated by VWC containing proteins is poorly understood.

This study describes the preparation, crystallization and structure determination of the binary complex consisting of BMP-2 and the first VWC domain of CV2. The complex consists of a single BMP-2 dimer and two CV2-VWC1 molecules. The VWC1 structure manifests two subdomains architecture plus an N-terminal clip peptide. The binding sites for CV2-VWC1 clip and N-terminal subdomain SD1 overlap with both BMP type I and type II receptor binding sites.

Mutagenesis/interaction studies enabled us to understand how affinity and specificity in the BMP-2/CV2-VWC1 are generated. One mutant that only contains clip and SD1 has a similar affinity for BMP-2 to that of the wt CV2-VWC1, which suggests that the binding part of CV2-VWC1 locates in the N-terminal subdomain. The N-terminal clip plays an important role in binding, when the clip was deleted, CV2-VWC1 showed more than 2000-fold lower affinity than that of the wt VWC1. Residues on clip and N-terminal β -sheets of CV2-VWC1 that form concave surface work cooperatively for the binding to BMP-2, and the binding through both hydrogen bonds and hydrophobic interactions. It is also found that CV2 binds to BMPs as well as BMP regulator Chordin, and the binding is not from one VWC domain, but a composite interface from at least two VWC domains.

Abstracts

This study also shows the biological activity of CV2/CV2-VWC1 *in vivo* and *in vitro*. The blocking of BMP-2 wrist and knuckle epitopes by CV2-VWC1 can inhibit BMP signaling, therefore resulting to the CV2 anti-BMP activity. It is possible that the binding of CV2 to Chordin leading to its pro-BMP activity *in vivo*.

Signale von morphogenetischen Proteinen des Knochens („bone morphogenetic proteins“ im Englischen) (BMP) regulieren zahlreiche Prozesse der Embryogenese und Organbildung während der Entwicklung von Wirbeltieren und Wirbellosen. Die Funktion der BMP wird im Extrazellularraum durch viele Modulator-Proteine reguliert, solche, die eine von-Willebrand-Faktor-TypC (VWC)-Domäne enthalten, miteingeschlossen. Crossveinless2 (CV2) ist eines der extrazellulären BMP-Modulator-Proteine, das 5 VWC-Domänen enthält. Die strukturelle Grundlage und der Mechanismus, durch den BMP durch VWC beinhaltende Proteine reguliert werden, ist bis heute schlecht verstanden.

Diese Studie beschreibt die Aufbereitung, Kristallisierung und Strukturbestimmung eines binären Komplexes, der aus BMP-2 und der ersten VWC-Domäne von CV2 besteht. Der Komplex besteht aus einem einzelnen BMP-2-Dimer und zwei CV2-VWC1-Molekülen. Die VWC1-Struktur zeigt eine Architektur von zwei Unterdomänen, die durch eine Bindung verknüpft sind. Die Bindungsstellen der N-terminalen CV2-VWC1-„Klammer“ und der N-terminalen Unterdomäne decken sich mit den Bindungsstellen sowohl des BMP-Typ1- als auch des Typ2-Rezeptors.

Mutagenese/Interaktions-Studien haben uns ermöglicht zu verstehen, wie Affinität und Spezifität im BMP-2/CV2-VWC1-Komplex generiert wird. Eine Mutante, die nur die N-terminale Unterdomäne enthält, hat eine vergleichbare Affinität für BMP-2 wie Wildtyp (wt) CV2-VWC1. Das deutet darauf hin, dass sich die Bindungsstelle von CV2-VWC1 in der N-terminalen Unterdomäne befindet. Die N-terminale „Klammer“ spielt eine wichtige Rolle in der Bindung. Wurde die „Klammer“ entfernt, zeigte CV2-VWC1 eine 2000 fache geringere Affinität als wt CV2-VWC1. Aminosäureketten der N-terminalen „Klammer“ und β -Faltblattstrukturen des CV2-VWC1 sind beide an der Bindung zu BMP-2 beteiligt und bilden eine konkave Oberfläche. CV2-VWC1 bindet an BMP-2 sowohl über Wasserstoffbrückenbindungen als auch durch hydrophobe Wechselwirkungen. Darüber hinaus wurde herausgefunden, dass CV2 an BMP und auch an den

Abstracts

BMP-Regulator Chordin bindet. Die Bindung wird nicht durch eine einzelne VWC-Domäne bewerkstelligt, sondern durch die zusammengesetzte Oberfläche von mindestens zwei VWC-Domänen.

Diese Studie zeigt auch, die biologische Aktivität von CV2/CV2-VWC1 in vivo und in vitro. Eine Blockade der BMP-2-Hand- (wrist) und Fingergelenk- (knuckle) Epitope durch CV2-VWC1 kann die BMP-Signalwirkung verhindern, und deshalb eine CV2-anti-BMP-Aktivität zur Folge haben. Es ist ziemlich wahrscheinlich, dass die Bindung von CV2 an Chordin in vivo zu pro-BMP-Aktivität führt.

CURRICULUM VITAE

Family name: Qiu

Given name: Liyan

Gender: Female

Date of birth: 27 Nov. 1977

Nationality: China

EDUCATION AND RESEARCH EXPERIENCE

Since 2005.03

PhD student under the supervision of Professor Walter Sebald and Dr. Jinli Zhang at the Institute of Physiological Chemistry II, **University of Wuerzburg**, Germany.

2004.05-2004.12

Research Assistant at the Institute of plant physiology and ecology, **University of Tuebingen**, Germany.

2000.09-2003.07

Graduate education in the School of Life Sciences, **Zhejiang University**, China.

1996.09-2000.07

Undergraduate education in the **Yantai Normal University**, Shandong, China.

ERKLÄRUNG

ERKLÄRUNG

Hiermit erkläre ich, dass ich die vorliegende Arbeit selbständig verfasst und dabei keine anderen als die hier angegebenen Quellen und Hilfsmittel verwendet habe.

Ferner erkläre ich, dass ich diese Arbeit weder einer anderen Prüfungsbehörde vorgelegt, noch anderweitig mit oder ohne Erfolg versucht habe, eine Dissertation einzureichen oder mich der Doktorprüfung zu unterziehen.

Ich erkläre, dass ich bisher keine akademischen Grade erworben oder zu erwerben versucht habe.

Würzburg, den Liyan Qiu

Acknowledgement

Acknowledgement

This work was undertaken in the Institute of Physiological Chemistry II, University of Wuerzburg under the guidance of Prof. Dr. Walter Sebald.

First of all I would like to show my gratitude to my supervisor Professor Sebald for giving me the opportunity to do my PhD work in his lab, for his supervision and support.

I am grateful for Prof. Dr. R. Benz from Faculty of Biology, University of Wuerzburg for being my tutor.

I would like to thank Dr. Jinli Zhang for his detailed instruction during my study and many thanks to Professor Thomas Mueller for his help in Crystallography. I appreciated so much the help of Dr. Joachim Nickel, Dr. Werner Schmitz, and I also want to show my thanks to Alexander and Stella for their collaboration on my PhD project.

I greatly appreciate my coworkers in the lab for their friendship, Yi, Christian, Stefan, Edwine, and other colleagues, for talking, eating, and working together and helping one another. I would like to express my gratitude to all the people in Physiological Chemistry II who helped me during my PhD study.

Thanks John for reading and modifying my thesis and Verena for translating the abstracts part to German.

Special thanks to Xuanmao for his love, his care and support.

Dedicate to my parents!